Publications of the
Astronomical Society of the Pacific

Vol. 104 1992 August No. 678

Publications of the Astronomical Society of the Pacific
104: 599–662, 1992 August

A Critical Review of Selected Techniques for Measuring Extragalactic Distances[1]

GEORGE H. JACOBY

Kitt Peak National Observatory, National Optical Astronomy Observatories, P.O. Box 26732, Tucson, Arizona 85726
Electronic mail: gjacoby@noao.edu

DAVID BRANCH

Department of Physics and Astronomy, University of Oklahoma, Norman, Oklahoma 73019
Electronic mail: branch@phyast.nhn.uoknor.edu

ROBIN CIARDULLO

Department of Astronomy and Astrophysics, Penn State University, 525 Davey Lab, University Park, Pennsylvania 16802
Electronic mail: rbc@astro.psu.edu

ROGER L. DAVIES

Department of Physics, Astrophysics Group, Oxford University, Keble Road, Oxford OX1 3RH, England
Electronic mail: rld@astro.ox.ac.uk

WILLIAM E. HARRIS

Department of Physics and Astronomy, McMaster University, Hamilton, Ontario L8S 4M1, Canada
Electronic mail: harris@physun.physics.mcmaster.ca

MICHAEL J. PIERCE

Dominion Astrophysical Observatory, Current address: Kitt Peak National Observatory, P.O. Box 26732, Tucson, Arizona 85726
Electronic mail: mpierce@noao.edu

CHRISTOPHER J. PRITCHET

Department of Physics and Astronomy, University of Victoria, P.O.B. 3055, Victoria, British Columbia V8W 3P6, Canada
Electronic mail: pritchet@clam.phys.uvic.ca

JOHN L. TONRY

Department of Physics, Massachusetts Institute of Technology, 77 Massachusetts Avenue, Cambridge, Massachusetts 02139
Electronic mail: jt@antares.mit.edu

DOUGLAS L. WELCH

Department of Physics and Astronomy, McMaster University, Hamilton, Ontario L8S 4M1, Canada
Electronic mail: welch@physun.physics.mcmaster.ca

Received 1992 April 30; accepted 1992 June 3

ABSTRACT. We review seven of the most reliable indicators used for deriving distances to galaxies as far away as 100 Mpc: globular-cluster luminosity functions (GCLF), novae, type-Ia supernovae (SN Ia), H I linewidth (Tully–Fisher) relations, planetary-nebula luminosity functions (PNLF), surface-brightness fluctuations (SBF), and fundamental-plane relationships for elliptical galaxies (D_n-σ). In addition, we examine the use of Cepheid variables since these serve to set zero points for most of the methods. We pay particular attention to the uncertainties inherent in these methods, both internal and external. We then test these uncertainties by comparing distances derived with each technique to

[1]Invited review paper.

distances derived from surface-brightness fluctuations. We find that there are small systematic offsets between the PNLF, GCLF, and SBF methods, with the PNLF and GCLF distances being on average 6% and 13% larger than those of the SBF method. The dispersion between the PNLF and SBF distances is 8%; the GCLF-SBF dispersion is 16%, the SN Ia-SBF dispersion is 28%, the D_n-σ-SBF dispersion is 26%, and the Tully–Fisher-SBF dispersion is 32%. The latter value drops to 14%, however, when one considers only well-mixed groups, suggesting that the spiral galaxies measured with Tully–Fisher are not always spatially coincident with the groups' elliptical galaxies. In the mean, all the methods agree extremely well. We also present a summary of distances to the Virgo cluster. Weighted and unweighted averages of the seven methods yield Virgo distances of 16.0 ± 1.7 and 17.6 ± 2.2 Mpc, respectively. The overlap among all the indicators is well within the expected accuracies of the methods. Using the weighted or unweighted Virgo distances to bootstrap to the Coma cluster, we find the Hubble constant to be either 80 ± 11 or 73 ± 11 km s^{-1} Mpc^{-1}, respectively.

TABLE OF CONTENTS

"Gerard de Vaucouleurs on the one hand, and Allan Sandage and Gustav Tammann on the other, arrived at estimates of the size of the universe, as measured by the Hubble constant, differing from each other by a factor of two. Moreover, when I asked the protagonists what was the range outside which they could not imagine the Hubble constant lying, these ranges did not overlap. Given that they were studying more or less the same galaxies with rather similar methods, often using the same observational material, I found this incredible."

Michael Rowan-Robinson, in *The Cosmological Distance Ladder* (1985)

1. INTRODUCTION

Aristarchus of Samos, in the third century B.C., may have been the first person to try measuring the size of his universe when he estimated the ratio of the distances between the Sun and Moon. His efforts, which were later followed by the work of such well-known scientists as Eratosthenes, Hipparchus, Ptolemy, Copernicus, and Kepler, led to a set of reasonably good relative distances within the solar system. With the advent of radar measurements in the mid-20th century, these relative values were placed on an absolute scale with unprecedented accuracy.

Once outside the solar system, however, there is an enormous loss in the accuracy of distance determinations. Measurements of nearby stars and galaxies typically carry uncertainties of 10%–20%, and are thus six orders of magnitude less accurate than solar-system measurements. (But the latter, of course, are more than six orders of magnitude closer!) For the more distant objects (up to 11 orders of magnitude more distant than solar-system objects), even this seems remarkable, especially when one considers the number of rungs on the distance "ladder" (Fig. 1), and the fact that each rung has its own "10% errors." Nevertheless, a number of steps are sufficiently redundant and secure that the accurate measurement of extragalactic distances seems a real possibility.

On the other hand, it is over 2000 years since Aristarchus, and yet we are still unable to determine the scale of our universe to the satisfaction of the astronomical community. By itself, this failure is not a serious transgression; it takes time to solve difficult problems. It is, however, a major embarrassment that the leading proponents in the field have historically failed to agree within their stated errors. If we dismiss the possibility of repeated oversights in the analyses, then the most likely cause of the discrepancy is that the measurement uncertainties, internal and/or external, have continually been underestimated.

It is this line of reasoning that led Rowan-Robinson (1985, 1988) to survey the field of extragalactic distance determinations, and we strongly encourage anyone interested in this topic to consult these reviews. Other recommended reading on the subject includes Balkowski and

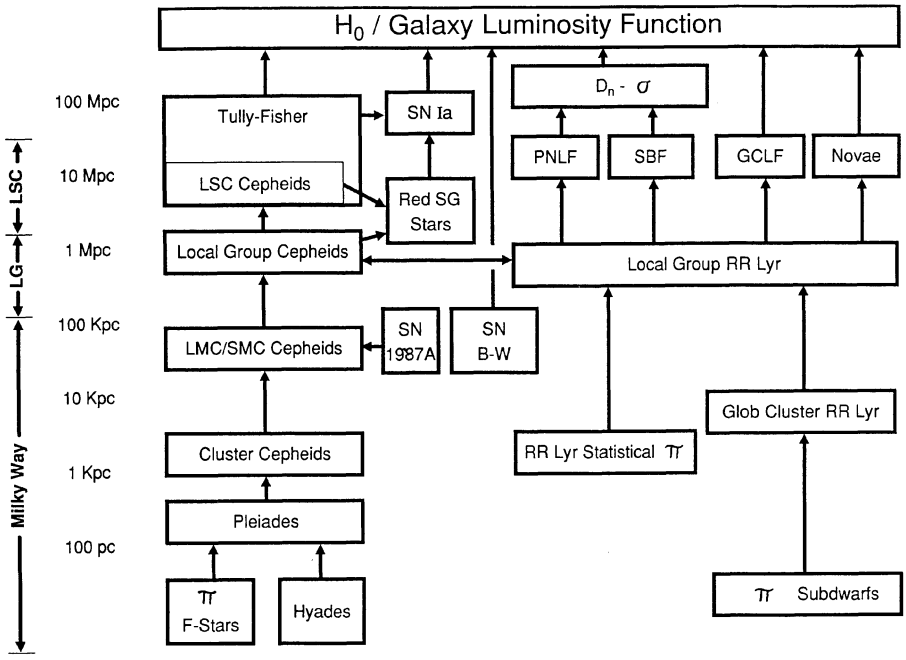

Pathways to Extragalactic Distances

FIG. 1—In this diagram we illustrate the various modern routes which may be taken to arrive at H_0 and the genealogy and approximate distance range for each of the indicators involved. Population I indicators appear on the left-hand side and Population II on the right-hand side. The distance increases logarithmically toward the top of the diagram. The following abbreviations have been used to conserve space: LSC—Local Super Cluster; SG—Supergiant; SN—Supernovae; B-W—Baade–Wesselink; PNLF—Planetary-Nebula Luminosity Function; SBF—Surface-Brightness Fluctuations; GCLF—Globular-Cluster Luminosity Function; π—parallax.

Westerlund (1977), de Vaucouleurs (1982), Aaronson and Mould (1986), van den Bergh and Pritchet (1988), and van den Bergh (1989). In this paper, we examine very recent developments in the field. More importantly, we present detailed critiques of the principal methods currently used for measuring the extragalactic distance scale. In particular, we pay careful attention to the uncertainties in each method with the hope that the reader will derive a greater appreciation for the true range of acceptable values for galaxy distances.

We begin with a discussion of the Cepheid variable stars which are used to calibrate distance indicators within the Local Group and to measure distances out to $\sim$5 Mpc. Despite major advances in technology during the past decade, Cepheids are too faint to use directly in distance determinations of cosmological interest (but see Pierce et al. 1992). These objects are, however, the primary calibrator for the secondary standard candles that are applied at much greater distances. Because of their vital role in establishing the distance scale, we review the basis for using Cepheids and the uncertainties incurred by adopting them as distance standards. Unless otherwise stated, we adopt the Cepheid distance to M31 of 770 kpc (Freedman and Madore 1990) and a differential extinction to M31 of $E(B-V)=0.08$ (Burstein and Heiles 1984) throughout this review. In fact, we will adopt the Burstein and Heiles (1984) reddening values for all galaxies discussed in this review. The various approximation techniques (cf. Sandage and Tammann 1976, 1981; de Vaucouleurs 1981) necessarily impose a smoothing function to the Galactic extinction, whereas the empirical approach of Burstein and Heiles (1978, 1984) appears to offer significantly improved individual values.

We then turn our attention to other methods currently used to measure the extragalactic distance scale. Although many techniques have been proposed over the years, we restrict our discussion to those which are applicable to at least 20 Mpc and for which a detailed error analysis can be performed. For example, we reject arguments based on the relative size of M31 compared to that of spirals in distant clusters (Sandage and Tammann 1990) since this method in its most recent use provides neither a resultant distance nor an uncertainty (but see Stenning and Hartwick 1980). We also reject methods based on an extreme property, such as the brightest or largest object in a class (e.g., red supergiants, H I regions, emission rings) since these techniques are susceptible to Malmquist effects, population sample size effects (the "Scott" effect; Neyman et al. 1953), and usually provide no quantitative assessment of errors. (Humphreys 1988 has demonstrated that brightest red stars, corrected for parent-galaxy absolute magnitude, are relatively good standard candles. However, like all methods based on a few extreme objects in a galaxy, it needs to be developed further to provide good statistical estimates of the errors arising from small sampling statistics and selection effects.) Instead we concentrate on the remaining methods (in no particular order) discussed by Sandage and Tammann (1990): the globular-cluster luminosity function, novae, type-Ia supernovae, the H I linewidth-luminosity relation for spiral galaxies (Tully–Fisher), the planetary-nebula luminosity function, the amplitude of surface-brightness fluctuations, and the fundamental plane relationships for elliptical galaxies (D_n-σ).

A separate section of the paper is devoted to each technique. Within each section, we discuss the physical basis of the method, its assumptions and calibration procedures, its observational requirements, and, most importantly, its strengths and weaknesses. We try to bring all internal and external errors, both random and systematic, to the surface so that the reader can judge the relative merits of each technique. We also attempt to identify additional observations and tests that would further strengthen or discredit the method.

For the purposes of this review, we define internal errors to be those which are intrinsic to the method, such as measuring magnitudes of galaxies, or fitting a function to a set of data points. These should be random since all systematic effects are removed during the reduction and calibration phase of the data analysis. Thus, the net internal error can usually be reduced by making additional measurements. External errors are those which accompany a measurement that is needed to apply the method, such as errors in Galactic extinction and absolute calibrations. These generally carry a higher probability of introducing a systematic error into the result than do the internal errors, and are more difficult to assess accurately. Note that for distance measurements beyond the point where geometrical methods apply, there is no way to define external uncertainties accurately since the true distances are never known exactly. We can assess the validity of the error estimates to some degree, however, by comparing the results from the different methods. We discuss our analysis of such a comparison in Sec. 11.

We also present a table of the distances to the Virgo cluster, the one common landmark for all the methods. The critical column in the table is not actually the distance, but rather the uncertainty in the distance. If the derived distances do not overlap within one or two times the stated errors, then something is very wrong. As will be seen from this table and the general comparison, we find good agreement among the methods, and we find that the errors are generally, but not always, well understood. If a distance-scale controversy exists at all, it is in the difficult task of estimating the uncertainties.

2. PRELIMINARY REMARKS

2.1 The Value of Testing

There is no perfect standard candle. Each method has limitations and uncertainties which can only be determined by thorough testing. We cannot emphasize this approach too strongly, as it is fundamental to the scientific method. Every standard-candle candidate must be subjected to direct observational tests to measure its sensitivity to various parameters such as galaxy luminosity, color, metallicity, and Hubble type. Some of the candles discussed here have not yet been examined so completely, and thus further work is implied.

In some cases, complete testing is simply impossible. For example, all the techniques we discuss are applicable to giant elliptical galaxies (except, of course, for the Cepheids and the H I linewidth-luminosity relation). Unfortunately, nature has not provided us with even one giant elliptical galaxy which is close enough to be used as an absolute calibrator. Consequently, it is impossible to test these techniques directly in galaxies with well-determined distances. Indirect tests, however, are possible for certain methods, and these are discussed in the sections that follow.

An issue which some feel quite strongly about is that a distance indicator must have a solid physical basis if it is to be given any weight (Aaronson and Mould 1986; Hodge 1981). Each of the methods discussed here rests on a physical prescription to some degree, and although none of the methods can be said to be completely understood, our ability to model the relevant physics in these objects is improving all the time. Thus, the apparent robustness of a computer model should have only limited influence on our estimate of the quality of a real physical system as a distance indicator. In fact, an empirical candle that has survived a rigorous testing program should carry far more weight than an untested candle that has a superb physical basis. Conversely, we should welcome those occasions when a candle is shown to be excellent in the empirical sense, but was predicted to be poor from first principles. Such a direct confrontation between observation and theory provides us the best opportunity to learn something new about the universe.

While most of the foregoing may seem trivially obvious, the concepts are absolutely critical. For example, two new methods for deriving the Hubble constant have been proposed recently: the time delay in a gravitational lens system (Rhee 1991; Roberts et al. 1991; Kochanek 1991), and the application of the Sunyaev–Zeldovich effect (Birkenshaw et al. 1991). These are extremely alluring methods because they bypass the entire chain of local calibrators and secondary indicators to give a direct measure of the Hubble constant. There are, however, some model dependencies which must be tested before the systematics of the techniques can be properly evaluated, and following the precepts of the above paragraphs, work is progressing toward that end (e.g., Press et al. 1992).

2.2 Biases

Another major issue deserves special mention. Correcting for biases that may be present in the data or data samples is a topic for the statistics of data analysis which extends beyond the scope of this paper. The problems associated with sample statistics are complex and involved, more so for some distance indicators than for others, although all indicators are affected to some degree. Unfortunately, there is no single prescription that is appropriate in all circumstances, and a complete discussion is better addressed in another review (Bertschinger 1992). For the purposes of this paper, we call the attention of the reader to a few common biases that afflict several techniques, and these should be kept in mind throughout this review.

A true Malmquist (1920) effect may be present such that any sample of objects becomes more and more restricted to brighter members as distance increases. Thus, a sample of distant galaxies will have a higher average luminosity than a nearby sample. This effect, in itself, does not mandate biased distances *provided* that any parameter used to predict the galaxy luminosity is not also biased.

A more subtle effect can arise if the galaxy sample is chosen from a set of biased parameters and those parameters are also used to estimate distances (e.g., magnitudes or diameters taken from a photographic catalog). If those same parameters, which have some measurement uncertainty, enter into the calculation of distances, then the sample will include galaxies near the selection limit that should have been rejected (i.e., they appear brighter or larger than the selection limit). The improper sample selection introduces biased distance estimates near the completeness limit which, in turn, biases the sample mean.

Biases can also result from differences in the environments of the samples. For example, most methods are calibrated locally but applied in large galaxy clusters. If the galaxies in clusters are somehow different from those in the Local Group, a very simple bias arises. Similarly, first-ranked galaxies may foster unusual objects (e.g., extremely bright planetary nebulae, globular clusters, red supergiants) which do not develop in the Local Group, again leading to a simple calibration bias.

Another subtle form of bias can be introduced in the analysis phase of distance determination by binning data. A histogram of globular clusters or planetary nebulae, for example, will have a bias which scatters objects from heavily populated bins into bins with fewer objects. Proper analysis techniques (e.g., maximum likelihood, numerical simulations) can account for this effect, first discussed by Eddington (1913, 1940), and more recently by Trumpler and Weaver (1962). A variant of the problem is discussed by Lynden-Bell et al. (1988) in the context of deriving the average distance to a cluster of galaxies. When the distance measuring technique has an uncertainty which is large enough that a significant number of background and foreground galaxies are inadvertently included in the sample, the mean distance for the cluster sample may be biased, depending on the spatial density of the sample and interloper galaxies.

2.3 Why Do We Care About Distances?

As a final note, it is worth considering why extragalactic distances warrant so much attention. Consider one of the most basic issues: the luminosity of an object. If the distance is not known to better than a factor of 2, then the power output could be in error by a factor of 4. This uncertainty undermines our claim to know one of the most basic properties of distant sources: their energy-generation mechanisms.

Perhaps the most widely publicized aspect of the distance-scale controversy is that the ages of the oldest

stars (e.g., those in globular clusters) are inconsistent with an age of the universe deduced from a large value for H_0. There are, of course, a variety of models for the universe in which this problem is resolved, but those are not necessarily the simplest models.

For the purposes of this paper, we emphasize that distances represent only one of the parameters in the definition of H_0, the other being the recession velocity corrected for large-scale motions. The uncertainty in any estimate of H_0 must include the contributions from distances *and* velocities (which must also include the uncertainties in the large-scale motion corrections). In order to interpret an estimate of H_0 in terms of an age parameter, we must also know the density of the universe (complete with uncertainties), *and* we must estimate the uncertainties in the computer models that predict stellar ages. Consequently, we feel that the age argument demands much more investigation before it can be used to constrain the observational results for H_0. In any case, our primary concern in this review is the distances.

There is an often ignored aspect of the distance-scale controversy. It seem fairly innocuous, but it adds a continuous element of distraction, annoyance, and cost to extragalactic astronomy. Our inability to "scale the universe" means that we must adopt a parametric treatment of distance through the variable $h(=H_0/100)$. This parameter now pervades the journals (and even appears in this review!) by introducing more ambiguity to an already difficult field. It is our sincere hope that the distance-scale controversy can be resolved within this decade so that everyone can move on to solving other important astrophysical problems.

3. CLASSICAL CEPHEID VARIABLE STARS

3.1 Background

Classical Cepheid variable stars are potentially the most accurate distance indicators available for the near field (0.5 kpc–10 Mpc). Their suitability as distance indicators arises from a number of factors including luminosity ($M_V = -2$ to -7), ease of detection through variability, precision, permanence, and understanding of the pulsation phenomenon. The classical (or type I) Cepheids are young, disk objects and as such are only found in galaxies with recent star formation (primarily spiral or irregular galaxies).

There is a vast literature on Cepheid variables as distance indicators and a full historical review is beyond the scope of this paper. Fernie (1969) gives a thorough and entertaining discussion of the early years. Other useful reviews of Cepheids as distance indicators are found in Feast and Walker (1987), Freedman (1988a), Walker (1988), and Madore and Freedman (1991).

The advantages of modern detectors for Cepheid work are legion and a number of known extragalactic Cepheids have been reobserved with CCDs and IR arrays. However, few discovery surveys have made it into print at this writing. Rather than discuss such surveys on a case-by-case basis, we summarize the observational papers on extragalactic Cepheids in Table 1 (excluding LMC and SMC work). Future surveys are likely to be tied to specific calibration needs such as the luminosity-linewidth relations or supernovae.

The sequence of operations required to find and use Cepheids for estimating distances is the same for any region of the visible spectrum, and we describe this process in the next section. We then discuss the tradeoffs between optical and near-infrared photometry.

3.2 Method

The traditional path to a Cepheid-based distance to a galaxy has involved the following steps: (1) acquisition of plate material at several epochs; (2) discovery of variables; (3) magnitude estimates; (4) determination of periods; (5) estimation of mean magnitudes and colors on a standard system; and (6) correction of absorption and distance estimate (given an absolute calibration).

A common feature of many of the earliest surveys for extragalactic Cepheids was the acquisition of *huge* numbers of plates. For instance, Hubble (1929) obtained 350 plates of M31 over 18 years—270 of which were of one field. From this only 40 confirmed Cepheid variables were identified. It is clear that such a large number of plates is not required to extract a reasonable distance estimate to a galaxy, particularly if photometric errors are sufficiently small that variability is obvious from only a few measurements.

The process of blinking plates is extremely tedious and inefficient. The earlier searches made up for inefficiency with plate area, but even with this advantage, sometimes only a handful of Cepheids were identified and characterized. For typical Cepheid light-curve amplitudes, only about 20% of the variables will be detected by blinking one plate pair under ideal conditions. Hence, large numbers of plate pairs need to be blinked to assure the largest sample of variables. Since modern detectors can obtain photometry of much higher precision, an automated means of selecting variables for further study is obviously desirable.

It is not widely appreciated how difficult it was to obtain *accurate* photometry of extragalactic Cepheids from photographic plates. The variables were most often superimposed on a nonuniform and crowded background. Furthermore, photoelectrically calibrated standards were rarely available on the same plate. These problems were dealt with in the most efficient way possible at the time. Typically, plates of a nearby standard field were taken on the same night as the program plates, with identical exposures, and developed at the same time. Then, local standards in the variable fields were established by comparing the stellar images on both plates by eye. This procedure attempted to use the ability of the eye to compensate for the differences in background and crowding, since iris photometry could not be trusted in such situations. A recent example of the use of this technique for M33 is found in Sandage (1983).

Increasing the quality of the photometry dramatically reduces the number of observations required to unambiguously determine the correct period. The large numbers of plates used in early studies were necessary to combat a

combination of poor photometry and aliasing introduced by scheduling. (Even so, 270 plates was a little extreme!) In the best case of ideal scheduling and high S/N photometry only about 8 epochs are required, as demonstrated by Cook et al. (1986). While it might seem that so few epochs might not sample the light curve adequately, this is not true for *detected* variables. To be discovered, the photometry must have sampled a significant fraction of the light-curve amplitude.

The difficulties in setting up a magnitude system have been mentioned above. While the zero point and scale of the chosen system are unimportant for establishing a period, they are critical to the distance determination. For CCD detectors used to date, the field of view has usually been too small to contain enough stars free from background and crowding. Hence, one of the major difficulties encountered in establishing local standards has been applying aperture corrections to magnitudes derived from profile fitting at small radii. For frames of NGC 2403 and M81, Freedman and Madore (1988) estimated the aperture-correction uncertainty as ± 0.07 mag. Fortunately, the recent availability of large-format CCD detectors should alleviate this problem considerably.

Once mean magnitudes and colors are in hand, it is necessary to estimate the correction for absorption. With only two colors, it is not possible to estimate the reddening for individual stars, and hence the most common expedient has been to adopt a global reddening correction. Properly calibrated CCD photometry permits the mean reddening to be estimated from the upper main sequence, since these stars are the precursors of Cepheids and are found in the same regions. Another approach, described in Freedman (1988b), is to "slide fit" the *P-L* relations for different bandpasses to match the *P-L* relation for a calibrating object such as the LMC. The trend in zero-point differences may then be used to estimate the differences in mean absorption between the two objects by fitting a universal extinction curve. Obviously, the onus on the calibration then falls on the LMC where individual corrections for reddening are possible.

The actual distance must be obtained by appealing to a more local calibration. The most trusted existing calibration technique is that obtained from cluster main-sequence fitting. The largest part of the systematic error in determining distances to external galaxies still lies in the Galactic calibration. The reasons for this will be discussed in Sec. 3.5.

3.3 Detection Regimes in Perspective

The difference between observations in the optical and near-infrared are sufficiently great that they warrant discussion. In this section, we will discuss the relative merits of optical (0.4–0.9 μm) and near-infrared (1.0–2.5 μm) observations of Cepheids. To accomplish this, we will consider, in turn, the wavelength dependence of observables, factors affecting the detected signal, and factors contributing to the noise.

3.3.1 Wavelength Dependence of Observables

Panoramic detectors used in the optical (0.4–0.9 μm) and the near infrared (1.0–2.5 μm) are unity gain devices which produce a single electron for every detected photon. A blackbody at an effective temperature of 5500 K—typical of longer period Cepheids—has slowly varying photon spectral density from the V bandpass (0.5 μm) out to K (2.2 μm). (We will come back to this fact again when we discuss the signal.) However, the near-infrared spectra of stars of this effective temperature are strongly distorted by the H^- opacity minimum at 1.6 μm, centered on the photometric H bandpass. The effect of this opacity minimum is to allow radiation characteristic of a hotter source function to escape, and consequently a Cepheid will appear approximately 20% brighter at 1.6 μm than predicted by a blackbody spectrum scaled to, say, a V magnitude. (A second and less important effect which works in the same direction is the smaller amount of limb darkening in the near-infrared.)

One consequence of the H^- opacity feature is the near constant $H-K$ of Cepheids (and for that matter, RR Lyrae stars) through their pulsation cycle. Since the $H-K$ index varies extremely slowly in this temperature regime, a useful value for the total absorption for bandpasses in the 1–2.5 μm regime may be estimated on the basis of the $H-K$ index at one phase point.

During pulsation, both the effective temperature and radius of a Cepheid vary. Since the relative change in radius rarely exceeds 5% in Cepheids (except for the longest-period stars), the areal change is only of order 10%. Therefore, the large light-curve amplitudes observed in the optical are primarily a reflection of the changes in surface brightness during the pulsation cycle, due to the changes in effective temperature. This variation is illustrated in Fig. 2, where the relative number of photons at minimum and maximum effective temperature are easily compared. For detection of variation, a short-wavelength bandpass such as B or V is indicated, whereas for measurement of mean light-curve characteristics, a long-wavelength bandpass such as I, J, H, or K is advantageous.

Other well-known advantages of longer-wavelength observation are the smaller total absorption, reduced sensitivity to flux redistribution due to metallicity, and reduced sensitivity to possible photometric contamination by an upper main-sequence companion.

3.3.2 Signal

Earlier, the slowly varying photon spectral density for Cepheid stars was described. If, for the purposes of this discussion, we take it to be constant, then the number of detected photons will vary as the throughput of the atmosphere and telescope optics, the width of the bandpass, and the quantum efficiency of the detector. It is not widely appreciated that the near-infrared is competitive with or superior to, say, the I (0.8 μm) bandpass in each of these respects.

The popular notion is that near-infrared transparency is quite poor. In fact, this is only true between the band-

TABLE 1
Extragalactic Cepheid Studies

Galaxy	Reference	Detector	Comments
Local Group			
M31	Hubble, 1929	pg	Discovery survey
	Gaposchkin, 1962	pg	Discovery survey, Field II
	Baade and Swope, 1963	pg	Discovery survey, Field IV
	Baade and Swope, 1965	pg	Discovery survey, Fields I,III
	Welch *et al.*, 1986	InSb	
	Freedman and Madore, 1990	CCD	Metallicity effects
	[Metcalfe and Shanks, 1991]	CCD	Corrections to standard sequence
M33	Hubble, 1926	pg	Discovery survey
	van den Bergh, Herbst, and Kowal, 1975	pg	Discovery survey
	Sandage, 1983	pg	Discovery survey
	Sandage and Carlson, 1983	pg	Discovery survey
	Madore *et al.*, 1985	InSb	
	[Christian and Schommer, 1987]	CCD	Corrections to standard sequence
	Mould, 1987	CCD	Single epoch
	Kinman, Mould, and Wood, 1987	pg	Discovery survey, r, automated
	Freedman, Wilson, and Madore, 1991	CCD	
	[Metcalfe and Shanks, 1991]	CCD	Corrections to standard sequence
NGC 6822	Hubble, 1925	pg	Discovery survey
	Kayser, 1967	pg	
	McAlary *et al.*, 1983	InSb	
IC 1613	Sandage, 1971	pg	Discovery survey
	McAlary, Madore, and Davis, 1984	InSb	
	Freedman, 1988b	CCD	
Phoenix	Caldwell and Schommer, 1988	CCD	Discovery survey, progress report
WLM	Sandage and Carlson, 1985b	pg	Discovery survey
M81 Group			
M81	Freedman and Madore, 1988	CCD	
	Mould *et al.*	CCD	Discovery survey (HST Cycle 1)
NGC 2403	Tammann and Sandage, 1968	pg	Discovery survey
	McAlary and Madore, 1984	InSb	
	Freedman and Madore, 1988	CCD	
	[Metcalfe and Shanks, 1991]	CCD	Corrections to standard sequence
Sculptor Group			
NGC 247	Freedman *et al.*, 1988	CCD	Discovery survey, progress report
NGC 253	Freedman *et al.*, 1988	CCD	Discovery survey, progress report
NGC 300	Graham, 1984	pg	Discovery survey
	Madore *et al.*, 1987	InSb	
NGC 7793	Freedman *et al.*, 1988	CCD	Discovery survey, progress report
Other			
Sex A	Sandage and Carlson, 1982	pg	Discovery survey
	[Walker, 1987]	CCD	Corrections to standard sequence
Sex B	Sandage and Carlson, 1985a	pg	Discovery survey
NGC 3109	Demers, Kunkel, and Irwin, 1985	pg	Discovery survey, automated
	Sandage and Carlson, 1988	pg	Discovery survey
	Capaccioli, Piotto, and Bresolin, 1992	CCD	
IC 5152	Caldwell and Schommer, 1988	CCD	Discovery survey, progress report
DDO 216	Hoessel *et al.*, 1990	pg	Discovery survey (aka Pegasus dwarf)

TABLE 1
(Continued)

Galaxy	Reference	Detector	Comments
Leo A	Hoessel, Saha, and Danielson, 1991	pg	Discovery survey
NGC 5068	Walker, 1990	CCD	In progress
NGC 5128	Walker, 1990	CCD	In progress
NGC 5236	Caldwell and Schommer, 1990	CCD	In progress
NGC 5408	Walker, 1990	CCD	In progress
324-g24	Walker, 1990	CCD	In progress
444-g84	Walker, 1990	CCD	In progress
381-g20	Walker, 1990	CCD	In progress
IC 4182	Sandage *et al.*	CCD	Discovery survey (HST Cycle 1)
M101	Cook, Aaronson, and Illingworth, 1986 Cohen *et al.*	CCD CCD	Discovery survey In progress (Palomar Consortium)
Virgo Cluster			
NGC 4571	Pierce *et al.*	CCD	In progress
NGC 4321	Pierce *et al.*	CCD	In progress

passes! The total atmospheric absorption in the *J*, *H*, and *K* bandpasses rarely exceeds 0.2 mag and the extinction coefficient is typically 0.04–0.10 mag airmass^{-1} for these bandpasses, which is the same range expected for photometry at *I*. [The near-infrared extinction curves are nonlinear, so quoting extinction coefficients alone would be slightly misleading (Manduca and Bell 1979).]

The bandwidths of the *J*, *H*, and *K* filters are typically 0.3–0.35 μm, compared to 0.2 μm at *I* and 0.08–0.10 μm at *B* or *V*. Furthermore, the quantum efficiency of thinned CCDs at *I* is typically 30%–35%, whereas quantum efficiencies greater than 60% over the *J*, *H*, and *K* bandpasses can be realized with HgCdTe detectors. The reflectivity of aluminum is 93%–96% in the 1.0–2.5 μm region compared to 86% at *I*.

Optical CCD chips continue to outperform near-infrared detectors in terms of field size, and this optical advantage is likely to remain for the immediate future.

3.3.3 Noise

Far and away the biggest disadvantage for ground-based near-infrared work is the high (and variable) sky brightness, primarily due to emission bands of the OH^- radical. The surface brightness of the sky climbs toward the red throughout the bandpasses of interest, being 19.2, 14.8, 13.4, and 12.6 mag arcsec^{-2} for the *I*, *J*, *H*, and *K* bandpasses, respectively (*CFHT Observer's Manual* 1990). Part of the *K* sky-brightness value is undoubtedly due to the emissivity of the telescope optics, so the true *K* sky brightness may be as low as 14 mag arcsec^{-2}. The $V-K$ color of the night sky has been referred to as the "Infrared Decade" (Schechter, private communication). Since the emitting layer for this airglow is at an altitude of about 90 km, it is necessary to go to space to escape its effects. There is a break in the OH^- band spectrum in the long-wavelength side of the *K* bandpass, but this is just where thermal emission starts to become a problem. (It is possible that this break could be exploited from a cold site such as Antarctica.)

A second important contribution to the noise in the photometry is crowding of stellar images. The difference between long-wavelength optical and infrared photometry is not substantial with respect to crowding. The *K*-giant background against which Cepheids will be detected acts as a background having statistical fluctuations due to variations in the number of giant stars per pixel, but is significantly redder ($V-K=3.3$) than the variables ($V-K=2.0$). The effects of both crowding and sky noise are obviously reduced when the FWHM of the stellar images is small (i.e., good seeing conditions).

3.3.4 Bandpasses of Choice

For the near field, optical ground-based photometry is likely to remain dominant for the foreseeable future, as a result of the lower-sky surface brightness in this regime. However, due to the substantial advantages of the near-infrared (particularly when unconstrained by molecular atmospheric absorption, since a single 1–2.5 μm bandpass could then be used) in terms of number of detected photons, the most distant Cepheid moduli can be obtained in the near-infrared from space–possibly with the NIC second-generation *HST* instrument.

3.4 Physical Basis

The physical processes behind the pulsation are relatively easy to understand, although they are by no means

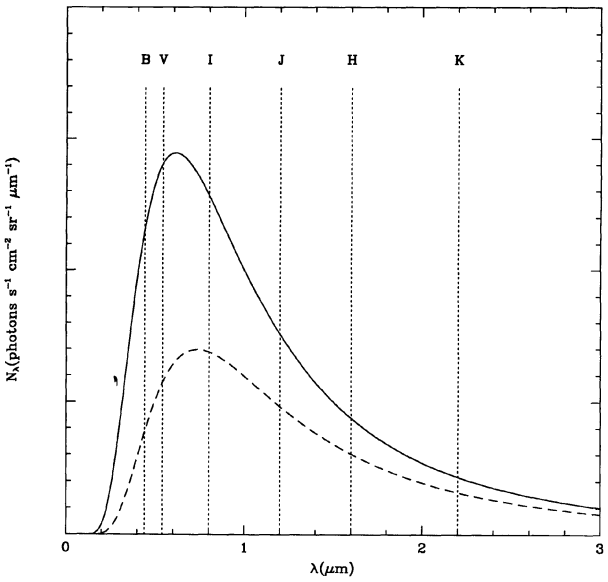

FIG. 2—In this diagram, the photon spectral density of a blackbody at 6000 K (solid line) and 5000 K (dashed line) is illustrated. These effective temperatures represent the range encountered during the pulsation of a typical 10-day Cepheid. The positions of the *B, V, I, J, H,* and *K* bandpasses are indicated. The number of detected photons from sources of these effective temperatures is proportional to the area under the curve for each bandpass. Wider bandpasses and higher quantum-efficiency detectors in the near infrared are particularly advantageous for the cooler and brighter long-period Cepheids. The increased near-infrared flux due to the lower H^- opacity is not shown in this diagram.

trivial to model. The interested reader is directed to Cox (1980, Chap. 10) for a full discussion. Normally, the compression of an element of gas will result in an increased rate of energy loss. However, near the boundary of an ionization zone of an abundant element, the gas can absorb heat when most compressed and release it after the instant of maximum density. If this interaction occurs at a resonant radius in the interior of a star, pulsation will ensue.

In Cepheid variables, the $He^+ \rightleftharpoons He^{++}$ zone is believed to be responsible for most of the driving. However, the $H \rightleftharpoons H^+$ zone does have an influence on the form and phasing of the light and velocity curves. The regularity of Cepheid pulsation is astonishing, corresponding to oscillator Q's of 10^9–10^{10} in most cases. As clocks, Cepheids are as good as the rotation rate of the earth. The repeatability of Cepheids is a significant asset allowing reexamination at a later date with only minimum calibration time.

The usefulness of Cepheids rests on the obvious correlation of period with luminosity. How does this arise? Every star has a characteristic oscillation period, but pulsation in stars outside the instability strip is strongly damped. The strong period-luminosity correlation arises because the temperature width of the instability strip is so narrow (due, in turn, to the need for the partial ionization zone to be at an appropriate depth in the atmosphere). If the temperature width of the strip were much larger, the period-luminosity relationship would be much less apparent, but a period-luminosity-color (*P-L-C*) relationship would retain its precision.

This interplay of parameters can be better understood by the following argument. The dependence of the period, P, on the stellar mass, M, and radius, R, follows from Newtonian gravitation

$$P \propto R^{3/2} M^{-1/2}. \tag{1}$$

The luminosity of the star, L, is correlated with its mass due to the strong density and temperature dependencies of the energy-generation equations:

$$L \propto M^k. \tag{2}$$

However, luminosity is also determined by the stellar radius and effective temperature, T, by

$$L \propto R^2 T^4, \tag{3}$$

so we can eliminate mass as a variable and the period is determined from two parameters: luminosity and temperature. The corresponding observational quantities are magnitude and color index.

The period-luminosity-color (*P-L-C*) relation is an equation for a plane. Cepheid variables are found only in the swath of the plane where stars are pulsationally unstable (and where real stars are actually found due to evolution!). Projections of this plane along each axis result in (1) the color-magnitude diagram, (2) the period-color diagram, and (3) the period-luminosity diagram. This is illustrated in Fig. 3, where the data on galactic calibrating Cepheids is taken from Table 2 of Feast and Walker (1987). Note that changing the boundaries of the allowed region of instability in the plane does nothing to reduce the quality of the *P-L-C* fit, but will change the widths of the distributions in all the projected planes. Incomplete filling of the instability strip by evolutionary tracks can therefore affect distance determinations using the *P-L* relation, but will not affect distances derived from a *P-L-C* relation. (The reader should note the similarities between the *P-L-C* plane and the so-called "fundamental plane" of the D_n-σ relation.)

Recent work on Galactic and LMC Cepheids by Fernie (1990) and Mateo et al. (1990) has demonstrated that the instability strip does not seem to have a constant width in color. Rather, the instability strip is better described by a wedge in the color-magnitude diagram opening at $(B-V)=0.4$, $M_V=-2$ with blue and red edges proceeding toward $(B-V)=0.6$, $M_V=-5$, and $(B-V)=1.1$, $M_V=-5$, respectively. This is most likely due to the filling of the instability region by evolution—the existence of pulsating δ Scuti stars and white dwarfs is evidence that the instability strip exists at lower luminosities.

The values of the coefficients of the *P-L-C* are still a topic of active discussion (especially with regard to metallicity dependence). However, a representative *P-L-C* relation from Feast and Walker (1987) is

$$\langle M_V \rangle = -3.53 \log_{10} P + 2.13(\langle B_0 \rangle - \langle V_0 \rangle) - 2.13. \tag{4}$$

The bracket notation indicates flux weighting and the zero subscript indicates a dereddened magnitude. Similarly, a representative *P-L* relation from the same source is

$$\langle M_V \rangle = -2.78 \log_{10} P - 1.35. \quad (5)$$

3.5 Calibration and Uncertainties

The luminosities of Cepheids are difficult to calibrate with high accuracy because of their low space density, since they are massive stars in a very brief evolutionary phase. The nearest Cepheids are about 200 pc away. Trigonometric parallaxes to these stars at 5% accuracy would require a precision of 0.25 milliarcsec. This is at the frontier of the capabilities of pioneering CCD astrometric programs under ideal conditions according to Monet (1988), and the difficulty in achieving this precision is exacerbated by the brightness of the Cepheids relative to field reference stars (usually a difference of 8 mag or more!). Thus, for even the nearest Cepheids, a precision of 10% from trigonometric parallax programs is probably optimistic.

An alternative to trigonometric parallax is statistical parallax. In this technique, one is still faced with the dramatic brightness differences between the program object and field reference stars for proper motion, but the linear increase in proper-motion signal-to-noise ratio with time allows this technique to be competitive. The most complete statistical parallax analysis of Cepheids to date is that of Wilson et al. (1991). Their derived zero point for the *P-L* relation is in excellent agreement with that of Caldwell and Coulson (1986) and Feast and Walker (1987), although the uncertainty is roughly three times as large. This agreement between kinematic and photometric calibrations suggest that there is no systematic error at the 0.3 mag level.

In Fig. 4, four modern paths to the calibration of Cepheid luminosities are illustrated. The first two involve cluster main-sequence fitting and the last two require angular diameters and radii of field Cepheids. The use of the Magellanic Cloud Cepheids as intermediaries is necessary when the period distribution of the calibrators is significantly different from the period distribution of the extragalactic Cepheids. The final path requires the fewest links and will be based on the most direct measurements of distance, but will not be realized until the completion of the Sydney University Stellar Interferometer–SUSI (see below).

Very recently, the promise of direct distance determination to the LMC has been realized by the precise measurement of the SN 1987A circumstellar-ring light echo by Panagia et al. (1991). This determination has resulted in a true distance modulus of 18.55 ± 0.13 mag to SN 1987A, which corresponds to a distance uncertainty of only 6%. Using an inclination of 27 deg and a position angle for the line of nodes of 170 deg, and assuming that the supernovae resides in the disk, we obtain a distance modulus of 18.57 ± 0.13 for the center of mass of the LMC. [The east side is known to be closer from the work of de Vaucouleurs (1980) and Gascoigne and Shobbrook (1978)]. While this distance is likely to remain the most precise for some time to come, the still open question of a luminosity-metallicity

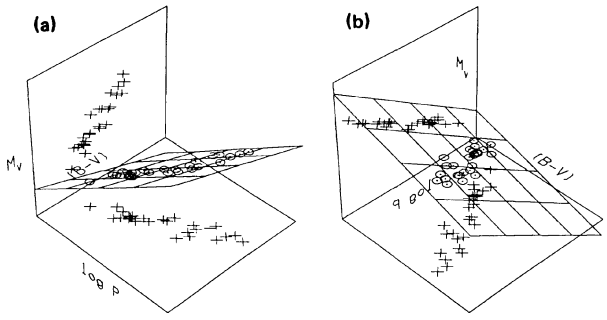

FIG. 3—Three-dimensional representations of the *P-L-C* relation given in the text with the points from Table 2 of Feast and Walker (1987) plotted. In (a) the projections onto the color-magnitude and period-color diagram are shown. The viewpoint in (b) has been chosen to highlight the period-luminosity and period-color projections.

dependence suggests that we retain the (independent) techniques for calibration of Cepheid luminosities, and these are now discussed in more detail. [Note that the interpretation of the LMC Ring data has been called into question by Dwek and Felten (1992).]

A number of galactic Cepheids are found in clusters or associations. A recent list is contained in Table 2 of Feast and Walker (1987). This table reveals a total of 28 potential calibrating Cepheids, of which 17 are believed to be in clusters, eight are believed to belong to associations, and three are calibrated by geometry or binarity. The cluster Cepheids are predominantly short-period stars (most have periods shorter than 12 days) and the association Cepheids are long-period stars (with periods between 15 and 70 days). Clusters are attractive because they permit a distance and reddening estimate independent of observations of the Cepheid. (Future work may also allow individual metallicity estimates for some clusters.) However, the technique is probably not capable of precisions exceeding ± 0.2 mag in distance modulus (equivalent to 10% in distance) *per cluster.* There are a number of reasons for this. First, the most obvious and most easily measured stars in the cluster are those near the turnoff. These stars lie on a near-vertical segment of the main sequence where any photometric error will be magnified dramatically into an error in the cluster-distance modulus. Second, stars near the turnoff may also lie an unknown distance redward of the actual zero-age main sequence due to evolution. In addition, such stars are frequently fast rotators (of unknown inclination) or binaries. Thus, an irreducible intrinsic scatter is introduced in the cluster main sequence and different distances may be derived solely from different interpretations of the same data.

Relief from the steep and sparsely populated upper main sequence may be obtained by attempting measurements of lower-mass stars but here field contamination overwhelms the CMD. Discrimination may be possible using proper

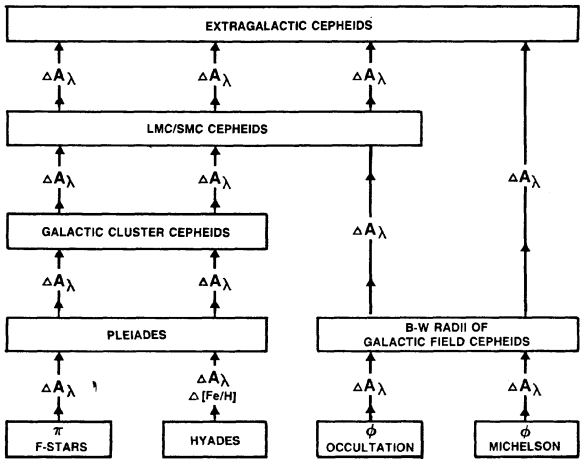

FIG. 4—Four modern paths to extragalactic Cepheid distances. The links indicate observationally determined corrections such as absorption (ΔA_λ) and metallicity (Δ[Fe/H]).

motions or radial velocities since velocity dispersions for galactic clusters are expected to be less than 1 km s^{-1}, but early-epoch plates did not go sufficiently deep for effective proper-motion measurements, and stars cool enough for modern radial-velocity spectrometers are very faint, leading to little progress in this area. Both upper and lower main-sequence stars may also suffer from differential reddening across the face of the cluster.

Once the position of the main sequence is deduced from the observations, it is necessary to determine the difference in distance modulus between the cluster in question and a local cluster: the Pleiades or Hyades. Originally, the Hyades was the cluster of choice because the smaller distance (40 pc) resulted in a more accurately determined distance modulus. However, the age of that cluster and its high metallicity made it less than ideal for comparison with young, Cepheid-bearing clusters. In the last decade, the Pleiades has been the cluster of choice, at a true distance modulus of 5.57 ± 0.08 mag (130 pc) according to the field-star parallax fit of van Leeuwen (1983). The Pleiades may also be calibrated relative to the Hyades after appropriate determination of the metallicity difference and its effect on the absolute magnitude and color, as discussed by Turner (1979). These two techniques are in good agreement.

If the mean radius of a Cepheid variable can be determined by independent means, then in principle a measurement of the angular size of the Cepheid will determine its distance. Such geometric techniques are referred to as "Baade–Wesselink" methods after Baade (1926) and Wesselink (1946) who first described how the light and color curves could be combined with the integrated radial-velocity curve to obtain the mean stellar radius. An excellent critique of the application of these methods is given by Gautschy (1987). While the full promise of these techniques is yet to be realized, the problems encountered to date are not fundamental in origin. Feast and Walker (1987) have reviewed the zero points determined from Baade–Wesselink techniques and compared them to the cluster and association zero point. They find that Baade–Wesselink luminosities tend to be 0.05–0.15 mag brighter. An unresolved question regarding these techniques is the most appropriate color index for use in the Baade–Wesselink solutions.

The angular radius can be determined from direct measurement or inferred from photometry after correction for reddening. The apparently largest Cepheids have angular diameters in the range of 1.0–1.5 milliarcsec. Direct techniques for measuring the angular radius include lunar occultation and Michelson interferometry. Lunar occultations are necessarily restricted to stars near the ecliptic, the most favorable being ζ Geminorum, X Sagittarii, and W Sagittarii. Ridgway et al. (1982) have measured the angular radius of ζ Gem, but with a precision of only 20%. Ground-based Michelson interferometry also shows significant promise with angular resolutions of 4×10^{-5} arcsec being obtainable with the 1 km baseline proposed by Davis (1985). Such observations do not suffer from the severe positional and scheduling restrictions of lunar occultation work and hence long-period Cepheids may be observed. Program Cepheids for SUSI are listed in Shobbrock (1992).

Indirect techniques for estimating the angular diameter rely on establishing a surface brightness from a color and measuring the flux in some bandpass. The relationship between surface brightness and effective temperature is calibrated by measuring colors of giants whose angular diameters have been accurately measured from lunar occultations. While a correction for absorption is required, the derived angular diameter is very insensitive to the value of the absorption used for the $(V-R)$ relationship. A very clear introduction to this technique is given in Barnes et al. (1977).

The nature of the uncertainties associated with a Cepheid-based distance to a galaxy can best be elucidated by considering individual cases. Here we will consider the existing uncertainties in distances to the LMC (0.051 Mpc), M33 (0.84 Mpc), NGC 2403 (3.2 Mpc), and M101 (7.5 Mpc).

LMC: In this nearby galaxy, high-precision photometry of Cepheids of all periods is possible with 1-m-class telescopes. Individual reddening estimates are possible using *BVI* photometry and the scatter in observed reddenings is found to be of order 0.04 mag. According to Caldwell and Laney (1990), 141 Cepheids in the LMC have published photometry using modern detectors. The error in the distance estimate is therefore dominated by the Galactic calibration errors of order ± 0.13 mag or 7% in distance, comparable with the geometric determination of Panagia et al. (1991).

M33: The recent work of Freedman et al. (1991) is the most comprehensive CCD study of M33 Cepheids to date. Their distance estimate is based on *BVRI* photometry of 10 Cepheids with good phase coverage. With smaller sam-

ples of variables, the finite width of the instability strip in temperature and its manifestation as a nonzero luminosity scatter in *P-L* relations become increasingly important. The mean magnitudes derived from their data have uncertainties of order 0.1 mag which are too large for meaningful individual reddening corrections. Instead a global reddening correction is used. The final internal error in their distance estimate is ±0.09 mag or 5% in distance. This uncertainty must be added quadratically to the Galactic calibration error, resulting in a total uncertainty of ±0.16 mag or 8% in distance.

NGC 2403: Freedman and Madore (1988) have obtained few-phase *I*-band photometry of eight Cepheids in NGC 2403. Their final estimate of the distance modulus uncertainty is ±0.24 mag or 12% in distance (including the uncertainty in the LMC distance modulus which they estimate as ±0.15 mag). Interestingly, the contribution of photometric errors to the distance uncertainty is now similar in magnitude to the effects of the instability strip temperature width.

M101: This galaxy is the most distant object in which Cepheid variables have yet been discovered. Cook et al. (1986) found and characterized two Cepheid variables using CCD photometry. A quantitative error analysis was not attempted in that paper, but following the reasoning of Freedman and Madore (1988) we expect the distance uncertainty to be of order ±0.3 mag or 15% in distance.

Perhaps the most important lesson to be learned from these studies is that the Cepheid distance uncertainty for a galaxy with single-band photometry of two Cepheids at 7.5 Mpc is only twice that of the very nearby and well-studied LMC. Said another way, if photometry is of sufficient quality to allow period determination, an uncertainty of 15% in distance (or less) is virtually assured.

3.6 Future Needs and Directions

There are numerous improvements possible in the detection and use of Cepheid variables that have been made possible by new detectors, fast-computing hardware, and reduction software. In this section we will discuss some of the more important developments. Madore and Freedman (1985) were the first to discuss possible procedural changes in the way Cepheids are used to determine distances. They correctly point out that Cepheid periods have traditionally been determined to precisions far greater than required for distance estimation and suggested an expedient technique for estimating periods based on photometry obtained at two phases. Their method attempts to exploit the rate of brightness decline on the descending branch of the light curve which is correlated with period. Unfortunately, the first application of this technique by Cook et al. (1986) on Cepheids in M101 was not encouraging (although it should be recognized that this is the most distant object in which a search has yet been attempted).

There are a number of ways in which Cepheid searches can be streamlined and improved. The first involves the acquisition of observations. In more distant galaxies, only the longer-period Cepheids are going to be detected. A convenient breakpoint in terms of total numbers and brightness occurs at a period of 10 days. If observations are obtained across three consecutive dark runs (at intervals of 2 or 3 days), there will be practically no ambiguity in period for 10–20 and ⩾40 day Cepheids. In Fig. 5, the window function for eight nights of observing spread over three dark runs is shown. Note how little aliasing occurs for periods between 10 and 20 days. (The 30-day alias is difficult to avoid if dark time is required!) Since the frequency distribution of Cepheids is heavily weighted toward shorter periods, the selected dates can be chosen to ensure a high success rate in period determinations. A similar case can be made for more distant galaxies where the less common 40–50-day Cepheids will be the targets of choice.

The discovery of variables by blinking is notoriously inefficient and difficult. Now that photometry for all objects in a program field can be obtained with reasonable effort, a number of options for variable detection avail themselves. Most obvious among these options is to examine the photometry for every star of an appropriate color. This technique still requires a significant amount of time and is fraught with pitfalls such as crowded stars resolved on some frames but not on others, deviations caused by chip defects, and so on.

Period determination has a long and well-documented history. (For a very readable overview, see Fullerton 1986.) We offer few insights here. Suffice it to say that the use of small numbers of observations demands signal-to-noise ratios of at least 10. One bad point can completely skew a period determination. While some discrimination is possible by examination of colors, there is no substitute for good data. The most generally useful and easily implemented algorithm for Cepheid period searches is to search the data *phased* with a range of trial periods for minimum "string length."

The bandpasses of choice for ground-based observations with CCDs are *V* and *R*. The *R* bandpass occurs near the peak sensitivity of most currently used CCDs. While the *V* bandpass falls at a slightly less sensitive wavelength than *R*, most chips have still lower quantum efficiencies at *B*. Furthermore, Cepheids are typically a half magnitude brighter (or more) at *V* than *B*, leading to higher S/N photometry with the same exposure. The amplitude of variation decreases to the red of *R*, but so does the quantum efficiency of CCDs. A further detriment to photometry at the longest optical wavelengths is night-sky emission by OH^- radicals, which is much stronger at *I* than at *R*. Since the $V-R$ color still provides good discrimination between types of variable stars, the *R* bandpass is the better long-wavelength choice for CCD detectors.

Cepheid variables are likely to remain the most precise distance indicators in the near field for a considerable time to come. They are far brighter than RR Lyr stars and can be detected and characterized in a reasonable number of nights if optimum scheduling is allowed. The greatest distance to which they can be used is determined more by image size (seeing plus optical quality) than by photon statistics, at present (due to crowding). As 8–10-m-class telescopes become available and high-resolution imaging

techniques improve, we can expect the limit for Cepheid distances to be pushed out at least as far as the spirals in Virgo. In fact, the search for Cepheids in Virgo cluster galaxies has already begun with a study in NGC 4571 by Pierce et al. (1992). Near-infrared space-based (NIC) measurements may well be able to detect the longest-period Cepheids in more distant galaxies.

4. GLOBULAR CLUSTERS

4.1 Background

The old star clusters found in the halos of all large galaxies have long been realized to have mean luminosities that are at least roughly the same everywhere we look. Typical globular clusters have absolute visual magnitudes $M_V \simeq -7$ to -7.5, comparable to the brightest supergiant stars; and in giant E galaxies which may contain many thousands of globular clusters, the brightest individual clusters reach luminosities of $M_V \simeq -11$, more luminous than any stellar indicators (except supernovae), and detectable at distances of more than 100 Mpc with today's ground-based CCD imaging capabilities. These characteristics are the basis of their attraction as standard candles (see Fig. 6).

The use of clusters for distance measurement is mentioned in passing by Hubble (1932, 1936b), though only in reference to large *spiral* galaxies (M31, M81, M101) for which they are intrinsically much less suitable. Their first published use in a giant elliptical, their most natural application, seems to be by Baum (1955), who simply compared the brightest globulars in M87 with those in M31. Other attempts were made to match the brightest clusters in the Virgo and Local Group galaxies (Racine 1968; Sandage 1968; van den Bergh 1969; de Vaucouleurs 1970; Hodge 1974), but these were eventually given up when it became clear that the numbers of globular clusters in these galaxies were very different, and that large statistical differences in the true luminosity of the brightest clusters could therefore be expected (but see Sec. 4.6 for a modern recasting of this approach).

The pioneering concepts developed by Racine in the early 1970's suggested that the luminosity function of the *entire* set of globular clusters in a galaxy had identifiable structure which must hold considerably more distance information than did just the brightest few clusters. Along these lines, the first fully modern use of globular clusters as standard candles is the work of Hanes (1977a,b, 1979), with deep photographic samples of clusters around several Virgo ellipticals. However, further major progress had to await the advent of CCD imaging, which permitted the key Virgo galaxies to be surveyed to much greater depth (van den Bergh et al. 1985; Cohen 1988; Harris et al. 1991), and brought the brightest clusters around far more distant galaxies immediately within reach (Harris 1987a; Thompson and Valdes 1987; Pritchet and Harris 1990).

4.2 Method

Detailed descriptions of the present-day use of globular-cluster luminosity functions (or GCLFs) can be found in Hanes and Whittaker (1987), Harris (1988a), and Harris et al. (1991) along with their results for the distance scale and H_0. The basic ideas are illustrated in Fig. 7, which is a plot of the GCLF [the relative number $\phi(m)$ of globular clusters as a function of magnitude m] for the Virgo giant ellipticals. The functional shape of $\phi(m)$ is characterized by two simple parameters: the magnitude level or *turnover point* (m_0) where the population of clusters reaches a maximum; and the *dispersion* [$\sigma(m)$] or standard deviation of the distribution. As an empirical curve, the observations show that a Gaussian or log-normal function

$$\phi(m) = Ae^{-(m-m_0)^2/2\sigma^2} \qquad (6)$$

(where A is a normalization factor representing the total population of globular clusters in the galaxy) does an excellent job of describing the GCLF in all galaxies studied to date. The log-normal fitting function gives a convenient way to parametrize the data and to intercompare the GCLFs from different galaxies. For the nearest *rich* systems of galaxies containing giant ellipticals (the Virgo and Fornax clusters) the deepest limits achieved at present reach to just about 1σ fainter than the turnover (Harris et al. 1991).

The actual use of the GCLF method, in its simplest form, goes as follows. The "standard candle" is essentially the magnitude of the turnover, m_0. The goal in observing any distant galaxy is then to obtain photometry of its halo clusters which reaches sufficiently faint to estimate m_0 accurately. In practice, the GCLF is normally found as the residual excess of starlike objects (see Fig. 6), after a background LF for the field has been subtracted and photometric detection incompleteness at the faintest levels has been accounted for. By fitting an analytic interpolation function

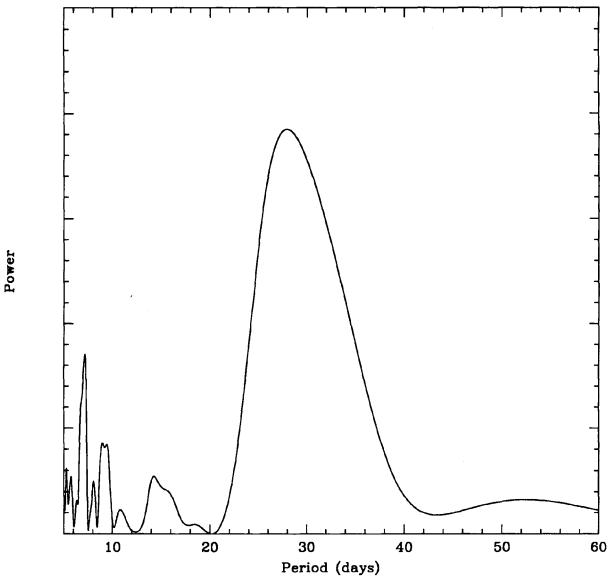

FIG. 5—The power in the "window function" for eight nights spread over three consecutive dark runs. The actual sequence of days used was 0, 4, 8, 29, 33, 36, 56, and 63. The power near 30 days is difficult to avoid if the dark time is required!

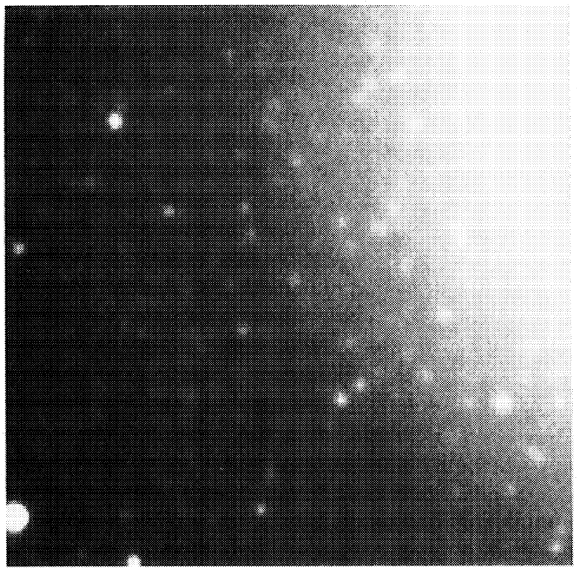

FIG. 6—CCD image of a 1-arcmin field near the center of NGC 3311, the central cD galaxy in Hydra I at a redshift $V_0 = 3400$ km s^{-1}. This image is a 7 × 1000-s exposure in B taken at the CTIO 4-m telescope. Even under average (1″) seeing conditions, large numbers of globular clusters are measurable.

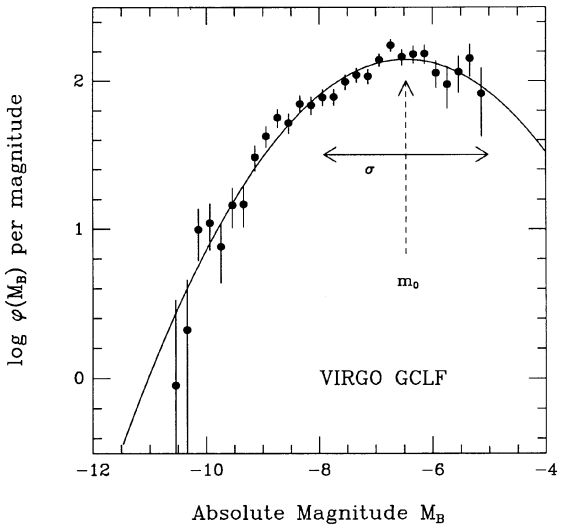

FIG. 7—The luminosity function for the globular clusters in four Virgo ellipticals combined (NGC 4365, 4472, 4486, 4649), from Harris et al. (1991). This composite GCLF was constructed from a total sample of about 2000 clusters brighter than $B = 26.2$ (the vertical scale units shown are arbitrary). Here ϕ is the relative number of clusters per unit magnitude interval, plotted against absolute magnitude M_B *assuming* d(Virgo) $\simeq 17$ Mpc. A Gaussian interpolation curve is superimposed, with a "turnover" or peak indicated by the dashed arrow (m_0), and a standard deviation $\sigma = 1.45$ mag.

(such as the Gaussian model above) to the observed data, or else by using a maximum-likelihood fit to the total observed LF (GCLF plus background), the curve parameters (A, m_0, σ) and their internal uncertainties can be estimated (van den Bergh et al. 1985; Pritchet and van den Bergh 1985b; Hanes and Whittaker 1987; Harris et al. 1991). Adopting an absolute magnitude M_0(turnover), and any necessary correction for foreground reddening, immediately yields the distance modulus.

If the limiting magnitude of the photometry goes clearly past the turnover as in the example of Fig. 7, both m_0 and σ can be solved for simultaneously. Ideally, the uncertainty $e(m_0)$ would be equal to $\sigma/\sqrt{N}$, which for a sample size N of several hundred or more clusters should be ± 0.1 mag or smaller. In practice, the extra noise introduced by the background LF subtraction and completeness corrections, and the uncertainty in σ itself, lead to best-case results near $e(m_0) \simeq \pm 0.2$ mag *for a single galaxy.* However, if the limit of the data falls at or a bit short of the turnover, then the fitted solutions for m_0 and σ become strongly correlated (Hanes and Whittaker 1987). It is still possible to estimate m_0 to a typical precision of ± 0.3 mag, but only by performing a restricted function fit with an assumed, externally known value of σ (hence the importance of the basic premise that the GCLF parameters are the same for galaxies of the same type; see Sec. 4.4). An alternative is to adopt the well-defined Virgo GCLF (Fig. 7) as a fiducial function and to match any other galaxy to it by adjusting its distance relative to Virgo until a best fit is achieved.

The range of applicability of the GCLF method, and its basic strengths, are readily summarized:

(1) The GCLF works by far the best in giant E galaxies, which contain the largest globular-cluster populations ($N \gtrsim 1000$ is observationally feasible in such galaxies). On the other hand, the GCLF method is immensely more difficult to employ in late-type galaxies (Sc, Sd, Irr), and so in most cases it is difficult to match the GCLF distance scale *directly* with any of the Population-I techniques.

(2) Because the clusters are nonvariable objects, they do not require repeated or carefully scheduled time-series observations. Telescope time is thus employed efficiently.

(3) Because it applies to objects in the halos of large galaxies, the method is free of a host of observational problems that affect all Population-I standard candles, such as internal reddening differences, crowding and source confusion, and inclination-angle corrections.

(4) The distance range of the primary GCLF method is set by the limiting magnitude at which the turnover M_0 is still detectable. With current ground-based capabilities, the limit should be near $d \simeq 50$ Mpc (Harris 1988a).

4.3 Physical Basis

So far, the motivation for the GCLF as a standard candle is almost totally empirical rather than theoretical. The astrophysical basis for its similarity from one galaxy to another is a challenging problem, and is probably less well understood than for any other standard candle currently in use. Because globular clusters are old-halo objects that probably predate the formation of most of the other stellar populations in galaxies (e.g., Harris 1986, 1988b, 1991; Fall and Rees 1988), to first order it is not surprising that they look far more similar from place to place than their

parent galaxies do. Methods for allowing clusters to form with average masses that are nearly independent of galaxy size or type have been put forward by Fall and Rees (1985, 1988), Larson (1988, 1990), Rosenblatt et al. (1988), and Ashman and Zepf (1992) under various initial assumptions. Other constraints arising from cluster metallicity distributions and the early chemical evolution of the galaxies are discussed by Lin and Murray (1991) and Brown et al. (1991). None of these yet serve as more than general guidelines for understanding why the early cluster-formation process should be so nearly invariant in the early universe.

After the initial formation epoch, dynamical effects on the clusters including tidal shocking and dynamical friction, and evaporation of stars driven by internal relaxation and the surrounding tidal field, must also affect the GCLF within a galaxy over many Gyr, and these mechanisms might well behave rather similarly in large galaxies of many different types. Recent models incorporating these effects (e.g., Aguilar et al. 1988; Lee and Ostriker 1987; Chernoff and Shapiro 1987; Allen and Richstone 1988) show that their importance decreases dramatically for distances $\gtrsim$2–3 kpc from the galaxy nucleus, and for the more massive, compact clusters like present-day globulars. In addition, recent photometry (Grillmair et al. 1986; Lauer and Kormendy 1986; Harris et al. 1991) extending in close to the centers of the Virgo ellipticals has shown no detectable GCLF differences with radius. The implication is therefore that today's GCLF resembles the original mass-formation spectrum of at least the brighter clusters, perhaps only slightly modified by dynamical processes. Many qualitative arguments can be constructed as to why the GCLFs should, or should not, resemble each other in different galaxies, but at the present time these must take a distant second place to the actual data.

4.4 Calibration

The calibration of the method reduces, in essence, to determining the absolute turnover magnitude M_0 and GCLF dispersion σ independently in as many galaxies as possible, with the Milky Way GCLF as the fundamental starting point. We do *not* suppose that either M_0 or σ are "universal" (identical) in all galaxies, although such assumptions were sometimes made of necessity in the earlier history of the subject. The basic requirement of the method is simply that the shape parameters (M_0, σ) must *behave regularly along the Hubble sequence of galaxies,* i.e., that they do not differ unpredictably between galaxies of the same type.

The full job of calibrating the GCLF self-consistently is not yet complete, though much recent progress has been made. For the GCLFs in giant ellipticals, the *dispersion* falls consistently in the range $\sigma \simeq 1.4 \pm 0.1$ mag (H. Harris et al. 1988b; Geisler and Forte 1990; Harris et al. 1991). For the Local Group galaxies (the Milky Way, M31, and the dwarf ellipticals), a smaller value $\sigma \simeq 1.2 \pm 0.2$ provides a better match, but the samples (particularly in M31) need to be improved and augmented further; see Harris (1991), Racine (1991), and Reed et al. (1992).

For the fundamental calibrating GCLF sample in the Milky Way, the turnover luminosity is at $M_B^0 = -6.8 \pm 0.17$. In M31, the turnover may be $\sim(0.2 \pm 0.2)$ mag more luminous, depending on the exact Local Group distance scale adopted and also on the still-uncertain degree of incompleteness in the faint half of the M31 halo-cluster sample (Racine 1991; Reed et al. 1992). Among four Virgo giant ellipticals including the high-specific-frequency M87 system (van den Bergh et al. 1985; Harris et al. 1991), the intrinsic differences in M_0 from galaxy to galaxy are ± 0.2 mag or less. A direct match between M_0 (spirals) and M_0 (ellipticals) has not yet been made, e.g., by comparing the GCLFs in elliptical and disk galaxies that are known beforehand to be in the same group and thus at the same distance from us to the necessary precision. However, on elementary external grounds, for any distance scale H_0 in the range $\simeq$50–100 km s^{-1} Mpc^{-1} the difference ΔM_0 between the Local Group Sb spirals and the Virgo giant E's must be less than half a magnitude (Harris 1987b, 1991). The essential argument is shown in Fig. 8, which contains the currently measured M_B^0 values for 13 galaxies of all types: four Local Group dwarfs, M31, and the Milky Way (Harris 1987b; Harris et al. 1991); two large ellipticals in the Leo group, NGC 3377 (Harris, 1990) and NGC 3379 (Pritchet and van den Bergh 1985b); NGC 1399 in the Fornax cluster (Geisler and Forte 1990; Bridges et al. 1991); and the four Virgo ellipticals mentioned above (van den Bergh et al. 1985; Harris et al. 1991). For the five giant E's, the values plotted in the figure *assume* Fornax and Virgo distances corresponding to $H_0 = 75$. The near constancy of the turnover magnitude over more than a factor of 4000 in parent-galaxy luminosity is remarkable; excluding the four dwarfs, the unweighted average from the nine remaining large galaxies is $\langle M_B^0 \rangle = -6.6$ with an rms scatter of ± 0.26 mag.

Refining the trend of M_0 with parent-galaxy type will require cluster photometry in several more galaxies with independently established distances (see below). The zero point of the GCLF luminosity scale depends *primarily* on the Population-II RR Lyr scale which sets the distances to the Milky Way globulars. It then depends *secondarily* on near-field extragalactic standard candles including Cepheid and RR Lyr variables (for M31).

4.5 Uncertainties

We now summarize the error budget in the GCLF method as it actually works. Consider an application in which the GCLFs for two or three giant ellipticals in the same cluster of galaxies have been measured. Thus if the uncertainty $e(m_0)$ averages ± 0.3 mag per galaxy, the individual values can be combined and the mean $\langle m_0 \rangle$ for the entire group obtained to $\lesssim \pm 0.2$ mag (see Harris et al. 1991). The resulting distance modulus will then have an *internal* uncertainty due to the measurement process made up of the following:

(i) ± 0.2 mag for $e(\langle m_0 \rangle)$ (note that for the Virgo

system which represents the current best case, $e(\langle m_0 \rangle)$ is $\lesssim 0.1$ mag);

(ii) ± 0.2 mag for the internal uncertainty in M_0, as established from the calibrating galaxies;

(iii) ± 0.05 mag (typically) in the photometric scale zero point; and

(iv) ± 0.05 mag for foreground absorption uncertainty (in most cases of interest, A_V is quite small since the program galaxies are at high latitude; for Virgo, the uncertainty would be about half this value).

Since these uncertainties are uncorrelated, they should be added in quadrature and the net internal uncertainty $e(m-M)_0$ for the system will be typically ± 0.3 mag.

There are also several potential sources of *external* error having to do with properties of the galaxies themselves: as usual, these are harder to quantify, but the known items include the following:

(1) The uncertainty in the fundamental RR Lyr luminosity scale. Although M_V(RR) is a continuing matter of debate, recent discussions, both observational and theoretical (e.g., Hesser et al. 1987; Jones et al. 1988; Fernley et al. 1990; Sandage and Cacciari 1990; Lee et al. 1990; Walker 1992), indicate $e(M_0) \simeq \pm 0.15$ mag from this source.

(2) The *systematic* mean difference ΔM_0 (turnover) between galaxies of different types, and most importantly between the Local Group spirals and the more distant large ellipticals. Calibrating this term thoroughly is the most urgent observational need at the present time for developing the GCLF technique. With additional measurements of M_0 in several more key galaxies (see below), it should be possible to reduce the error due to ΔM_0 to a level less than ~ 0.1 mag.

(3) The intrinsic *scatter* of M_0 about the mean relation of M_0 vs galaxy type. Again, this is not well known at present, but the existing comparisons within the Local Group and Virgo (Fig. 8) suggest $e(M_0) \simeq \pm 0.2$ mag from this source.

(4) Scatter due to metallicity differences between globular-cluster systems in different galaxies. The clusters in giant ellipticals have mean metallicities consistently near [Fe/H] $= -1.0$ (Mould et al. 1986; Mould et al. 1990b; Geisler and Forte 1990; Couture et al. 1990, 1991), whereas in the Milky Way and M31 the average extends down to [Fe/H] $\simeq -1.6$ depending on the region of the halo (Zinn 1985; Elson and Walterbos 1988). For the usual broadband indices, such metallicity differences translate into ~ 0.1 mag shifts in mean color, or in luminosity if the observations are done in bands such as B, which are metallicity sensitive (Wagner et al. 1991; Bridges et al. 1991; Couture et al. 1990).

(5) Systematic errors in fitting the fiducial GCLF curve to the observations, leading to an incorrect estimate of m_0. This error can arise in cases where the photometric limit of the observations is near or at the turnover, so that the curve fitting must be done after having corrected the data for image-detection incompleteness, internal photometric uncertainty, and background contamination, all of which are strong functions of magnitude near the photometric limit. Effects of increasing photometric uncertainty with magnitude tend to bias m_0 brightward, while the other effects may bias the result either positively or negatively. Biases in either direction may also occur (see above) if the wrong dispersion σ is used for the fitted curve. Although these errors seem to be no larger than the other items on this list, they have not yet been completely modeled in most real cases to date; for other related comments, see Hanes and Whittaker (1987), van den Bergh et al. (1985), and Harris et al. (1991). More powerful maximum-likelihood methods for matching the data to a model including all these effects *simultaneously* are being developed (Secker and Harris 1992) and will enable more nearly unbiased fits to be made.

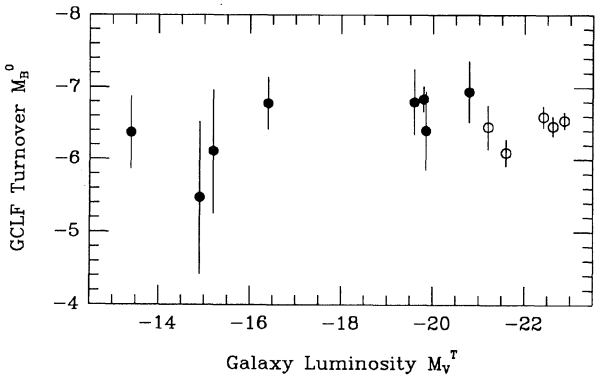

FIG. 8—Estimated turnover luminosities M_B^0 for 13 galaxies, plotted against total galaxy luminosity. The *filled circles* include six Local Group members (the Milky Way, M31, and the four dwarfs: NGC 147, 185, 205, and Fornax), plus the Leo ellipticals NGC 3377 and 3379, whose distance of $d = (10 \pm 1)$ Mpc is well established by the PN and SBF techniques (Ciardullo et al. 1989; Tonry et al. 1989). The *open circles* include four Virgo members (NGC 4365, 4472, 4486, 4649) and the central giant elliptical in the Fornax cluster, NGC 1399; note that for these, we *assume* $d = 17$ Mpc to derive the distances and turnover luminosities.

The total budget for the external errors, under the most pessimistic assumption that they are uncorrelated, is 0.27 mag. Combining this with the internal errors yields a total uncertainty for the method of 0.4 mag per galaxy.

As imaging capabilities continue to improve, other effects which are currently too small to be important may become noticeable. For example, over the past decade, technical improvements have pushed image quality to the point ($< 0''.4$) where globular clusters in galaxies as distant as Virgo can actually be resolved as nonstellar images. While this should not seriously affect the photometry when performing either point-spread function fitting or aperture photometry, it may also provide a means for better rejection of both field stars and background galaxies from the samples.

4.6 Future Needs and Directions

Aside from its presently incomplete calibration, the principal observational problem associated with the GCLF method is that it can be applied effectively only to giant ellipticals. This feature is perhaps best regarded as a limitation rather than a weakness, since the gE's are most often

found in the rich clusters that are the main landmarks in Hubble velocity space. But for any types of irregular and late-type spiral galaxies, it is unlikely that GCLFs will ever turn out to be useful standard candles.

On the theoretical side, prescriptions for future work are simple to state but quite challenging to execute. We need a theory of cluster formation specific enough to predict their complete mass spectrum and not just a mean globular-cluster size. Following this, the dynamical interaction of a system of clusters with its parent-galaxy environment needs to be modeled well enough to describe how the initial cluster-mass distribution evolved into what we see today. Matching the models to the observations for galaxies of widely different types can then begin in earnest.

On the observational side, the most pressing need is to calibrate GCLFs for selected *large* disk and elliptical galaxies which are close enough for the turnover to be clearly measured. The distances to these must, of course, be established independently. Requirements for the spirals are particularly stringent (they must be almost perfectly edge-on so that the halo clusters are clearly visible). For nearby giant Sa/Sb disk galaxies, especially important systems for which new GCLF data have been produced include NGC 4594 (Bridges and Hanes 1992), NGC 4565 (Harris et al. 1992), and M31 itself (Reed et al. 1992); other potentially valuable candidates are listed by H. Harris et al. (1988a). The edge-on S0 NGC 3115 will also be of interest, though it has a rather sparse cluster system. Well-situated, nearby large E galaxies are similarly scarce; the most interesting ones for extensive GCLF measurement may be NGC 3377 and 3379 in Leo (Pritchet and van den Bergh 1985b; Harris 1990), and NGC 4278 and 4494 in the Coma I group (Gregory and Thompson 1977). Adding these systems to the calibration should eventually lead to a fully self-consistent GCLF determination of the distances to Virgo and Fornax, the nearest rich galaxy clusters.

Once Virgo and Fornax are secured, the absolute distances to giant ellipticals in other systems at $V_0 \lesssim 4000$ km s^{-1} including Hydra I, Centaurus, Pegasus, and Perseus will then follow: these are close enough that the bright half of the GCLF is fully measurable (Harris 1988a), and thus can be fitted using the E-galaxy GCLF as a fiducial marker as described above. Finally, *HST* imaging with the WF/PCII camera has the capability to extend the reach of the GCLF technique by about 2 mag more. With it, photometry to the turnover level can be obtained out to the Coma cluster members (at $V_0 \sim 7000$ km s^{-1}) and slightly beyond.

There are also prospects for using the *bright end* of the GCLF as a secondary standard candle to continue much further out. The basis of the idea has been pointed out by Hanes and Whittaker (1987) and can be seen from Fig. 7. If the GCLF is already well populated, as it is in a typical giant elliptical, then $\phi(m)$ falls off so steeply at the bright end that further increases in the cluster population do not change the level of the brightest few clusters very much. When one images a distant galaxy, the effect is very much like that of the planetary-nebula LF technique: the globular clusters "switch on" rather suddenly as a critical magnitude level is reached. Near the top end ($M_V \simeq -10$), it may be shown easily that $\Delta M_V(n) \simeq 0.4 \Delta M_V^T$, where $M_V(n)$ is the mean luminosity of the brightest few clusters ($n \sim 10$–20) and M_V^T is the galaxy luminosity. The brightest ellipticals in clusters of galaxies have an intrinsic luminosity dispersion $\sigma(M_V^T) \simeq \pm 0.4$ mag (e.g., Sandage 1973b). Then, even if the cluster specific frequencies of giant E galaxies vary by factors of ~ 3 (Pritchet and Harris 1990), the parameter $M_V(n)$ may act as a standard candle to the ± 0.5 mag level of precision. With ground-based photometry and CCD imaging at half-arcsec quality now conventional at some sites, the brightest clusters will be detectable in giant E galaxies at $V_0(\mathrm{lim}) \simeq 12{,}000$ km s^{-1}. With the *HST*, the ultimate limits of the brightest-cluster technique should extend to about 7 mag more distant than the Virgo cluster, or a redshift $V_0 \simeq 35{,}000$ km s^{-1}. The method may then provide an interesting complement to the Tully–Fisher and D_n-σ techniques, which function over the same distance ranges.

5. NOVAE

5.1 Background

Novae possess a number of attributes that make them potentially valuable standard candles. They are luminous (approaching $M_V = -10$) and easy to recognize. Because they belong to an old stellar population, they are found predominantly in ellipticals and the bulges of spirals (Ciardullo et al. 1987); such environments are relatively dust-free and photometrically smooth, so that observations of novae beyond the Local Group are simpler and easier to interpret than observations of Cepheids. The available evidence suggests that observations of novae are not strongly affected by metallicity effects (van den Bergh and Pritchet 1986). Finally, the calibration of novae as standard candles possesses relatively low intrinsic scatter (van den Bergh and Pritchet 1986), and is well understood theoretically (Shara 1981a,b).

The first known observations of novae in external galaxies were made in the early years of the twentieth century (Ritchey 1917; Shapley 1917). As noted by van den Bergh (1988), these observations held the potential for resolving the fundamental distance-scale problems of that era, but failed to do so because of the confusion between novae and supernovae. The first systematic study of novae in an external galaxy was Hubble's (1929) survey of M31, a study that was greatly extended by Arp (1956); recent work on M31 has been summarized by Capaccioli et al. (1989). Other early observations of novae in Local Group galaxies are summarized by Pfau (1976). The first detection of novae beyond the Local Group was apparently by Hubble in the Virgo cluster elliptical M87 (Bowen 1952); Sandage (1987) has confirmed that Hubble's M87 nova candidates were probably real. More recent studies of novae in Virgo cluster ellipticals are by Pritchet and van den Bergh (1985a, 1987a). Sandage (1986) has also reported on observations of novae in the Sb spiral M81 made in the early 1950's.

All of the above observations of extragalactic novae were made in continuum blue light. More recently Ciardullo and collaborators have reported on Hα observations of novae in both M31 (Ciardullo et al. 1983, 1987, 1990a) and NGC 5128 (Ciardullo et al. 1990b). The relevance of Hα observations of novae to the extragalactic distance scale is discussed further in Sec. 5.6.

5.2 Method

The relationship between the maximum luminosity (magnitude) of a nova and its rate of decline (MMRD) is the usual starting point for deriving extragalactic distances. That luminous novae decay more rapidly than intrinsically faint novae was first noted by Zwicky (1936). The MMRD correlation for Galactic novae was confirmed and studied in more detail by McLaughlin (1945). Schmidt (1957), and Pfau (1976). The most complete recent study of the MMRD relation for Galactic novae is by Cohen and Rosenthal (1983) and Cohen (1985), who have derived expansion parallaxes for a number of (previously undetected) spatially resolved shells around old Galactic novae. The physical basis for the MMRD relation has been discussed by Hartwick and Hutchings (1978) and Shara (1981a,b) and is reviewed by Shara (1989). These authors show that more massive white dwarfs require less accreted matter to produce a thermonuclear runaway, and these lower-mass envelopes can be ejected more rapidly; thus the most luminous novae are also the fastest.

To measure the distance to an external galaxy using the MMRD relation, it is necessary to determine the apparent magnitudes of novae at maximum light, and a mean rate of decline over 2 mag. At present the calibration of the MMRD relation is in the B or m_{pg} bands (see below), so that observations through these bandpasses are preferred. It is essential that the observations sample the light curves of novae frequently enough near maximum light that m^{max} can be estimated for the fastest (i.e., brightest) novae. The signal-to-noise ratio of the photometry should be high enough that novae discovered near maximum light can be followed at least 2 mag below this level.

5.3 Calibration

The calibration can be effected in two ways: (1) using Galactic novae (in which case the use of the MMRD relation is a *primary distance indicator*, calibrated using geometrical techniques); or (2) using novae in M31 (in which case the distance scale is tied to the distance of M31).

The Cohen (1985) MMRD relation for Galactic novae is given by

$$M_V^{max} = -9.96 - 2.31 \log \dot{m}, \qquad (7)$$

where $\dot{m}$ is the mean rate of decline (in mag d^{-1}) over the first 2 mag. The mean scatter around this relation is ± 0.52 mag (1σ) for the high-quality subset of Cohen's data. The data and fit are shown in Fig. 9. A slightly different result is obtained if the Galactic data are corrected for the constancy of M_B 15 days after maximum light (Buscombe and de Vaucouleurs 1955). In principle, such a correction removes systematic errors in the absolute magnitudes, and results in a tighter MMRD correlation ($\sigma \simeq 0.47$ mag for *all* objects).

An alternate calibration of the MMRD relation is obtained by studying novae in the nearby spiral galaxy M31. The properties of the nova system in M31 have been reviewed by Ciardullo et al. (1987) and Capaccioli et al. (1989). Only about 1/3 of the known novae in M31 have sufficient information in their light curves to be useful in determining the MMRD relation, and only about 1/4 of these possess good-quality light curves with a well-observed maximum and rate of decay. The M31 MMRD relation is shown in Fig. 10. The 1σ scatter around the mean relation depends on the subset of data chosen, and is in the range 0.20–0.28 mag (cf. Capaccioli et al. 1989; van den Bergh and Pritchet 1986).

To compare the M31 MMRD data with the mean Galactic MMRD, we assume $(m-M)_B \simeq 24.6$ for M31 (e.g., Pritchet and van den Bergh 1987b and references therein), $(B-V)^{max} \simeq 0.23$ (van den Bergh and Younger 1987), and $(m_{pg}-B) \simeq -0.17$ (Arp 1956). With these assumptions, it can be seen from Fig. 10 that the agreement between the Galactic and M31 MMRD relations is not good: the flattening observed in the M31 MMRD relation for bright and faint novae is not seen for Galactic novae. In addition, there appears to be a systematic offset of about 0.3 mag between the two MMRD relations, in the sense that Galactic novae are *fainter* than M31 novae. [This offset would increase to ~ 0.5 mag if the mean *internal* absorption for M31 novae were 0.2 mag (van den Bergh 1977; Capaccioli et al. 1989). However, we note that Ford and Ciardullo (1988) have failed to find any systematic difference in the MMRD relation for novae close to and far from obvious dust patches in the bulge of M31.]

What could cause these differences between the Galactic and M31 MMRD relations? The flattening at faint magnitudes in the M31 MMRD relation may be due to Malmquist bias: in the presence of a magnitude limit, only the brightest novae will be detected. Whether or not this flattening is real has little effect on distance determinations outside the Local Group, because it is predominantly the most luminous novae that are detected at large distances. The flattening of the M31 MMRD relation for *luminous* novae is a more difficult problem. If one aligns the MMRD relations for Galactic and M31 novae in the "linear" ($-1.3 \lesssim \log \dot{m} \lesssim -0.7$) regime, then the luminous ($\log \dot{m} \gtrsim -0.6$) Galactic novae lie an average of ~ 0.8 mag above the M31 MMRD relation. One possible explanation for this is that maximum light for M31 novae is not as well sampled as it is for Galactic novae; this is particularly apparent in the light curves of Arp 1 and Arp 2 (Arp 1956).

The shift of the Galactic and M31 MMRD relations relative to each other seems to imply that the true distance modulus of M31 is 0.3 mag less than the value obtained with "quality" distance indicators (e.g., RR Lyr stars, IR observations of Cepheids). However, Capaccioli et al. (1989) have demonstrated that this discrepancy vanishes if a different sample of objects is chosen to define the Galactic

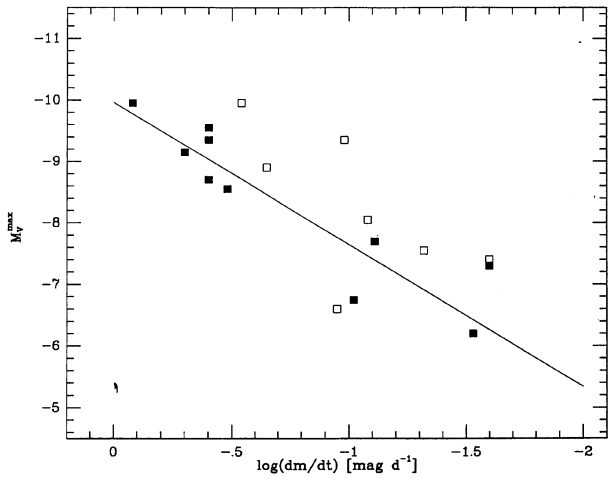

FIG. 9—Maximum magnitude–rate of decline relation for Galactic novae observed by Cohen (1985). Closed symbols represent the novae designated "high quality" by Cohen; the solid line [Eq. (7)] is a least-squares fit to the high-quality data.

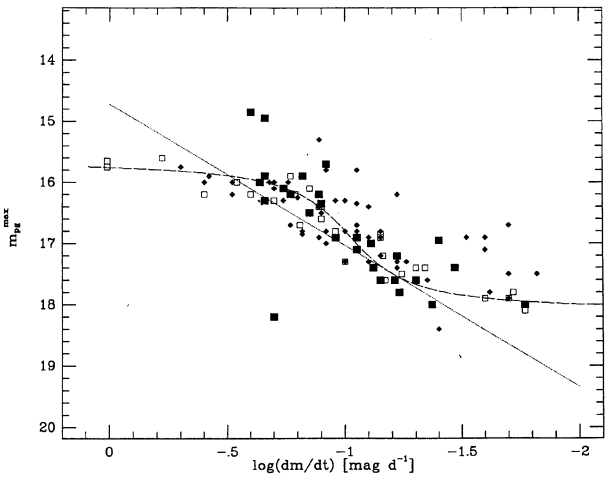

FIG. 10—Maximum magnitude–rate of decline relation for novae in M31. The data (from several sources) has been taken from Table VI of Capaccioli et al. (1989). *Solid squares:* high-quality data; *open squares:* medium-quality data; *dots:* low-quality data. The solid line represents the Galactic calibration (Fig. 9), shifted by $(m-M)_B=24.6$, and transformed to the m_{pg} system as described in the text. The dashed line represents the Capaccioli et al. analytical fit to the M31 data.

MMRD, and if uncorrected M_V^{max} values are used for the Galactic nova sample (instead of M_V values corrected for the Buscombe–de Vaucouleurs effect). It is also worth noting that the theoretical MMRD (Shara 1981b) possesses a flatter slope than that observed for Cohen's (1985) data on Galactic novae, and hence provides a better overall fit to the S-shaped MMRD relation observed for M31 novae.

Finally, it should be noted that the Galactic MMRD relation is defined with far fewer objects than is the case for M31; furthermore, the overall quality of the Galactic data (as demonstrated by the scatter in the MMRD relation) is considerably lower than for M31, probably due to such effects as uncertain Galactic absorption, and due to the assumption of spherical symmetry that is inherent in Cohen's application of the expansion parallax technique (Ford and Ciardullo 1988). In fact, the offset between the Galactic and M31 MMRD relations is almost exactly what would be expected if the prolate geometry of nova shells is not taken into account when applying the expansion parallax technique (Ford and Ciardullo 1988).

In view of all of the above, it seems somewhat safer to employ the M31 MMRD relation as the calibrator for the extragalactic distance scale. This makes the distance scale dependent on an assumed distance to M31. However, Pritchet and van den Bergh (1987b) and van den Bergh (1989) show that there is concordance in most distance estimates for M31 (except those derived using novae!); using the M31 calibration is therefore a more prudent approach at the present time.

5.4 Uncertainties

Existing problems with calibrating the MMRD relation in M31 have already been discussed above. The role of internal absorption in the M31 MMRD is probably small; more serious is the calibration uncertainty for the brightest M31 novae (has maximum light been observed?), and the inconsistency between Galactic and M31 MMRD relations (is it due to shell geometry?).

An additional problem is the existence of so-called "anomalous" novae. These novae, which represent roughly 10% of all novae in M31, are unusually bright or faint for their observed decay rate $\dot{m}$. At least one faint nova (Arp 4) was unusually red and hence probably heavily obscured (Arp 1956). However, most anomalous novae in M31 are $\gtrsim 1$ mag *brighter* than other novae with the same $\dot{m}$; nova 2 in the west field of the Virgo cluster elliptical NGC 4472 (Pritchet and van den Bergh 1987a) and Nova LMC 1991 (Della Valle 1991) may also be examples of such novae. Anomalous novae stand out clearly in the M31 MMRD relation (because of the small scatter in this relation), and hence can be ignored. But for Virgo cluster galaxies, the existence of anomalously bright novae has the potential to strongly bias distance determinations for at least two reasons: (1) Data on novae in the Virgo cluster are affected by an apparent magnitude cutoff, so that only the brightest novae are observed. (2) m_{max} and $\dot{m}$ are not well determined for novae at the distance of the Virgo cluster; anomalous novae may be confused with normal novae because of scatter in the MMRD relation. Luminous variable objects of unknown type, such as the red "nova-like" variable discovered by Mould et al. (1990a) in the bulge of M31, may also be confused with normal novae in MMRD diagrams of distant galaxies.

An even more severe (logistical) problem is that of scheduling observations. Because bright novae are so fast, repeated observations are required each night to estimate m_{max} and $\dot{m}$. But the nova rate per CCD field is only $\sim$0.1–0.2 d^{-1} for typical Virgo cluster ellipticals (Pritchet and

van den Bergh 1987a), and lower than this for the brightest novae—i.e., the yield per night of observing is low. The need for large amounts of observing time on 4-m-class (or larger) telescopes to observe novae in the Virgo cluster means that the observations of Pritchet and van den Bergh (1987a) are unlikely to be repeated in the near future.

For fainter, slower novae (say $M_B^{\max} \gtrsim -8.5$, $\dot{m} \lesssim 0.2$ mag d^{-1}), observations spaced one night apart suffice, so that a number of galaxies can be observed on a single night; observing faint novae also avoids uncertainties in the calibration of the bright end of the MMRD relation. But a nova with $M_B^{\max} \simeq -8.5$ in the Virgo cluster ($m-M \approx 31.5$) reaches $B \simeq +23$ at maximum light; novae much fainter than this cannot be followed the requisite 2 mag of fading, because of the bright background against which they are observed.

Nova light curves show a wealth of detail, and few if any are characterized by a simple linear decrease in magnitude. This irregularity poses several problems. Novae frequently have secondary outbursts; such outbursts can be confused with primary maxima if only a limited time series of observations is available (as is the case for most observations of distant novae). Unusual objects [such as the Mould et al. (1990a) object] might be flagged with an extensive time series of data; but with limited observations, such phenomena may be misidentified as normal novae.

To illustrate the *internal* errors that result in using novae to determine the distance scale, we take the specific case of the determination of the distance modulus of the Virgo cluster (Pritchet and van den Bergh 1987a) as an example:

(i) Photometric errors: typically ± 0.05 to ± 0.10 mag, (3.6-m telescope, 0.9 arcsec seeing, 1-h exposures).

(ii) Errors in the determination of $\dot{m}$: generally less than 10%, resulting in errors in distance modulus less than 0.1 mag.

(iii) Errors due to missed maximum light: A correction is made to remove the systematic bias resulting from missing maximum light. This correction is typically in error by ± 0.05 to ± 0.5 mag, depending on the speed of the nova.

(iv) Errors in absorption towards Virgo: ± 0.04 mag (blue light) is assumed throughout this entire review.

(v) Errors in d(M31): ± 0.1 mag assumed throughout this article.

The most important *external* error is the bias that is introduced because of the way in which the Virgo cluster light curves are sampled (compared with the M31 light curves). This bias has been estimated by Pritchet and van den Bergh (1987a) to be about 0.2 ± 0.1 mag on the basis of extensive Monte Carlo simulations.

It is difficult to know how to combine the above errors into a meaningful total error, since some of the errors are rms deviations, whereas others are "estimated" peak-to-peak errors. A reasonably conservative total uncertainty appears to be ± 0.4 mag (cf. Pritchet and van den Bergh 1987a).

5.5 Other Distance Indicators using Novae

Several other methods for using novae as distance indicators have been proposed in the literature. Here we give a brief discussion of some of these methods and their limitations.

$\langle M_{15} \rangle$: Buscombe and de Vaucouleurs (1955) first showed that the mean magnitude of an ensemble of novae 15 days after maximum light was a constant; from the most recent data on Galactic novae, Cohen (1985) has shown that $\langle M_{15} \rangle \simeq -5.60 \pm 0.14$, where the quoted error is the 1σ error in the mean. The rough constancy of $\langle M_{15} \rangle$ is a consequence of the MMRD relation, and has been explained theoretically by Shara (1981a). For Virgo cluster novae, $\langle B_{15} \rangle \approx +26$ if $(m-M) = 31.5$; hence the $\langle M_{15} \rangle$ distance indicator will be strongly affected by Malmquist bias at the distance of the Virgo cluster unless the observational completeness limit goes somewhat fainter than $B > 26$. Note that there are exceptional objects (e.g. M31 novae Arp 1, 2, and 3) that suggest this method be used with caution.

Luminosity Function of Novae: The luminosity function of novae at maximum light is approximately Gaussian in the data of Rosino (1973); de Vaucouleurs (1978) used the mean magnitude of this Gaussian to determine the distance to M31. More recently, Pritchet and van den Bergh (1987a) used this technique to determine the distance to the Virgo cluster, and obtained a result that was consistent with the MMRD relation. The most recent compilation of M31 nova data by Capaccioli et al. (1989) appears to show a double-peaked luminosity function; Capaccioli et al. use the magnitude of the *minimum* between the two peaks as a distance indicator. Yet another method is to use the *integral* luminosity function of novae at maximum light; this function is linear over a wide range of magnitude, and possesses a well-defined intercept (van den Bergh and Pritchet 1986).

The use of the luminosity function of novae at maximum light as a distance indicator demands large samples of novae that are essentially complete at the faintest magnitudes; it is therefore unlikely that this method will be useful for any but the nearest *luminous* galaxies (i.e., those with high nova rates). The Capaccioli et al. (1989) technique of using the dip between two peaks in the luminosity function is not completely reliable, because, as Capaccioli et al. demonstrate, different samples of M31 novae have luminosity functions with very different structure. (The very existence of this dip is in some question—cf. Rosino 1973; Capaccioli et al. 1989.)

Finally, it should be mentioned that the luminosity function of *all* M31 nova observations (i.e., random phases) possesses no useful information that can be used in determining extragalactic distances (van den Bergh and Pritchet 1986; Ford and Ciardullo 1988).

Period of Visibility: van den Bergh and Pritchet (1986) show that there exists a strong correlation between the mean period of visibility of novae (down to some limiting magnitude $m_{\rm lim}$), and the absolute magnitude that this $m_{\rm lim}$ corresponds to. Application of this correlation (calibrated

using M31 data) to the Virgo elliptical observations of Pritchet and van den Bergh (1987a) yields a distance modulus that is similar to that obtained using the MMRD relation. This method needs complete samples of novae down to some chosen $m_{\rm lim}$, but the samples do not have to be large. (With a large sample of novae, it would in principle be possible to apply this technique at several different $m_{\rm lim}$ values.)

5.6 Future Needs and Directions

There are a number of uncertainties in the MMRD calibration of novae, most of which have been discussed in Secs. 5.2 and 5.4. Although none of these uncertainties is debilitating, all must be addressed in future efforts to improve the nova distance scale. We describe two large projects below that would improve the calibration of the MMRD relation for distance scale work.

Galactic Calibration: The systematic difference between the Galactic and M31 MMRD relations needs to be understood better. Following Ford and Ciardullo's (1988) suggestion, it would be extremely helpful to have a new Galactic calibration based solely on novae whose shell geometry is well determined.

M31 Calibration: Problems with the existing M31 nova database include possible transformation errors from one set of observations to another, systematic photometric errors for novae observed photographically against the bright M31 bulge, sensitivity to reddening, and poor temporal sampling of nova light curves. A new CCD survey of the M31 bulge would solve many of these problems. Using the *I* bandpass would allow observing at all lunar phases (thus improving the continuity of the observations), and would lower the effect of internal reddening in M31 (if any). It is also possible that the effect of the "reddening pulse" near maximum light (van den Bergh and Younger 1987) may be smaller at longer wavelengths. The use of a detector with linear response would provide an effective means of standardizing the observations to a common photometric system, and removing the effects of the strongly varying background of the M31 bulge. If two 0.5–1.0-m telescopes (separated by $\sim 180°$ in longitude) were used, high-quality data on a number of novae could be obtained in only 2–3 years. The only problem with using longer-wavelength (*I*) data for the calibrations is that the contrast of novae against an underlying old (red) population would be decreased; this could be critical for observations of more distant galaxies. However, this decrease in contrast would be offset by the higher rate of detected photons in the red, and possibly by the use of active optics techniques (for galaxies beyond the Local Group).

Clearly nova surveys are feasible in a number of galaxies beyond the Local Group using large-format CCDs. Such surveys would be particularly valuable to tie the Cepheid distance scale to that of novae, and to add more calibrators to the Tully–Fisher relation. Certainly the M81 group is within reach, and, in subarcsec seeing, galaxies in the Leo Group may also be observable. Since the nova rate in ellipticals and spiral bulges appears to be substantially higher than in disks (Ciardullo et al. 1987), it follows that surveys in galaxies of morphological-type Sb and earlier would be most productive.

As pointed out by Ciardullo and collaborators (Ciardullo et al. 1983; Ciardullo et al. 1987; Ciardullo et al. 1990 a,b), there are several strong arguments for observing extragalactic novae in the light of Hα. This emission line remains bright for a much longer time than does continuum emission (e.g., Fig. 1 of Ciardullo et al. 1990a), and the contrast of a nova against the underlying background light is excellent when observed through a narrowband filter. Unfortunately, the available evidence (Ciardullo et al. 1990a) suggests that there is no correlation between the rate of decline and maximum brightness in Hα light. However, Ciardullo et al. have discussed how the rate of fading of intrinsically faint novae may still be obtained from "surrogate" Hα observations, because the late stages of nova light curves have similar rates of decline in *B* and Hα.

An alternate technique for using Hα observations in distance scale work involves the measurement of the nova rate (normalized per unit luminosity). Ciardullo et al. (1990b) argue that this quantity may be constant over a wide range of galaxy types, provided that the luminosity of the *old* stellar component is used to normalize the nova rate. From Figs. 2 and 3 of Ciardullo et al. (1990a), it is apparent that most novae in M31 remain brighter than $M_{\rm H\alpha} = -6.5$ for at least 15 days. It follows that, if observations of a galaxy were obtained more frequently than every 15 days, and if the limiting magnitude of the observations were deep enough to reach $M_{\rm H\alpha} = -6.5$, then the measured nova rate would sample all novae, and hence would be proportional to the old star luminosity of the region observed. A distance modulus could therefore be derived based solely on counting statistics, and the precision of the result would improve over the years as additional novae are observed. Calculations show that observations of almost complete samples of novae in the Virgo cluster are feasible in the 0.″5–0.″6 seeing conditions that are not uncommon on Mauna Kea. For this technique to be applied, more Hα data on M31 novae would be required—both to improve our estimate of the M31 nova rate per unit luminosity (upon which the distance determinations rest), and also to calibrate the optimal temporal spacing more accurately. Such a survey is well within the reach of a small telescope.

6. TYPE-Ia SUPERNOVAE

6.1 Background and Dispersion in Absolute Magnitude

Supernovae, as extremely luminous ($M_B \sim -19.5$) point sources, offer an attractive route to extragalactic distances. In this review the emphasis will be on supernovae of type Ia (SNe Ia). Type-II supernovae have a wide range in peak absolute magnitude and cannot be treated as standard candles. Distances to individual SNe II can be estimated by means of the expanding photosphere (Baade–Wesselink) and the expanding radiosphere methods, but only elementary applications based on simplifying assump-

tions have been made to SNe II beyond the Local Group (Kirshner and Kwan 1974; Branch et al. 1981; Bartel 1991). For applications of the method to SN 1987A in the Large Magellanic Cloud, based on detailed calculations, see Chilikuri and Wagoner (1988), Eastman and Kirshner (1989), Schmutz et al. (1990), and Höflich (1991). Supernovae of type Ib, type Ic, or type II-L may turn out to be good standard candles but the present samples are small and all three subtypes have the disadvantage of being less luminous than type Ia.

Supernovae of type Ia lack hydrogen lines and helium lines in their optical spectra; during the first month after maximum light they do have a strong absorption feature produced by the red doublet (λ6347, λ6371 Å) of singly ionized silicon. For a review of the spectral classification of supernovae see Harkness and Wheeler (1990). For the purposes of this review, we adopt the model that type-Ia supernovae are the result of the nuclear detonation of a white dwarf which is at or near the Chandrasekhar mass limit (see Sec. 6.2). Since such stars are present in the old stellar populations of all galaxies (but see Foss et al. 1991), there is good reason to believe that type-Ia supernovae behave as standard candles.

Numerous analyses of unrestricted samples of SNe Ia, involving various assumptions about relative distances and interstellar extinction, have produced values of the dispersion in peak M_{pg} or M_B that are generally consistent with the early results of Kowal (1968), who determined $\sigma=0.6$ mag. Smaller dispersions of 0.3–0.5 mag have been obtained by restricting the SN Ia samples to those beyond the Local Supercluster (Branch and Bettis 1978), in elliptical galaxies (Branch and Bettis 1978; Tammann 1978; Cadonau et al. 1985), in the Virgo cluster (Tammann 1978, 1988; Capaccioli et al. 1990), and in the Coma cluster (Barbon 1978; Capaccioli et al. 1990). The restriction to remote samples lowers the dispersion by a combination of two effects: (1) the avoidance of the problem of uncertain relative distances for the nearby galaxies, and (2) the tendency to select against SNe Ia that are observationally subluminous (whether they are intrinsically subluminous or are highly extinguished).

Several attempts have been made to divide SNe Ia (actually SNe I, prior to the recognition of SN Ib and SN Ic as separate subtypes in the 1980s) into photometric subclasses that may have different luminosities. Barbon et al. (1973) split SNe I into those having "fast" and "slow" light curves and saw some evidence that the fast events might be more luminous than the slow ones, but Barbon et al. (1975) found no significant brightness difference. Rust (1974) classified SNe I according to the rate of light-curve decline and found a correlation with brightness (see also de Vaucouleurs and Pence 1976). Pskovskii (1977, 1984) classified SNe I according to the immediate post-peak decay rate and found a similar correlation (see also Branch 1981, 1982).

The most recent studies, based on larger supernova samples and incorporating models for the retarded expansion of the local supercluster (Virgocentric flow), point to a low intrinsic dispersion in the peak brightness of SNe Ia that leaves little room for correlations with the light-curve decay rate. Leibundgut and Tammann (1990) review the data on SNe Ia in the Virgo cluster and find that when the sample is restricted to six SNe Ia for which photoelectric B photometry is available, the dispersion in M_B is only 0.18 mag, even with no extinction corrections; a larger dispersion of 0.41 mag in M_{pg} for seven Virgo SNe Ia is attributed to the poorer quality of the photographic photometry, but could be due, in part, to the intrinsic depth of the cluster. Leibundgut and Tammann conclude that the intrinsic scatter among Virgo SNe Ia could be vanishingly small. Tammann and Leibundgut (1990) find an observational dispersion of 0.53 mag in M_B for 35 SNe Ia that occurred in non-Virgo galaxies having recession velocities greater than 1000 km s^{-1} after correction according to Kraan-Korteweg's (1986) model of the retarded expansion of the local supercluster. An allowance for errors in the distances reduces the dispersion in M_B to 0.32 mag. Tammann and Leibundgut argue that errors in peak apparent magnitudes and the neglect of parent-galaxy extinction are responsible for a scatter of at least 0.2 mag, and conclude that the intrinsic SN Ia dispersion is $\lesssim$0.25 mag.

Miller and Branch (1990) take SN Ia apparent magnitudes (B or m_{pg}) from the *Asiago Supernova Catalog* (Barbon et al. 1989) and galaxy distances from the *Nearby Galaxies Catalog* (Tully 1988a) and find $\sigma=0.70$ mag for an unrestricted sample of 45 SNe Ia. For a sample of nine SNe Ia in elliptical galaxies the dispersion reduces to 0.32 mag. The dispersion in the unrestricted sample is strongly affected by six observationally subluminous SNe Ia, all of which turn out to have appeared in inclined disk galaxies (S or S0 galaxies having $i>50$). This suggests that the observationally subluminous SNe Ia are intrinsically normal but highly extinguished, as argued previously by Tammann (1982) on the basis of supernova colors. Miller and Branch find that by adopting a simple single-parameter thin-disk model for the extinction layer in the parent galaxies the dispersion for SNe Ia in disk and elliptical galaxies can be reduced to 0.27 mag. The SNe Ia absolute magnitudes, both before and after the parent-galaxy extinction procedure is applied, fail to correlate with Pskovskii's light-curve decline rates. Miller and Branch (1992) calculate the SN Ia dispersion not only on the basis of a Virgocentric flow model but also for a Great Attractor model (Burstein 1990) and an *IRAS* cluster model (Rowan-Robinson et al. 1990); for all three models the dispersion is about 0.3 mag.

The implication of the recent work cited above is that the intrinsic dispersion among SNe Ia is too small to be measured by the available data. Other evidence that supports or at least is consistent with a small ($\lesssim$0.5 mag) dispersion can be cited:

(1) Hamuy et al. (1991) present definitive photometry of two SNe Ia in the same galaxy, 1980N and 1981D in NGC 1316 (Fornax A), and find that the maximum-light magnitudes were the same to within 0.1 mag.

(2) SNe Ia show a small dispersion among the almost extinction-free infrared absolute magnitudes (Elias et al. 1981, 1985; Leibundgut 1988).

Direct or indirect evidence for a larger dispersion, on the other hand, is weak.

(1) Not only has the evidence for a correlation between brightness and light-curve speed deteriorated, but even the question of whether there *is* a significant range in the shapes of the light curves of ordinary SNe Ia is disputed (Younger and van den Bergh 1985; Cadonau et al. 1985; Leibundgut 1988; Filippenko 1989). Three relatively recent SNe Ia, SN 1986G (Frogel et al. 1987; Phillips et al. 1987; Leibundgut 1988; Christiani et al. 1992), SN 1991T (Filippenko et al. 1992a; Ruiz-Lapuente et al. 1992; Phillips et al. 1992; Jeffery et al. 1992), and SN 1991bg (Filippenko et al. 1992b) do appear to have had somewhat peculiar light curves, but all three definitely had peculiar spectra. Owing to uncertainties in extinction and distances, it is not clear that the absolute magnitudes of SNe 1986G and 1991T were unusual, but SN 1991bg occurred in the Virgo cluster and was subluminous by 3 mag in the B band. SN 1991bg demonstrates that spectroscopically peculiar SNe Ia must not be included in "standard-candle" samples.

(2) An intrinsic dispersion in a *spectroscopic* property—the blueshift of the red Si II absorption feature at and shortly after maximum light—has been demonstrated (Branch et al. 1988). This establishes that there are real differences (or asymmetries) in the outermost ejected layers of SNe Ia, but these could prove to be compatible with a uniform peak luminosity.

In summary, current evidence favors a small intrinsic dispersion for ordinary SNe Ia that may be $\lesssim 0.3$ mag. Most SNe Ia that are observationally subluminous tend to be red *and* in inclined disk galaxies, and probably just suffer high interstellar extinction. The peculiar, intrinsically subluminous SN 1991bg also was red. If observationally faint events enter into samples of remote SNe Ia, in spite of the selection against them, they can be recognized by their colors, and, in the case of those that are intrinsically abnormal, by their spectra. There is not yet any solid evidence for anomalously *bright* SNe Ia.

From the Hubble diagram for their sample of 35 SNe Ia, Tammann and Leibundgut (1990) infer

$$M_B = -18.13 \pm 0.08 + 5 \log h, \quad (8)$$

where h is the Hubble constant in units of 100 km s^{-1} Mpc^{-1}. From a sample of 40 SNe Ia, Miller and Branch (1990) find

$$M_B = -18.36 \pm 0.04 + 5 \log h. \quad (9)$$

The difference is primarily due to the fact that Tammann and Leibundgut do not apply any corrections for parent-galaxy extinction, while Miller and Branch do apply an inclination-dependent correction to those SNe Ia in spirals that appear to be subluminous. Perhaps the most accurate available estimate for the intrinsic absolute magnitude is that obtained by Miller and Branch for nine SNe Ia in ellipticals:

$$M_B = -18.33 \pm 0.11 + 5 \log h. \quad (10)$$

To find the value of the Hubble constant from SNe Ia, we need to make a velocity-independent determination of the intrinsic absolute magnitude of at least one SN Ia for insertion into Eq. (10).

6.2 Physical Basis and Self-Calibration

The standard model for a type-Ia supernova is the thermonuclear disruption of a carbon-oxygen white dwarf that has accreted enough mass from a companion star to approach the Chandrasekhar mass (Woosley and Weaver 1986; Wheeler and Harkness 1990 and references therein). The nuclear energy released in the explosion unbinds the white dwarf and provides the kinetic energy of the ejected matter, but adiabatic expansion quickly degrades the initial internal energy and the observable light curve is powered by delayed energy input from the radioactive decay of ^{56}Ni and ^{56}Co. This model brings with it a self-calibration of the peak luminosity. Arnett (1982a) predicted on the basis of an analytical model that the SN Ia peak luminosity would be equal to the instantaneous decay luminosity of the nickel and cobalt, in which case the peak luminosity follows directly from the ejected nickel mass and the rise time to maximum light. The rise time can be inferred from observation but owing to uncertainties in the physics of the nuclear burning front (e.g., Woosley 1990) the amount of synthesized and ejected ^{56}Ni cannot yet be accurately predicted by theory. Sutherland and Wheeler (1984) and Arnett et al. (1985) outlined how the nickel mass can be estimated indirectly from spectra and light curves. The more nuclear burning, the more ^{56}Ni and kinetic energy, and the greater the blueshifts in the spectrum and the faster the decay of the light curve. Arnett et al. (1985) argued from the blueshifts in the spectra that the nickel mass must be in the range 0.4–1.4 $M_\odot$ and favored a value of 0.6 $M_\odot$ (as in the particular carbon deflagration model W7 of Nomoto et al. 1984). Adopting a rise time to maximum of 17 ± 3 days and distributing the luminosity according to the observed ultraviolet-deficient flux distribution of SNe Ia, Arnett et al. estimated $M_B = -19.5^{+0.4}_{-0.9}$) at bolometric maximum, which corresponds to $M_B = -19.6$ with limits of -19.2 and -20.5 at the time of maximum blue light a few days earlier.

Harkness (1990) finds that LTE synthetic spectra for carbon-deflagration models are very sensitive to the amount (and location in mass coordinate) of the ^{56}Ni in the ejecta; other models do not fit the observed spectra nearly as well as model W7 of Nomoto et al. (1984). He concludes that a nickel mass of 0.6 $M_\odot$ may be optimum and that the upper limit is 0.8 $M_\odot$. From computed light curves for carbon-deflagration models, Woosley (1990) favors 0.8 or 0.9 $M_\odot$ with a lower limit of 0.4 or 0.5 $M_\odot$. If we accept 0.6 ± 0.2 $M_\odot$ as the best present estimate, then following Arnett et al. we have $M_B = -19.6 \pm 0.5$. The recent discovery of SN 1990N 17 ± 1 days before maximum light (Leibundgut et al. 1991) raises the possibility that the rise time is longer than 17 days. If the characteristic rise time should prove to be 20 days, for example, then the peak luminosity would be lowered by 0.16 mag.

Very recent investigations of the ejected nickel mass and the peak absolute magnitude, on the basis of the standard

SN Ia model, are in good mutual agreement. Using an extension of the approach of Arnett et al. (1985), Branch (1992) finds an ejected nickel mass of 0.6 $(+0.2, -0.1)$ $M_\odot$ and $M_B = -19.44 \pm 35$, Leibundgut and Pinto (1992) calculate the theoretical light curve of model W7 over the interval 60–130 days after explosion and use the observed SN Ia light curve to find a peak $M_B = -19.6$, and Ruiz-Lapuente et al. (1992) fit theoretical spectra to a 245-day observed spectrum of SN 1972E to find a nickel mass of 0.5–0.6 $M_\odot$. Ruiz-Lapuente et al. also find 0.4 $M_\odot$ for the peculiar and possibly subluminous SN 1986G.

6.3 Other Calibrations

6.3.1 Historical Galactic Supernovae

Early attempts to use the historical galactic supernovae to calibrate SNe Ia were based on Tycho's supernova of 1572 (van den Bergh 1970; de Vaucouleurs 1985). Recent improved estimates of distances to the remnants of historical supernovae (Strom 1988) imply, however, that SN 1572 ($M_B = -18.0$) was significantly less luminous than SN 1006 ($M_B = -20.0$) and Kepler's supernova of 1604 ($M_B = -19.7$), which has led Green (1986) and Strom (1988) to suggest that SN 1572 may have been a type Ib. In any case, SN 1572 should not be used to calibrate SNe Ia, which are the brightest supernovae. Distances from Strom, apparent magnitudes from Clark and Stephenson (1977, 1982), and extinction estimates from various sources lead to a mean absolute magnitude for SNe 1604, 1006, and the (extremely uncertain) SN 185 ($M_B = -20.2$) of $M_B = -20.0 \pm 0.5$. It seems likely that the remnant distance scale will decrease, because currently favored distances such as Strom's lead to a surprisingly high local supernova frequency that could be reduced by *increasing* the remnant distances (van den Bergh and Tammann 1991).

6.3.2 Nearby Extragalactic SNe Ia

Among the SNe Ia that have appeared in galaxies within a few megaparsecs, SN 1937C in IC 4182 and SNe 1895B and 1972E in NGC 5253 were observationally normal and not highly reddened, while SN 1986G in NGC 5128 was observationally peculiar *and* highly reddened and therefore cannot be trusted as a calibrator.

Sandage and Tammann (1982) derived a distance modulus $\mu_0 = 28.21 \pm 0.3$ (4.4 ± 0.6 Mpc) for IC 4182 by assuming an average $\langle M_V(3) \rangle = -7.72$ for its three brightest red stars. SN 1937C had $B = 8.7 \pm 0.2$ which, if extinction is negligible (Sandage and Tammann 1982), gives $M_B = -19.51 \pm 0.36$. Very recently Pierce et al. (1992), have derived a shorter distance to IC 4182 using I- and K-band photometry of its brightest red stars. Their calibration implies $M_B = -18.8$. Observation of Cepheids in IC 4182 are needed to resolve the discrepancy.

van den Bergh (1989) reviews the distance to the NGC 5128/5236 group, which he takes to include NGC 5253. Based on the planetary-nebula distance for NGC 5128 relative to that of M31 (Jacoby et al. 1988), van den Bergh recommends $\mu_0 = 27.95 \pm 0.13$ (3.9 ± 0.2 Mpc) for NGC 5128 and concludes that most of the group members have distances in the range 3.2–4.6 Mpc. With a mean $B = 8.35 \pm 0.2$ for SN 1972E and 1895B, a foreground extinction $A_B = 0.12$ (Burstein and Heiles 1978), and negligible parent-galaxy extinction (Caldwell and Phillips 1989), the distance range of 3.2–4.6 Mpc leads to $M_B = -19.77 \pm 0.45$.

With standard assumptions SN 1986G comes out to be less luminous. Adopting $B = 12.5 \pm 0.1$ and $E(B-V) = 0.9 \pm 0.1$ (Phillips et al. 1987; Rich 1987), $R = A_V/E(B-V) = 3.0 \pm 0.5$, and $\mu_0 = 27.95 \pm 0.13$ gives $M_B = -19.05 \pm 0.55$. This is fainter than SNe 1972E and 1895B unless NGC 5253 is in front of the NGC 5128/5236 group (de Vaucouleurs 1979, but see also van den Bergh 1980) or the extinction has been underestimated.

6.3.3 Thermal Emission

Current estimates based on thermal emission assume that the optical flux at the supernova photosphere can be approximated by the flux emitted by a blackbody having the same optical (or optical-infrared) color temperature. The radius of the photosphere can be derived by a method analogous to Baade's (1926) method for variable stars (Branch and Patchett 1973) or simply taken to be the product of the expansion velocity at the photosphere and an estimated rise time from explosion to maximum light (Arnett 1982b; Branch et al. 1983). During most of their evolution the energy distribution of SNe Ia is non-Planckian, but for a brief time near 25 days after maximum light the energy distribution from the U to the K band is close to that of a blackbody having $T = 6000 \pm 1000$ K (Leibundgut 1988). With a velocity at the photosphere of 9500 ± 500 km s^{-1} (Branch et al. 1988), a rise time to maximum light of 17 ± 3 days, and the assumption of blackbody emissivity, the absolute magnitude 25 days after maximum light becomes -18.2 ± 1.0, which corresponds to $M_B = -20.4 \pm 1.0$ at maximum light. Very recently Jeffery et al. (1992) have applied this method to near-maximum-light spectra to derive $M_B = -19.8$ for SN 1990N and -20.0 for the peculiar SN 1991T. These simple thermal emission estimates have the virtue of being independent of all intermediate astronomical distance calibrations but a critical uncertainty is how well the blackbody flux approximates the true optical flux (cf. Harkness 1987). The external error in the thermal emission estimates will become known when detailed spectrum calculations for SNe Ia (Branch et al. 1991) have been performed.

6.4 Uncertainties and Results

At present the self-calibration by means of radioactivity yields $M_B = -19.6 \pm 0.5$, while the other three calibrations give -20.0 ± 0.5, -19.77 ± 0.45, and -20.4 ± 1.0. Each calibration carries an external error that is difficult to quantify. The self-calibration perhaps should be regarded as the primary calibration, and the others as consistency checks (none is inconsistent with the self-calibration). Then the mean apparent magnitude of SNe Ia in the Virgo

cluster of $m_B=11.9\pm0.1$ (Leibundgut and Tammann 1990), combined with a typical Burstein and Heiles (1984) foreground extinction measure of $A_B=0.06$, yields a Virgo distance modulus of 31.44 ± 0.5 ($D=19.4\pm5$ Mpc), and Eq. (10) above yields $H_0=56\pm14$.

6.5 Future Needs and Directions

With modern search techniques, SNe are being identified more frequently than ever before (e.g., Muller et al. 1992). This increased rate offers the promise of validating type-Ia SNe across Hubble types. Furthermore, newly identified SNe will be observed with CCDs instead of photographic plates, thereby providing photometry of unprecedented accuracy against the background of their host galaxies. Extensive observational coverage of a few individual SNe Ia together with detailed modeling of spectra and light curves will allow the methods discussed above under the separate headings of thermal emission and radioactivity to merge into one physical method which should lead to a tightly constrained peak luminosity. An independent check can be obtained by calibrating SN 1937C via Cepheids in IC 4182; perhaps a way to determine a good distance to NGC 5253 also can be found. Measurements of peak apparent magnitudes of SNe Ia well out in the Hubble flow will then yield a Hubble constant independent of the Virgo cluster and undisturbed by peculiar velocities.

7. TULLY–FISHER RELATIONS

7.1 Background

The empirical relationship between the luminosity of a spiral/irregular galaxy and its rotational velocity, known as the luminosity-linewidth or Tully–Fisher relation (Tully and Fisher 1977), has become one of the most widely used extragalactic distance indicators. Despite the fact that a similar technique was applied to estimate the distance of M31 by Öpik (1922), Hubble (1936b) failed to recognize it as a useful way to measure extragalactic distances. The method languished until Roberts (1962) discussed a variant. Later, Balkowski et al. (1974) noted the more direct correlation between luminosity and H I 21 cm linewidth. Tully and Fisher (1977) were the first strong advocates of its use as a distance indicator. Consequently, they are now associated with the "Tully–Fisher relation" (hereafter referred to as the TF relation) and its application to the extragalactic distance scale problem.

Spiral and irregular galaxies are common in both the field and in all but the richest clusters. Consequently, the TF relation is an extremely valuable technique for extensive mapping of local large-scale structure, the Hubble flow, and any associated peculiar velocities. In addition, since the local population is dominated by spirals and irregulars, the TF relations can, at least in principle, be calibrated directly by Cepheids. The TF relations provide an opportunity to go from local calibrating galaxies to the "smooth" Hubble flow in a single step. As an example of the influence of the TF relations, Sandage and Tammann (1976) reassessed their previous work on the distance scale in light of the TF relation and also discussed many of the general uncertainties. A comparison of the distance to the Virgo cluster determined by Tully and Fisher (1977) with the value obtained by Sandage and Tammann (1976) is presented by Fisher and Tully (1977) and illustrates how differences in samples, extinction, and particularly linewidth corrections can lead to quite different results. For reference, Tully and Fisher (1977) obtained a distance for the Virgo cluster of 30.6 ± 0.2 mag, while Sandage and Tammann (1976) obtained 31.4 ± 0.2. The revision of the Hyades modulus to 3.23 mag (e.g., Hodge and Wallerstein 1966; Hanson 1975) shifts these two estimates to 30.8 and 31.6 mag.

The necessary data consist of apparent magnitudes, usually corrected for Galactic and internal extinction, and some measure of rotation velocities, corrected for projection effects, for a sample of galaxies. Usually, the rotational velocity is obtained via the doppler broadening of the H I 21 cm line, although Fabry–Perot imaging and long slit rotation curves (both obtained via Hα) are useful as well.

7.1.1 Photographic and B-Band Relations

As originally proposed by Tully and Fisher (1977), the observational parameters of the TF relation are (1) the photographic magnitude corrected for extinction, used as a measure of the luminosity of a galaxy, and (2) the global H I 21 cm linewidth corrected for projection, used as a measure of the galaxy's rotational velocity. The raw measurements must be corrected for inclination effects, with the corrections for extinction and projection going in the opposite sense; when extinction corrections to the magnitudes are small (i.e., the galaxy is nearly face-on) the projection corrections for the rotational velocity are large, and vice versa. Consequently, considerable care must be taken to determine the proper corrections to the fundamental observables, and several different prescriptions for these corrections have been proposed (cf. Tully and Fisher 1977; Sandage and Tammann 1976; Fisher and Tully 1977). Nevertheless, any systematics introduced by the use of different correction schemes should in principle scale out, provided that the "local calibrators" and the sample galaxies are treated in the same way.

The publication of the *Second Reference Catalog of Bright Galaxies* by de Vaucouleurs et al. (1976) greatly increased the size of the existing data base of total magnitudes for a wide variety of galaxies. In addition, the completion of extensive H I 21 cm surveys such as that by Fisher and Tully (1981) significantly improved the status of the linewidth data. These data were subsequently used by several groups to examine both the utility of the TF relation as a distance indicator and the character of the local Hubble flow (cf. Bottinelli et al. 1983, 1984, 1986; Fouqué et al. 1990; Giraud 1986, 1987; Richter and Huchtmeier 1984). Similar photoelectric data were obtained by Visvanathan (1981, 1983) in the *V*, *r*, and *IV* ($\lambda_0\sim1$ μm) bands. These papers, and the references therein, provide a history of the controversies regarding the use of the TF relation.

The introduction of CCDs as the primary optical detector in astronomical use has greatly improved the quality of

the surface photometry of galaxies and consequently the TF relations, for with them it is now possible to obtain total magnitudes for galaxies to a precision of ~5% (e.g. Pierce 1988). In addition, CCD surface photometry can produce improved and unbiased estimates of galaxy inclinations (e.g., Pierce 1988; Pierce and Tully 1988), which are crucial to correct the observed 21 cm linewidths for line-of-sight projection. Together these developments have prompted an extensive reexamination of the TF relations and their role in the extragalactic distance-scale problem (Pierce and Tully 1988, 1992a,b).

7.1.2 Infrared (H-Band) Relation

A significant improvement in the application of the TF relations occurred with the introduction of infrared *H*-band magnitudes ($\lambda_0 = 1.6\ \mu$m) by Aaronson et al. (1979). They realized that the infrared offered two distinct advantages over visible wavelengths: first, that the extinction at *H* is only 10% that in *B*, and second, that the infrared light is dominated by late-type giants. Thus, over the entire range of morphological types, the infrared is presumably a better tracer of the stellar mass than *B* luminosity. Subsequent observations proved that the infrared Tully–Fisher relation (hereafter referred to as the IRTF relation) has a significantly smaller dispersion than does the *B*-band relation, implying that uncertainties in the extinction corrections for the blue light (which were still rather crude at that time), and/or variations in mean stellar population, were significant. In a subsequent series of papers Aaronson et al. (1980) discussed the absolute calibration, while Mould et al. (1980) determined the distance to the Virgo cluster, along with the corresponding value for H_0. They restricted the sample of bright spirals to those with inclinations greater than 45° and with no morphological peculiarities, following Tully and Fisher (1977), and obtained a distance modulus for the Virgo cluster of 30.98 ± 0.09 mag (internal errors only) with the updated Hyades distance.

Aaronson et al. (1980) used the IRTF relation to estimate distances to four clusters at about four times the Virgo distance. They found significantly larger values for H_0 than they had found earlier for Virgo (i.e., 95 ± 4 km s^{-1} Mpc^{-1} vs 65 ± 4 from Virgo alone) and proposed that the larger value was representative of a global value, while the smaller value was the result of peculiar motion of the Local Group in the direction of the Virgo cluster. This was consistent with the models for the peculiar velocities associated with the local-mass distribution (e.g., Peebles 1976; Schechter 1980) and the dominant role of Virgo in the Local Supercluster (e.g., de Vaucouleurs 1953, 1956; Tully 1982). A more extensive analysis of the velocity field of the Local Supercluster by Aaronson et al. (1982) using distances estimated for a sample of ~300 galaxies via the IRTF relation produced convincing evidence of Virgocentric retardation or "infall." This model is now generally believed to be inadequate given recent observations implying larger-scale peculiar motions (e.g., Aaronson et al. 1986, 1989; Dressler et al. 1987). A recent application of the IRTF to the problem of local peculiar velocities can be found in Han and Mould (1990). The ongoing effort of estimating large-scale peculiar velocities using the IRTF (e.g., Mould et al. 1991) is beyond the scope of this review.

7.2 Method

The current lack of a strong theoretical basis for the TF relations (see Sec. 7.3) prevents a precise definition of the optimum luminosity and rotational parameters which produce the minimum scatter and best calibration for the relations. For luminosity, the choices are (i) the total magnitude for the galaxy, or (ii) a suitably defined aperture magnitude. The former offers the advantage of having a relatively simple definition, while the latter has been a necessity for infrared photometry, where until recently single-element detectors were state of the art. For the rotational-velocity parameter the choices are (i) the maximum of the rotation curve (V_{max}), or (ii) the rotational velocity at a suitably chosen radius, perhaps corresponding to a particular aperture magnitude definition (e.g., Madore and Woods 1987).

Total magnitudes have been the choice for the luminosity parameter over visible wavelengths, even when derived through multiaperture photometry and template growth curves (e.g., de Vaucouleurs et al. 1976; Visvanathan 1981, 1983). The use of total magnitudes was motivated by the availability of the data, the desire for a uniform magnitude system, and the expectation that the mass-to-light ratio of galaxies is constant, or at least a smooth function of mass. The latter is of particular concern at optical wavelengths where the large color difference between the bulge and disk components of spiral galaxies suggests differences in the mass-to-light ratio. This results in a significant morphological-type dependence for the TF relations at bluer wavelengths. Consequently, a TF relation based on blue photometry through small apertures is of limited use (see Pierce and Tully 1988). The numerous problems associated with multiaperture photometry (e.g., centering errors, contaminating stars, the use of circular apertures and mean growth curves, etc.) have been discussed by Corwin (1979). With the introduction of CCDs, full growth curves using elliptical annuli can be easily constructed with contaminating regions (e.g., stars, cosmetic defects) suitably dealt with. The sky level for each image can also be easily estimated, provided the field of view is sufficiently large. Together, these advantages of CCD photometry can result in total magnitudes with a precision ~5% (Pierce 1988, 1992).

Pierce and Tully (1988) found dispersions for the TF relations of 0.37, 0.31, and 0.28 mag for the *B*, *R*, and *I* bands, respectively, from CCD photometry of a complete sample of galaxies in the Ursa Major cluster. There is likely significant line-of-sight depth for this sample, since it spans about 8° on the sky, suggesting an intrinsic dispersion for the longer-wavelength TF relations of $\leqslant 0.25$ mag, or 12% in distance. Much of the improvement over previous work (typically with $\sigma \sim 0.5$ mag) was attributed to an increased accuracy of inclination estimates obtained via ellipses to galaxy isophotes. For example, they found a significant improvement in the dispersion for the IRTF relation using

photometry from the literature, provided that the linewidths were corrected with the improved inclinations. Apparently, the redder wavelengths are preferable, though the B band is still useful for comparative purposes.

Although the infrared aperture magnitudes have been very successful, they are not free of problems. The H-band magnitude ($H_{-0.5}$) is defined to be the apparent H magnitude through an aperture size (A) given by $\log(A/D_{25}^{b,i}) = -0.5$, where $D_{25}^{b,i}$ is the B-band diameter of the galaxy at the 25 mag arcsec^{-2} isophote, corrected for internal and Galactic extinction, as well as projection. This definition allows the use of small apertures that are more tractable with traditional infrared photometers, and also reduces the effect of the sky signal to a manageable level. (The H-band sky is very bright; $\mu_H \sim 13.4$ mag arcsec^{-2}. Compare this with a mean H-band surface brightness, over $D_{25}^{b,i}$ of $\mu_H \sim 18$ mag arcsec^{-2} for a moderate luminosity spiral and ~ 21 mag arcsec^{-2} for a typical dwarf irregular galaxy.) There are well-known observational techniques used in infrared astronomy to combat these high background levels. Nevertheless, nearby systems having low surface brightness and large angular size pose a special problem due to uncertainties in the sky level. In addition to the general problems associated with aperture photometry mentioned above, there is an additional difficulty in tying the infrared aperture size to the optical diameter (e.g., van den Bergh 1981; Aaronson et al. 1986). Significant systematic errors have been introduced into some of the IRTF distance estimates from biased B-band isophotal diameters, a consequence of using different catalogs of B-band diameters for different distance ranges (e.g., Cornell et al. 1987). CCD photometry is almost a necessity to provide a uniform and unbiased aperture definition, at which point aperture photometry itself becomes of limited value. The application of infrared imaging technology over the next few years should alleviate most of these concerns, provided the data reach a sufficiently faint surface-brightness level for total magnitudes to be estimated. An example of the application of infrared array technology to the IRTF can be found in Peletier and Wilner (1991).

7.2.1 Inclination Estimates

Although there has been some success at estimating the inclination of spiral galaxies by fitting the spiral structure to logarithmic templates (e.g., Danver 1942), there are clearly problems with this approach due to the nonuniformities in spiral galaxies. The approach suggested by Holmberg (1958) assumed that disk galaxies can be adequately represented as oblate spheroids such that

$$\cos^2 i = [(b/a)^2 - \alpha^2]/(1-\alpha^2), \qquad (11)$$

where i is the inclination, (b/a) is the observed axial ratio, and α is the axial ratio for an edge-on system. We can also allow α to be a function of morphological type (e.g., Heidmann et al. 1972; Bottinelli et al. 1983; Fouqué et al. 1990). This approach assumes that galaxies have circular isophotes, to which there are clearly counter examples (e.g., M101). Fortunately, the most severe cases are obvious and can be excluded. Less obvious cases increase the uncertainty in i, particularly at low i, but the effect due to variations in α may be equally important. Historically, axial ratios have been estimated by eye using the *Sky Survey* or larger-scale plates. This is an uncertain procedure, particularly when applied to systems whose inner (higher surface-brightness) isophotes are not circular. Pierce (1988) and Pierce and Tully (1988) have advocated the use of ellipse fitting to CCD images in order to estimate axial ratios and hence inclinations. They found that deep images reveal an apparent underlying old-disk population in dwarf systems which can be used to improve the accuracy of the inclination estimates for these systems. Even for bright galaxies, fitting ellipses to isophotes is more quantitative and objective than are eye estimates using photographic plates. Nevertheless, some personal judgment is still required as significant variations in ellipticity with radius are often present in typical galaxies.

An alternative, and promising technique makes use of the two-dimensional velocity field of the galaxy to constrain its inclination. This approach requires an extensive map of the velocity field of the galaxy, using either Fabry–Perot imaging at Hα or aperture synthesis techniques at 21 cm. While this requires considerably more effort, the technique offers real promise for improving inclination estimates. In this approach the gas is assumed to be rotating in circular motion and the velocity field defines the inclination. However, the gas is also subject to noncircular motions originating from nonaxisymmetric mass distributions (e.g., bars, ovals, spiral structure), and so inclination estimates will be somewhat model dependent, although independent of the photometric estimates. Work currently under way by Schommer et al. (1989) should clarify some of these concerns and provide sufficient data to access the technique more fully. Initial results indicate good agreement between the kinematic and photometric inclination estimates.

7.2.2 Internal Extinction Corrections

The corrections for internal extinction are based on models, but these have proven difficult to test due to a shortage of accurate surface photometry. The approach usually taken assumes that spiral and irregular galaxies are not optically thick, although the suggestion that galaxies are opaque has been expressed by Disney et al. (1989) and Valentijn (1990). There are three general forms for the optically thin models: (i) the light is assumed to be mixed evenly with the dust, (ii) the dust is assumed to lie in an infinitely thin obscuring layer, and (iii) a combination of the two, where the dust lies in a layer of finite thickness with a portion of the light being unobscured. While the second model is relatively simple and has some observational basis, the assumption of an infinitely thin absorbing layer results in a rapid variation of extinction between $i = 45°$ and $i = 90°$. Available data suggest that this is too severe (i.e., Tully and Fouqué 1985).

Tully and Fouqué (1985) discuss some of the problems with the first two formulations given above and offer a compromise between these extremes (the third model). This model is certainly the most physically sound, and it

appears to provide the best fit to the available data. Under the assumptions of the third model the extinction correction becomes

$$A^i = -2.5 \log\{f(1+e^{-\tau \sec i}) + (1-2f) \times [(1-e^{-\tau \sec i})/\tau \sec i]\}, \quad (12)$$

where, as before, i is the inclination and τ is the optical depth. The additional parameter f is the fraction of the light that is *unobscured* by the dust layer. Thus, $f=0.5$ leads to the infinitely thin layer model, while $f=0$ leads to the model proposed by Holmberg. Tully and Fouqué (1985) adopted $\tau \sim 0.55$ for the B band, $f \sim 0.25$, and suggested that the data are better fit if the extinction for $i > 80°$ is held at the value for 80°. At present, this simplistic two-component model appears to be the most reasonable formulation for the internal extinction within galaxies, provided that they are optically thin. Surface photometry data over a broad wavelength range would greatly help to clarify the values of f and τ, particularly any dependence on morphological type for these parameters.

7.2.3 Linewidth Definitions and Corrections

As mentioned in Sec. 7.2, the parameter used in the TF relations for predicting the luminosity for a particular galaxy is V_{max}, the maximum amplitude of the rotation curve. If the dark-matter distribution is isothermal (implied by flat rotation curves), then V_{max} is a measure of mass, provided that the distribution of mass within galaxies is similar (see Sec. 7.3). Since galaxies have flat rotation curves over much of their extent, V_{max} should be insensitive to differing measurement techniques, and has the additional advantage of being well defined. In the original formulation, Tully and Fisher used the Doppler width of the 21 cm line profile measured at 20% of peak (W_{20}), corrected for receiver broadening and galaxy inclination (i.e., $W^i = W_{20}/\sin i \sim 2V_{max}$). This was also the procedure used by Aaronson and collaborators. It has the advantage of being conceptually simple and it is easy to compare between different researchers when these minimally corrected linewidths are used. The 21 cm line is particularly well suited to sampling the outer rotation curves of galaxies since the extent of detectable H I is often several times that of the visible galaxy (e.g., Roberts 1962; Bosma 1981). It is also relatively easy to detect H I out to considerable distances (e.g., the Hercules cluster at $V_0 \sim 11{,}000$ km s^{-1} with Arecibo). It is worth emphasizing that errors in the corrected linewidths are likely to be the dominant source of observational error, so a signal-to-noise level of $\gtrsim 10$ is essential.

Other definitions of rotational broadening have been used (e.g., W_{50}), particularly if the signal-to-noise ratio is low. While alternative definitions are acceptable, in principle, the fact that estimates of V_{max} using W_{20} closely correspond to those values obtained from classical rotation curves via Hα implies that W_{20} is a good choice. The use of different definitions for linewidth become important when trying to compare results from the Hα and H I techniques, or even from different investigators.

Bottinelli et al. (1983, 1984) correctly pointed out that the simple inclination correction given above does not allow for the effects of the turbulent motion internal to the gas; these are expected to be a significant source of Doppler broadening for low-luminosity systems. Observations of significant linewidths for face-on systems (e.g., Lewis 1984) attests to the importance of this effect. Without a correction for turbulence, W^i, and hence V_{max}, would be progressively overestimated with decreasing luminosity (mass), resulting in a curved TF relationship (e.g., Aaronson et al. 1986; Mould et al. 1989). Using the observed velocity ellipsoid for the flattest Population-I components in the Galaxy, Bottinelli et al. estimated the turbulence at ~ 15 km s^{-1}. The amount of the correction was slightly inclination dependent due to the assumption of an anisotropic velocity ellipsoid. They then linearly subtracted this correction from the observed profile width and corrected for inclination to obtain $2V_{max}$.

Tully and Fouqué (1985) suggested a slight modification to the Bottinelli et al. procedure. They advocated an isotropic velocity dispersion for the H I and a quadrature subtraction of the turbulence term for dwarf galaxies on the grounds that the velocity profiles are more like Gaussians than the "boxcar" profiles of the higher-luminosity galaxies. Their prescription for correcting linewidths is consequently more complicated as it also includes a smoothing function to ease the transition between the two correction regimes:

$$W_R^2 = W_{20}^2 + W_t^2 - 2W_{20}W_t(1-e^{-(W_{20}/W_c)^2}) - 2W_t^2 e^{-(W_{20}/W_c)^2}, \quad (13)$$

where W_{20} is the measured width at 20% of peak intensity, W_t is the expected 20% width due to turbulence (38 km s^{-1}) for an isotropic velocity dispersion of 10 km s^{-1}, W_c is the characteristic transition width from "horned" to Gaussian-shaped profiles (120 km s^{-1}), and finally, $W_R^i = W_R/\sin i$ is the corrected rotational parameter ($\sim 2V_{max}$). Note that this procedure results in the transition width (W_c) being a function of inclination.

These two correction schemes are essentially indistinguishable for $W_R^i \geqslant 100$ km s^{-1}, but differ substantially from the case of no turbulence correction. Obviously, care must be taken when comparing corrected linewidths from different researchers. Naturally, the calibrators and the sample galaxies should span a similar range in luminosity and W_R^i to the program galaxies in order to minimize any systematic errors introduced by these correction procedures.

An optical alternative to H I velocity widths has been developed by Rubin et al. (1985) based on rotation curves measured at Hα. This technique is particularly promising because detection efficiencies are high for telescopes in the 2–3-m class out to velocities of $\sim 10{,}000$ km s^{-1}; thus they are competitive with 21 cm linewidths obtained with the Arecibo telescope, while offering full sky coverage. In addition, optical spectroscopy can be applied in the crowded cores of more distant clusters, where the large beam of even the Arecibo dish suffers from confusion. While the

Hα data can easily be corrected for inclination, the correction for internal turbulence in low-luminosity systems is complicated by outflow near star-forming regions. Recently, Courteau (1992) has reexamined the application of Hα rotation curves for estimating V_{max}, and finds good agreement between optical and radio estimates. Dressler and Faber (1990b) have used an optical version of the TF relation to examine the velocity field in the vicinity of the "Great Attractor."

7.2.4 Malmquist Effects

There has been a great deal of discussion in the literature during the past decade concerning the significance of selection effects in the determination of extragalactic distances, particularly for those obtained via TF relations. Since the TF relations are applicable to spiral and irregular galaxies, they have until recently been the only quantitative distance indicator which had been applied to a sufficient sample of galaxies such that the effects of Malmquist "bias" on distance determinations can be adequately tested.

The samples in question are typically selected on the basis of apparent magnitude. In such samples, the resulting luminosity function is progressively biased toward intrinsically brighter systems with increasing increasing *true distance*. This bias is usually referred to as a "Malmquist effect," although this is not quite the situation Malmquist (1920) described. Tammann (1987) and Sandage (1988), for example, argue that the distances are biased, leading to an apparently small dispersion of the TF relations. The fact that the *luminosity function* of an apparent magnitude-limited sample is progressively more biased for ever increasing distance is without a doubt (e.g., Sandage et al. 1979). At issue is whether the *estimated distances* for such a sample are biased.

Additional confusion has arisen when analytical solutions to similar bias problems (e.g., Teerikorpi 1984, 1987; Bottinelli et al. 1986; Lynden-Bell et al. 1988) are applied to the TF samples. However, those solutions may suffer from simplifying assumptions, or they may not be general solutions. In fact, the problem described by Malmquist (1920) is only a special case of the overall problem of estimating astronomical distances.

For example, errors in predicted distance modulus can arise from both random and systematic errors. Purely random errors obviously do not result in biased distance estimates, unless they propagate into both the sample selection criteria and the estimated distance moduli. An example of this would be the use of cataloged apparent magnitudes to *both select the sample and estimate individual distance moduli.* Note, however, that this coupling can be broken if new photometry is obtained for a sample selected on the basis of cataloged photometry.

An example of a systematic error with distance is that described originally by Malmquist (1920). In this case, an observable (i.e., spectral type) is used to predict the *mean* absolute magnitude of a particular class of stars. This predicted absolute magnitude is then used to estimate distance moduli, even though the sample selection criteria have already biased the distribution in absolute magnitude, such that the mean of the parent population is not the mean of the selected sample. However, this need not be the case for all apparent magnitude-selected samples.

Simulations of the TF relations demonstrate that for the case in which the dispersion in inclination-corrected linewidth dominates the dispersion in apparent magnitude (e.g., Bothun and Mould 1987), either due to an intrinsic scatter or due to observational errors in W_{20} and inclination, then there is essentially no bias introduced into the TF distances due to selecting the sample on the basis of apparent magnitude. The fact that the true luminosities of the sample members are biased becomes irrelevant, since the unbiased predictor of luminosity (i.e., W^i_R) will produce an *unbiased predicted luminosity.* That is, the sample members which are at larger distance, and hence more luminous than would be expected for members of an unbiased sample, will have linewidths which predict them as such. As a result, *the predicted distances* for such a sample are unbiased. This point was first discussed by Schechter (1980) in the context of the Faber–Jackson relations for elliptical galaxies (Faber and Jackson 1976) and later by Pierce and Tully (1988), and Tully (1988) in the context of the TF relations.

7.2.5 Sample Selection

For the TF relations to be successfully applied, the galaxies must have detectable gas in essentially circular motion; otherwise, the estimate of V_{max} will be inaccurate. Although there is occasionally detectable H I in lenticular systems (van Driel and van Woerden 1991), defining a TF relation for E/S0 galaxies involves several complications; the origin of the gas is uncertain, the gas is usually patchy, its detection is difficult, and its motion may not be circular. Because of these difficulties (and the potential for significant M/L variations among early-type galaxies as discussed in Sec. 73), it is best to limit samples of galaxies to types Sb–Irr having no signs of peculiar morphology, due, for example, to recent interactions. In addition, the galaxies must have enough gas in their exterior regions such that the observable rotation curve reaches a peak and V_{max} can be adequately sampled. It is now clear that disk galaxies within the cores of even moderately poor clusters like Virgo suffer significant stripping of their outer envelope of H I gas (e.g., Haynes and Giovanelli 1986; Cayatte et al. 1990). Fortunately, only a few systems in Virgo are gas-stripped to radii within the turnover in their rotation curves. The most serious cases also have morphological peculiarities and would likely have been excluded on this basis alone (e.g., NGC 4438). However, this remains an uncertainty for galaxies in the cores of more distant clusters; for these galaxies a full rotation curve may be necessary to assure that the rotation curves do indeed turn over.

The modest morphological-type dependence mentioned earlier (i.e., earlier types having low luminosities for their linewidths, see Sec. 7.2) is a consequence of late-type galaxies being systematically bluer than those of earlier type, coupled with the historical use of the *B*-band TF relation. Because the effect decreases dramatically toward longer

wavelengths, a likely cause is the smaller bulge-to-disk ratio and the larger fraction of young stars in the low-mass, gas-rich systems. Some of the effect may also be the result of a decrease in dust content for the later morphological types (e.g., van den Bergh and Pierce 1990). If so, the assumption of a mean optical depth for all morphological types could contribute to a morphological-type dependence, especially at the shorter wavelengths where extinction estimates would be significantly overestimated.

As mentioned above, the kinematics of lower-luminosity irregular galaxies become progressively more dominated by turbulence and less by rotational motion. Consequently, the TF relations must progressively break down below some luminosity. Tully and Fouqué (1985) discuss the linewidth corrections for extending the TF relations to low-luminosity systems. Some of the motivation for this was to increase the number of local calibrators available (e.g., Richter and Huchtmeier 1984). However, the TF relations for systems fainter than $M_B \sim -15.0$ become rather poorly defined as the corrections to the linewidths become large and the inclinations become more uncertain. With these factors in mind, it is recommended that samples be limited to galaxies brighter than $M_B \sim -16.0$ for which the kinematics are dominated by rotation.

7.3 Physical Basis

The fact that luminous disk galaxies have flat rotation curves over the entire extent of their optical region and beyond (e.g., Rubin et al. 1980; Bosma 1981) implies the existence of large amounts of nonluminous matter. If spherical symmetry is imposed, then the integrated mass ($\sim V^2R/G$) grows linearly with radius, with the implication that the "dark-matter" density scales as $\rho \sim R^{-2}$. This also is the expectation for an isothermal halo (e.g., Binney and Tremaine 1987), along with a flat rotation curve at large R. If we also assume that galaxies have roughly constant surface brightness ($L \sim R^2$) and that the mass-to-light ratio (M/L) is constant, then we have $R \sim V_{\max}^2$, or $L \sim V_{\max}^4$. This is roughly the slope of the TF relations at the longer wavelengths ($M_H \sim 10 \log W_R^i$). A similar argument was originally presented by Schechter (1980). More elaborate physical justifications have been presented by Aaronson et al. (1979) in an attempt to explain the origin of the slope of the H-band TF relation.

Unfortunately, the situation is considerably more complicated than these derivations would suggest. It is now clear that the basic photometric scaling properties of low-luminosity systems differ from those of luminous systems (e.g., Binggeli et al. 1984; Pierce 1988, 1991). For example, the I-band M/L begins to increase rather abruptly for galaxies less luminous than about $M_B \sim -19.5$ (Pierce 1988, 1991). These results suggest that while the visible matter in luminous galaxies is self-gravitating, the low-luminosity systems are dark-matter dominated (e.g., Persic and Salucci 1988, 1990). Consequently, the existence of a tight TF relation over this broad range in luminosity becomes difficult to understand, yet searches for second parameters in the TF relations have thus far been unsuccessful (e.g., Cornell 1989; Bivano et al. 1990).

Central to this problem is the fact that disk galaxies have flat rotation curves over a broad range of luminosity and mass, with dark matter dominating at moderately large radii. At the same time, it is clear that the TF relation implies a "disk-halo conspiracy," such that the mass within some characteristic optical radius is coupled with the mass (Sancisi and van Albada 1985). One of the more successful attempts at understanding this phenomena is given by Blumenthal et al. (1984). They find that gravitational interplay between the luminous and nonluminous matter in luminous disk galaxies is sufficient to redistribute the total mass in such a way as to produce the flat rotation curves which are observed. Dekel and Silk (1986) have developed a model for the formation of dwarf galaxies in an attempt to explain some of the properties of these systems, including their distinctive photometric scaling properties. They suggest that low-mass galaxies are more susceptible to significant sweeping of gas via supernovae-driven winds during protogalactic collapse than are more massive systems due to a lower binding energy. In such a situation, star formation can be radically slowed and, in some cases, essentially quenched. As a result, these systems today would have a larger dark-to-luminous matter ratio than more massive systems since the dark matter (assumed to be nonbaryonic) would be unaffected by radiation and gas dynamics.

While this model is capable of reproducing the general trend of M/L with L, including the characteristic onset mass (luminosity), it cannot explaining the tight TF relations found for low-luminosity systems (Pierce 1991). Evidently, some important physics is still missing and a complete understanding of the TF relations will have to wait for a more highly developed model of the formation of galaxies. Nevertheless, the TF relations remain strong empirical relations between the photometric and kinematic scaling properties of spiral and irregular galaxies.

7.4 Absolute Calibration

At the time of Tully and Fisher (1977), only two local calibrating galaxies had moderately secure distance determinations, M31 and M33. Subsequently, there has been some debate as to the distance of M33 (see Sec. 3). Pierce and Tully (1988) presented an absolute calibration based upon CCD photometry of M31, M33, and NGC 2403 in the B and R bands with I-band data provided only for the latter. However, Burstein and Raychaudhury (1989) pointed out some significant problems with the Pierce and Tully photometry of M31. This was a particular concern given the small number of local calibrators available.

Recently, the situation has changed dramatically, with extensive CCD photometry of Cepheids and RR Lyrae variables in nearby galaxies. There are now reliable distance estimates to three systems in or near the Local Group (M31, M33, NGC 3109), two systems in that M81 group (M81 and NGC 2403), and one galaxy in the Sculptor group (NGC 300). If, in addition to these systems, we could make use of the other members of the M81 and

Sculptor groups with $M_B \leqslant -16.0$, the total number of calibrators would be 15.

Pierce and Tully (1992a) have recently completed an analysis of the absolute calibration of the TF relations which addresses many of the concerns expressed by Burstein and Raychaudhury (1989). The relations are shown as the upper sequence of panels in Fig. 11. The solid points represent those systems with individual distance estimates provided by Cepheids and/or RR Lyrae variables, while the open symbols represent additional members of the M81 and Sculptor groups (square and triangles, respectively). These are assumed to be at a mean distance given by those systems with individual distance estimates. The distribution of the additional members of the M81 group is consistent with a small dispersion, implying a small line-of-sight depth for the group. The large dispersion for members of the Sculptor group is consistent with previous suggestions of significant line-of-sight depth for the group (e.g., de Vaucouleurs and Davoust 1980). The dispersions are $\sim$0.20 mag for the systems with individual distance estimates, implying a precision in distance estimates from the TF relations of $\sim$10% for an individual galaxy.

On the other hand, Sandage (1988), Kraan-Korteweg et al. (1988), and Tammann (1988) suggest that the intrinsic dispersion of the TF relations may be as large as 0.7 mag (see Sec. 7.5). However, the data shown as the upper sequence of Fig. 11 are not consistent with that result, nor is Freedman's (1990) demonstration that the intrinsic dispersion is small for the IRTF relations.

From the six local calibrating galaxies currently with individual distances, the zero point of the calibration is established to an uncertainty of 0.08 mag (Freedman 1990; Pierce and Tully 1992a). The distances assumed for the local calibrators are well estimated relative to the distance of the LMC, which is tied to the Galactic calibration of Cepheids and RR Lyrae variables. The distance of the LMC is uncertain to $\sim$7% (e.g., Feast and Walker 1987) and so the primary source of error in the TF calibration lies with the Galactic calibration of the Cepheid *P-L* and *P-L-C* relations.

Pierce and Tully (1992a) find a significant systematic color difference between field (i.e., the "local calibrators") and cluster galaxies (see also Holmberg 1958). This results in a systematic variation in the estimated distances with bandpass. A small ($\sim$0.25 mag) correction is necessary in the *B* band in order to produce consistent distance estimates over all bandpasses and environments. The resulting calibration is given by

$$M_B^{b,i} = -7.48(\log W^i_R - 2.50) - 19.55 + \Delta_B \pm 0.14, \quad (14)$$

$$M_R^{b,i} = -8.23(\log W^i_R - 2.50) - 20.46 + \Delta_R \pm 0.10, \quad (15)$$

$$M_I^{b,i} = -8.72(\log W^i_R - 2.50) - 20.94 \pm 0.10, \quad (16)$$

$$M_H^{b,i} = -9.50(\log W^i_R - 2.50) - 21.67 \pm 0.08, \quad (17)$$

where the correction factors $\Delta_B = 0.25$ and $\Delta_R = 0.06$ are required for statistically consistent distances between the different bands for "cluster galaxies." The corrections for "field galaxies" should be zero. The existence of a "color correction" diminishes the utility of the *B*-band relation and implies that longer-wavelength bandpasses produce more reliable distance estimates. Note that these calibrations apply only to the Tully and Fouqué (1985) prescriptions for extinction and linewidth corrections.

7.5 The Virgo Cluster

Virgo, as the largest nearby cluster, also plays a central role in the study of the TF relations in that it is often used to define both the slope and intrinsic dispersion for the TF relations. Pierce and Tully (1988) obtained CCD photometry for the brighter cluster members in Virgo and a complete sample in the Ursa Major cluster; the systems were found to be about the same distance. These results are comparable to those obtained previously for the two clusters by Tully and Fisher (1977) and Mould et al. (1980). Pierce and Tully (1988) found greater dispersion in Virgo than in Ursa Major and interpreted this as the result of an infalling cloud of galaxies superposed on the Virgo cluster core (e.g., Fig. 12), whereas Kraan-Korteweg et al. (1988; hereafter referred to as KKCT) interpreted the dispersion as an intrinsic property of the TF relations. They also suggested that the large values of H_0 found by Aaronson and collaborators for more distant clusters were the result of selection biases producing both artificially small observed dispersions for the TF relations, as well as resulting in systematically low distances via "Malmquist effects," as discussed in Sec. 7.2.5.

Pierce and Tully (1992b) have recently obtained CCD photometry for the fainter members of Virgo. Their sample includes essentially all the galaxies used by KKCT. The data are presented here in the lower panels of Fig. 11. Clearly, KKCT were correct in the assertion that the dispersion in the TF relations increases when the fainter sample is added. In Fig. 12 the individual distance estimates are shown against radial velocity for both the Pierce and Tully (1992b) and the KKCT data (and calibrations). The superimposed lines are the predicted envelopes in velocity that a galaxy infalling into the cluster for the first time will follow (Tully and Shaya 1984). The concentration of points with a distance of $\sim$21 Mpc is evident in both data sets, suggestive of a "background cloud." Note that the distance range with the highest velocity dispersion corresponds to $\sim$15–16 Mpc, or a distance modulus of $\sim$31.0. This is also the distance obtained for the brighter members by Pierce and Tully (1988), who interpreted this region of the diagram as the virialized core of the cluster. The "background cloud" defines a distinct, well-known distribution when projected on the sky: the *S'* or *B* cloud (de Vaucouleurs 1961). Figure 13 shows the distribution of these "background candidates" projected upon the sky.

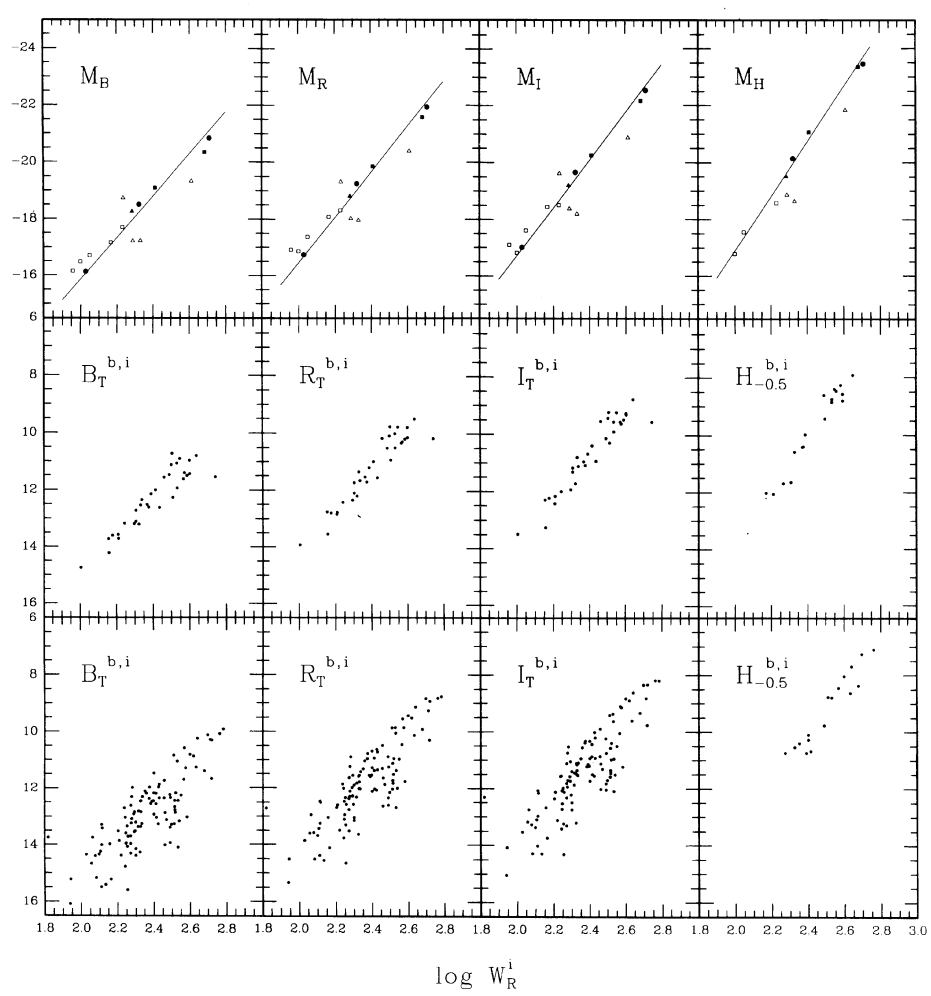

FIG. 11—*B*-, *R*-, *I*-, and *H*-band Tully–Fisher relations for the Local Calibrators (top), Ursa Major cluster members (middle), and Virgo cluster members (bottom). It is apparent from the figures that the slope of the relations increases going to longer wavelengths and the dispersion decreases. The variation in slope is thought to arise from the differing contributions to the observed bandpass made by greater fraction of young stars found in the lower-luminosity systems. The smaller dispersion at longer wavelengths is likely due to a reduction in the sensitivity to these effects, as well as those expected from extinction variations. Note the much larger dispersion found for the Virgo cluster data.

7.6 Uncertainties

As discussed above, CCD photometry can reduce the errors in the apparent magnitudes to ~5%. It is difficult to reduce errors in W_{20} much below about 10 km s^{-1}, given that the observed 21 cm profiles often have low-intensity "bumps" or "wings." In addition, inclination errors are currently limited to about 3° for galaxies with an inclination near 45°. As a result, corrected linewidths (W^i_R) have a typical rms dispersion of ~16 km s^{-1}, or ~0.02 in log W^i_R. This corresponds to an internal error of 0.17 mag or 8% in distance, leaving very little room for intrinsic dispersion in the TF relations. However, there is no assurance that the TF relations are strictly linear. Both the Ursa Major and local calibrating samples are deficient in high-luminosity systems and there is some evidence for curvature or a change in slope at the high-luminosity end (e.g., Aaronson et al. 1986; Pierce 1988; Mould et al. 1989). However, the available data for a broad range of environments from the local field to the relatively dense core of the Virgo cluster indicate no sign of any significant variations in slope with local density. It might be expected that low-luminosity galaxies would be more sensitive to environmental influences and, if this is the case, a change in slope of the TF relations in differing environments would result. The intrinsic dispersion among galaxies (i.e., any lack of coupling between mass and luminosity) probably adds an uncertainty of ~0.15 mag (see Secs. 7.4, 7.5, and Fig. 11). It is unclear whether such effects would be random or systematic. In any event, it appears that the internal rms dispersions for the redder TF relations are ~0.25 mag, or 12% in distance. In addition, the uncertainty in the physical basis for the TF relations opens the possibility for a subtle systematic variation of the TF relations with environment, although no evidence for such effects has been

found. Finally, the distance scale via the TF relations is tied directly to the distance of the LMC and the Galactic calibration of the Cepheid and RR Lyrae variables. Ultimately, the precision of TF relations is limited by this calibration.

7.7 Future Needs and Directions

It is unlikely that the accuracy of visible-light CCD photometry will improve much in the future. On the other hand, it is likely that the use of large-format IR arrays will reduce the uncertainties in the estimates of Galactic and internal extinction. With the dispersion in the relations currently being dominated by uncertainties in the corrected linewidths (W_R^i), significant improvements are most likely to originate from better values of W_{20} and/or inclinations. The use of two-dimensional velocity-field measurements may help in both respects but this would still be somewhat model dependent. A careful investigation of the shape of the TF relations, particularly at the bright end, would help to address current uncertainties regarding the shape and the morphological-type dependence of the TF relations.

8. PLANETARY NEBULAE

8.1 Background

It is common to think of using the brightest stars to determine extragalactic distances. Indeed, over 50 years ago, Hubble (1936a) first attempted to resolve stars in other galaxies to quantify the expansion of the universe, and since then, the use of blue and red supergiants for extragalactic distance determinations has been explored several times (e.g., Sandage and Tammann 1974; Humphreys 1983). However, only recently has it been appreciated that young planetary nebulae also fall into the "brightest stars" category and are therefore potentially useful as standard candles. As can be seen in the $H-R$ diagram of Fig. 14, the central stars of these objects are almost as luminous as the brightest red supergiants—the fact that their continuum emission emerges in the far ultraviolet, instead of the optical or near infrared, does not affect their detectability. On the contrary, since their surrounding nebulae reprocess the EUV radiation into discrete emission lines, planetaries can be viewed through interference filters which suppress the starlight from the host galaxy. As a result, observations made through a narrow-band λ5007 filter can detect $\sim$15% of the energy emitted from these extremely luminous objects, with little contamination and confusion from continuum sources.

Planetary nebulae have several advantages over other extragalactic distance indicators. Because PN are not associated with any one stellar population, they can be found in galaxies of all Hubble types, and hence are particularly valuable for probing the E and S0 galaxies which define the cores of large groups and clusters. Likewise, internal extinction is usually not a problem in extragalactic PN observations: unlike blue supergiants or Cepheids, PN can be found far away from star-forming regions, in areas of the galaxy which are relatively dust free. Since PN are observed through narrow-band filters which suppress the continuum, the identification and measurement of these objects does not require complex, crowded-field photometric procedures, and, unlike variable-star standard candles, PN observations are required only once. Perhaps most importantly, in a large galaxy there may be several hundred planetaries populating the brightest two magnitudes of the planetary-nebula luminosity function (PNLF). With the luminosity function so well defined, distance derivations are straightforward, and the internal errors can be as small as 3% (cf. Jacoby et al. 1989).

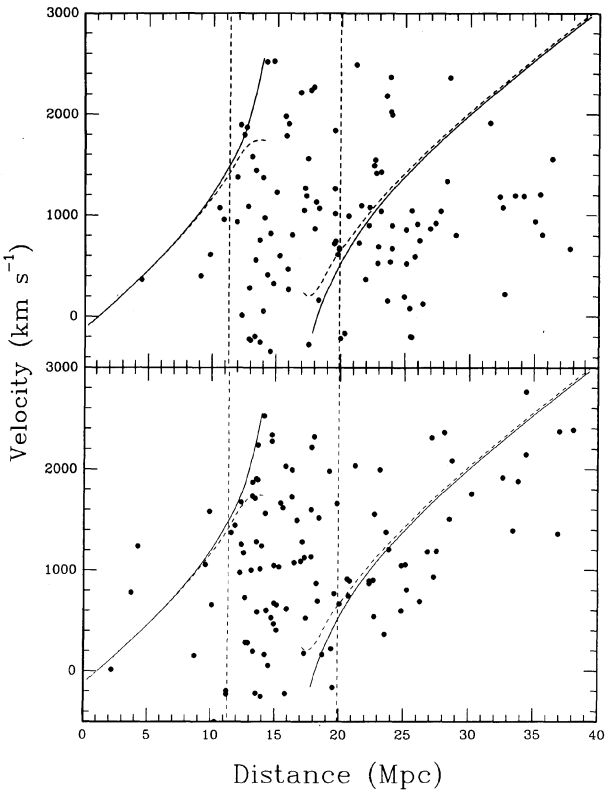

FIG. 12—Distance-velocity diagram for the 6° region of the Virgo cluster from Pierce and Tully (1988), and from data given by Kraan-Kortweg et al. (1988) shown as the upper and lower panels, respectively. The data are from independent data sets and independent calibrations. The superimposed lines represent envelopes of predicted peculiar velocities for a Virgo mass constrained by a virial analysis of the cluster (Tully and Shaya 1984). The evidence for a background contamination of the Virgo cluster sample is clear, with the mean distance for the virialized core of the cluster being $\sim$15.5 Mpc. The background group with low-velocity dispersion at a distance of $\sim$25 Mpc is also localized on the sky and has been referred to as the S' or B cloud.

Despite these facts, the use of PN to determine extragalactic distances is a relatively new phenomenon. The first suggestion that PN might be a useful standard candle can be found in the book *Galaxies and Cosmology* by Hodge (1966), where it is listed in Table 12.1 along with such well-known distance indicators as Cepheids, RR Lyrae and novae. Actual PN distance measurements, however, were not made until the 1970's, when Ford and Jenner (1978) used a 50 Å wide λ5007 filter and the SIT

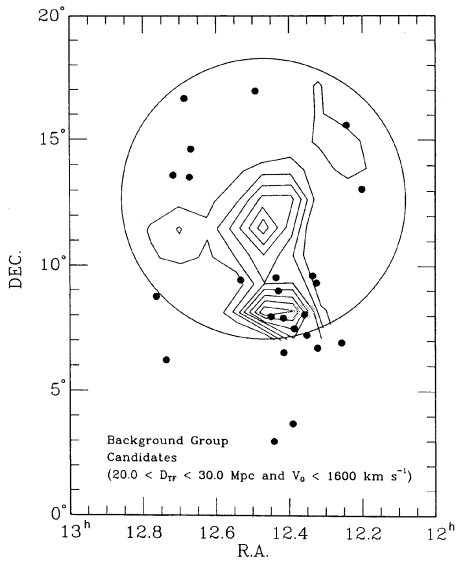

FIG. 13—The "background candidates" projected upon the sky. The superimposed contours illustrate the density distribution of all Virgo galaxies with $500 \leqslant V_0 \geqslant 1500$ km s^{-1} taken from Huchra (1985).

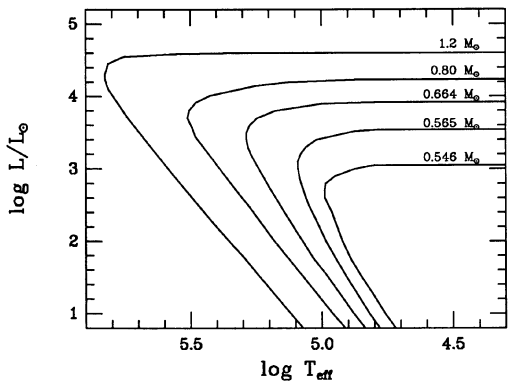

FIG. 14—A schematic $H-R$ diagram showing the evolutionary tracks of planetary nebula central stars. The tracks illustrate the strong dependence of magnitude and lifetime with core mass: the luminosity of a helium burning central star goes approximately as $L \sim M^{3.5}$, but the lifetime of the object goes as $\tau \sim M^{-9.5}$. It is these two relationships, coupled with a sharply peaked core-mass distribution, which causes the abrupt truncation in the planetary-nebula luminosity function.

Video Camera on the Kitt Peak 4-m telescope to find and measure the brightest PN in the bulge of M81. Ford (1978) had noticed that the absolute [O III] λ5007 flux of the brightest PN in each of seven Local Group galaxies varied by less than 25%. Thus, by comparing the [O III] λ5007 fluxes of M81's brightest PN with those of the brightest PN found in M31, Ford and Jenner (1978) estimated the distance ratio between these two galaxies to be $\sim$4. A few years later, Jacoby and Lesser (1981) used a similar argument to place limits on the distances to five Local Group dwarfs, and Lawrie and Graham (1983) estimated the distance modulus of NGC 300.

None of the above results was exceptionally persuasive, however. Some of this skepticism arose from the analysis method which excluded all but the brightest objects from consideration. However, the main concern at the time was that little was known about the luminosity function of planetaries; hence the uncertainties associated with these distances were completely unknown. It is an irony of the subject that distances to Galactic planetary nebulae are extremely difficult to obtain, and that a single PN is definitely not a standard candle. [For instance, NGC 7027, one of the best studied Galactic PN has recent distance estimates that range from 178 pc (Daub 1982) to 1500 pc (Pottasch et al. 1982).] However, while a single PN may not be a standard candle, an ensemble of these objects can yield a well-determined distance. The reason for this is the invariance of the [O III] λ5007 planetary-nebula luminosity function.

8.2 The Planetary-Nebula Luminosity Function

In his study of Magellanic Cloud planetaries, Jacoby (1980) showed that the [O III] λ5007 luminosity function for faint planetaries is well represented by an exponential law formed by combining a uniformly expanding shell with a nonevolving central star (Henize and Westerlund 1963). However, as the CCD observations of PN in M31 (Ciardullo et al. 1989), M81 (Jacoby et al. 1989), the Leo I group (Ciardullo et al. 1989), the NGC 1023 group (Ciardullo et al. 1991), the Magellanic Clouds (Jacoby et al. 1990), and Virgo (Jacoby et al. 1990) have shown, the bright end of this function is truncated rather dramatically, in a manner similar to that predicted by the theoretical models of Jacoby (1989). Ciardullo et al. (1989) therefore modified the Henize and Westerlund law by adding a cutoff exponential, proposing that

$$N(M) \propto e^{0.307M}(1-e^{3(M^*-M)}), \qquad (18)$$

where the magnitude, M, is related to the λ5007 flux of a planetary by

$$M = -2.5 \log F_{5007} - 13.74, \qquad (19)$$

and M^* is the absolute magnitude of the most luminous planetary.

To set the zero point of the function, Ciardullo et al. (1989) used 104 unobscured PN in the bulge of M31. By adopting the infrared Cepheid distance of 710 kpc (Welch et al. 1986), and a total foreground extinction of $A_{5007} = 0.39$, Ciardullo et al. found the best-fit value for M^* to be $M^* = -4.48$ with a 1σ internal error of $+0.036$, -0.046. Because these 104 PN serve as the sole absolute calibrator for PNLF distances, this internal error, as well as the external uncertainty in M31's true distance and reddening, propagates directly into all subsequent PNLF measurements. Future observations may reduce the internal error by enlarging the sample of PN used in the calibration, but because PN are secondary standard candles, PNLF distances will always be subject to uncertainties in the Local Group distance scale. In fact, recent estimates for M31's distance (770 kpc; Freedman and Madore 1990) and reduced extinction ($A_{5007} = 0.28$; Burstein and Heiles

1984) suggest a cutoff that is 0.06 mag more luminous.

Since the Ciardullo et al. PNLF is not a power law, and, in fact, shows a rapid decline over the brightest magnitude of the luminosity function, a fit of the observed PNLF to Eq. (18) yields a distance directly, provided, of course, that the function is invariant. Fortunately, there is good evidence to show that this function, if not invariant, is at least insensitive to galaxy color, metallicity, or Hubble type. Well-defined PNLFs currently exist for 17 giant spiral, elliptical, and irregular galaxies. In none of these objects is there any evidence for a change in the shape of the PNLF cutoff (cf. Fig. 15). More importantly, the zero point of this function also appears to be constant. In the Leo I group, Ciardullo et al. (1989) found that the PNLF distances for three elliptical and S0 galaxies, NGC 3377, 3379, and 3384, all fell within 0.5 Mpc, or 5% despite the fact that the galaxies differ by 0.8 mag in absolute luminosity, 0.3 mag in $(U-V)$, and 0.1 in [Fe/H]. Jacoby et al. (1990) derived a similar result for six early-type galaxies in the Virgo cluster core: although the galaxies span a range of 0.19 in [Fe/H], 0.22 mag in $(U-V)$, and 2.2 mag in $(m_{1550}-V)$, the 1σ dispersion in their computed distances was again only 5% (0.8 Mpc). Perhaps the strongest internal confirmation of the insensitivity of the PNLF to stellar population, however, comes from the agreement between the PNLFs of NGC 1023, a gas-rich S0 galaxy, and fellow group member NGC 891, the edge-on Milky Way lookalike. Ciardullo et al. (1991) measured identical distances to these two galaxies, using as their data a complete sample of PN in NGC 1023's disk and NGC 891's halo. Since the halo stars of NGC 891 are undoubtedly much older than the disk objects of NGC 1023 [NGC 1023 formed stars $\sim$3 Gyr ago (Gregg 1989)], this result strongly supports the contention that a galaxy's star-formation history does not play an important role in determining the PNLF cutoff. Moreover, since the total number of PN found in NGC 891's halo is a factor of 3 less than that discovered in NGC 1023, the similarity in the derived distances to these two galaxies is additional evidence that the PNLF cutoff is indeed an exponential, rather than a power law as proposed by Bottinelli et al. (1991).

External comparisons have also proved that PNLF distances do not depend strongly on the properties of the underlying stellar population. PNLF surveys in the bulge of the Sb galaxy M81 and in the Large Magellanic Cloud have resulted in derived distances to these galaxies (Jacoby et al. 1989; Jacoby et al. 1990) that are statistically indistinguishable from that found from the I-band and infrared observations of Cepheids (cf. Freedman and Madore 1988; Welch et al. 1987; Feast and Walker 1987). Moreover, Pottasch's (1990) PNLF-based estimate of 8.1 kpc for the distance to the Galactic Center is completely consistent with that determined by other methods (Reid 1989). Finally, it should be noted that the PNLF distances to the Leo I, NGC 1023, and Virgo clusters are in excellent agreement with those estimated from the Tully–Fisher method (Pierce and Tully 1989; Aaronson and Mould 1983), and a comparison between the PNLF and surface-brightness fluctuation distances for 14 galaxies measured by both methods yields a dispersion of only 0.19 mag, a number consistent with the internal error estimates of the two methods (Sec. 11).

8.3 Method

The identification and accurate measurement of planetary nebulae in external galaxies requires special care which begins with the selection of the narrow-band filter. The best way to image PN in distant galaxies is through an interference filter with a full width at half maximum bandpass of $\sim$30 Å. (Filters much narrower than $\sim$ 25 Å may suppress planetaries which are redshifted onto the filter wings by the velocity dispersion of the galaxy. Broader filters, however, admit too much continuum light from the host galaxy and degrade the signal-to-noise ratio.) Unfortunately, observations of emission-line sources are difficult to calibrate photometrically, and the narrowness of the filter compounds the problem. In order to compare the flux of an emission-line object with that of a continuum source (e.g., a standard star), the transmission of the filter at the wavelength of the emission line must be compared to the filter's mean transmission (Jacoby et al. 1987). This presents a problem, since the properties of a narrow-band filter change with temperature and illumination angle. In particular, a drop in temperature will cause a filter to shift its bandpass to the blue, while fast optics will lower a filter's peak transmission and drastically alter the shape of the transmission curve (Eather and Reasoner 1969). These effects limit the accuracy of PN flux measurements made with a fast beam (e.g., the prime focus of the KPNO and CTIO 4-m telescopes) to a few percent. A complete discussion detailing the difficulties and calibration procedures for narrow-band filters appears in Jacoby et al. (1989).

While the selection and calibration of an appropriate narrow-band filter may be difficult, identifying and measuring planetary nebulae on a CCD frame is relatively easy. PN are visible on λ5007 frames but are completely invisible on comparably deep off-band frames. Thus, by "blinking" the two images, planetary nebulae can be found almost immediately. Unfortunately, it is sometimes difficult to measure faint PN superposed on a bright, rapidly varying background of a galaxy. One method of handling this problem is to use a low-order polynomial to flatten the sky around each object prior to photometry. A more effective technique, which is particularly useful in the bright inner regions of galaxies, is to create a "difference" picture. In this procedure, an off-band image taken through a filter adjacent to λ5007 is scaled to, then subtracted from, the on-band frame, until the background continuum disappears. What is left, aside from the imperfect subtractions of foreground stars, are isolated images of emission-line sources, which can then be measured with either aperture photometry or point-spread-function fitting techniques (cf. Fig. 16). This differencing technique works best if the read noise of the detector is low. Unlike broadband observations for stars in distant galaxies, narrow-band PN images are not always sky-noise limited; hence the subtraction of poor

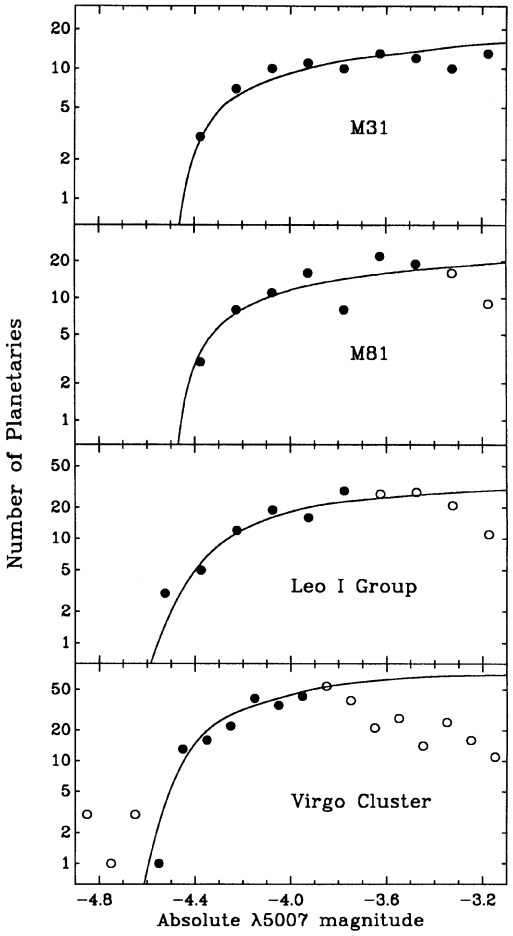

FIG. 15—The observed planetary-nebula luminosity functions for M31, M81, three galaxies in the Leo I group, and six galaxies in the Virgo cluster. Aside from small differences caused by the photometric errors associated with each observation, the shapes of the four functions are identical, demonstrating the form of the PNLF does not depend on Hubble type. Open circles display points which were not used in the solution. The solid lines show the best empirical luminosity functions.

signal-to-noise frames increases the photometric errors. For modern low-noise detectors, however, this additional error is small, and is more than compensated for by the precision of the flattened background (cf. Jacoby et al. 1990).

Once the PN of a galaxy have been identified and measured, their distance can be obtained by comparing their luminosity function to that of M31, as represented by Eq. (18). This can best be done using the method of maximum likelihood (Ciardullo et al. 1989). An analysis of this type, however, requires a proper statistical sample of PN and an appropriate model for the empirical function. Unsharp masks and color maps may be used to exclude objects affected by internal extinction, but a more serious issue concerns the inclusion of objects near the frame limit. Because the detectability of planetary nebulae varies with background surface brightness, the selection of a homogeneous sample of objects requires knowing how the limiting PN magnitude changes with position in the galaxy. Fortunately, Renzini and Buzzoni (1986) have shown that the luminosity specific stellar death rate for a stellar population is insensitive to the population's age, initial mass function, and metallicity. Hence, the probability of finding a planetary nebula at any location within a galaxy should be roughly proportional to the galaxy's surface brightness at that location. Observations in M31, M81, Leo I, and Virgo confirm this conclusion, and offer a direct and simple method of statistically validating a sample of PN candidates. Since the distribution of PN should follow the bolometric light of the host galaxy, if the two distributions disagree, then the sample of PN is either contaminated by the inclusion of spurious images, or, more likely, reduced by incompleteness.

If the PN identification are found to be incomplete, two alternatives are available: one can either use all the data and correct for the incompleteness, or one can restrict the sample to a subset of objects which is complete. The former option is difficult and tedious, and introduces an unnecessary uncertainty. Since PN measurements must be made within the body of the galaxy, the correction factors which are needed depend both on the apparent PN magnitude and the background surface brightness. Procedures which attempt to measure these factors must therefore be two-dimensional in nature and involve a large number of simulations. Fortunately, for most applications, such complex models are not needed. Unlike the globular-cluster luminosity function, whose accurate measurement requires observations as far past the turnover as possible, PNLF distances depend more on the photometry of the brightest objects than the faintest. Thus, while faint PN do contribute to the fit, accurate ($\sim$10%) distances can be obtained with PN measurements that extend only $\sim$1 mag down the luminosity function. This being the case, a simple and straightforward method exists for defining a homogeneous set of planetaries. To create a complete sample, one need only compare the distribution of PN with that of the galaxy light for samples of objects with differing limiting magnitudes. When the two distributions agree, the PN sample can be considered complete (Ciardullo et al. 1989).

After defining the PN sample, the information most needed for modeling the PNLF is some knowledge of how the photometric error varies with magnitude. Since the observed PNLF should be the convolution of the universal PNLF with the photometric error function, this correction, if ignored, can lead to an underestimation of the true distance (Ciardullo et al. 1989). Similarly, if a PNLF survey is conducted in the central regions of a distant galaxy and the model luminosity function does not provide for the occurrence of chance PN superpositions, then the true distance will again be underestimated (Jacoby et al. 1990). Under most circumstances, however, these factors only change the derived distance to a galaxy by a few percent, and, if appropriate care is taken with the photometric measurements and the modeling of PN superpositions, neither effect should be important.

Thus far PN have been used primarily for early-type galaxies. The major reason for this is the possible contam-

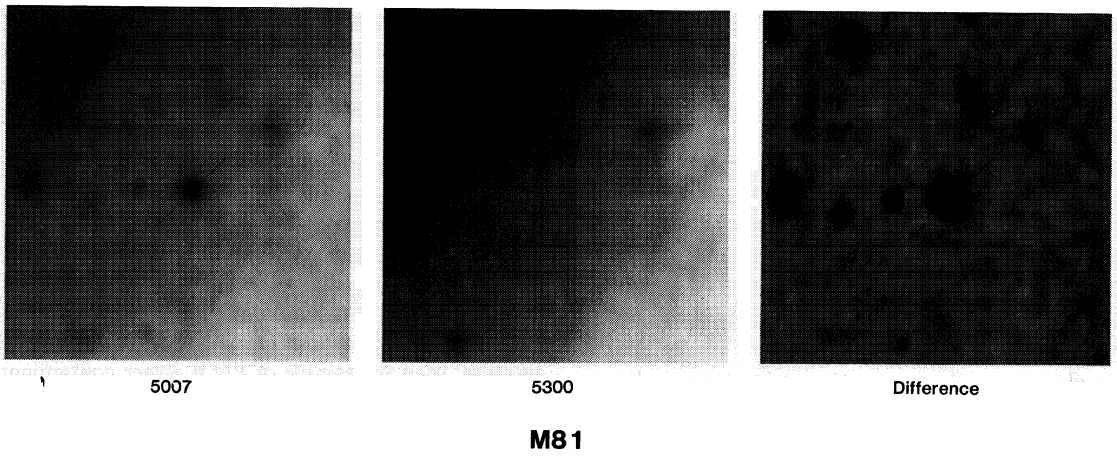

FIG. 16—Difference images are effective tools for identifying faint planetary nebulae in distant galaxies. Displayed is small section of a halo field in M81 obtained with the KPNO 4-m telescope and a TI CCD. The left-hand panel shows the frame in the light of redshifted λ5007, the center panel shows an offband λ5250 image, and the right-hand panel displays the scaled difference between the two images. A bright planetary and two fainter ones are easily visible on the difference frame.

ination of the PNLF by compact H II regions. In their survey of M81's bulge, Jacoby et al. (1989) discriminated between PN and H II regions by requiring that all PN be stellar and have an [O III] λ5007 to Hα ratio much greater than one. The theory behind this is that PN central stars are much hotter than typical OB associations, and their nebulae have much higher excitation temperatures. Unfortunately, some H II regions, such as NGC 2363 in NGC 2366 (Kennicutt et al. 1980) do have high [O III]-to-Hα ratios and at large distances, objects such as these can be confused with planetaries (Ciardullo et al. 1991). For early-type galaxies with few H II regions, the probability of seeing one of these high-excitation objects is small, and, unless the object has an absolute λ5007 magnitude within $\sim$0.2 mag of M^*, its misidentification will not significantly alter the derived distance. (An H II region that is much brighter than M^* can be statistically excluded from the sample on the basis of its deviation from the empirical law. Faint interlopers, on the other hand, are numerically unimportant compared to the population of true PN.) However, in late-type spiral and irregular galaxies, where the total number of H II regions far exceeds the number of bright planetaries, these [O III] bright regions can distort and possibly overwhelm the PNLF. The only way to positively discriminate between H II regions and planetary nebulae in these galaxies is by size—planetary nebulae further than $\sim$2 Mpc away will always appear stellar, even with a diffraction-limited *Hubble Space Telescope*. H II regions, on the other hand, are usually larger than $\sim$20 pc across, and one can hope to resolve them even at distances as large as $\sim$15 Mpc. To do this, PNLF measurements in late-type galaxies must be performed from space, or from a ground-based telescope capable of high spatial resolution.

When an empirical model is compared with an uncontaminated sample of planetaries, two independent variables are fit: the distance modulus, μ, and the total PN population, N. For understanding the three-dimensional distribution of galaxies, the distance modulus is, of course, the more important parameter, but the latter quantity is of considerable interest from an astrophysical standpoint. When the total number of planetaries is normalized to bolometric luminosity, the result is the luminosity-specific PN density, a quantity which is closely related to the population's evolutionary flux and the specific stellar death rate. As mentioned above, Renzini and Buzzoni (1986) have shown theoretically that the luminosity-specific stellar death rate should be insensitive to a population's age, metallicity, or initial mass function. However, the PNLF analyses to date suggest that the rate of PN production correlates with $(U-V)$ index, in the sense that blue galaxies produce more PN per unit luminosity than galaxies with a redder population (Peimbert 1990; Ciardullo et al. 1991; Richer and McCall 1992). If this preliminary result holds true, then this PNLF by-product will be an important tool for helping us to understand the late stages of stellar evolution.

Figure 17 displays contours of probability in distance modulus and PN density for the observed PNLF of the elliptical galaxy NGC 4406 in the Virgo cluster. This result, which is based on a homogeneous sample of 59 PN extending 0.7 mag down the luminosity function, is typical of what is possible with a 3-h λ5007 exposure on a 4-m telescope, with 1″ seeing and a low-noise, blue-sensitive CCD. The displayed 1σ contour corresponds to an uncertainty of $+0.051$, -0.059 mag. However, these contours only reflect the formal internal precision of the fitting procedure. The true error of any PNLF distance determination also includes uncertainties in the standard star measurements and filter calibration ($\sim$0.05 mag), the foreground extinction to the galaxy ($\sim$0.05 mag), the definition of M^*($\sim$0.04 mag), and the distance and extinction to the calibration galaxy, M31 (0.10 mag). Hence, although the precision of NGC 4406's measurement is

$\lesssim 0.06$ mag, the true error in its distance modulus is closer to 0.14 mag.

Implicit in the likelihood contours of Fig. 17 is the assumption that the empirical form of the PNLF, as given in Eq. (18) is correct. Because Bayesian statistical methods only compare probabilities, the solutions which arise from likelihood analyses must also be checked with a χ^2 or Kolmogorov–Smirnov (hereafter referred to as KS) test. If a best-fit empirical law is excluded by such a test, then the maximum likelihood solution must be discarded. Conversely, any alternative law that does not pass a χ^2or KS test cannot be considered viable. It is, in fact, on this basis that the power-law PNLF cutoff proposed by Bottinelli et al (1991) can be rejected at the 5σ level.

As with all stellar-based standard candles, the usefulness of the PNLF method is limited by the size of the telescope, the brightness of the background sky, and, most importantly, by the image quality. With 0".5 seeing on a dark night, a 4-m class telescope can measure PN as faint as $m_{5007} \sim 28.9$ in ~ 3 h. Thus, in theory, galaxies as far away as ~ 30 Mpc can be measured with today's telescopes. In practice, however, the true limit of the PNLF technique is slightly less than this, due to the background luminosity of the host galaxy and the limitations of variable seeing over long exposures. Nevertheless, clusters such as Crater, Pavo-Indus, and even the lower-redshift component of the Centaurus cluster, which stands half-way between us and the Greater Attractor (Lucey et al. 1986; Burstein et al. 1990), should all be measurable with current instrumentation via the PNLF technique.

8.4 Uncertainties

Despite the internal and external consistency exhibited in the PNLF method, the use of planetary nebulae for extragalactic distance determinations is still relatively new and the limitations on the technique are not fully known. One concern about PNLF distances arises from the observations of PN in the Virgo cluster (Jacoby et al. 1990). In these galaxies, there is clearly a small population of overluminous objects which do not fit the $\lambda 5007$ luminosity function. Jacoby et al. arbitrarily excluded these objects from their analysis, stating that their inclusion would shorten the derived distance to Virgo, and degrade the quality of the fits. To date, however, the nature of these objects is not completely known. Observations in NGC 1023 performed in subarcsec seeing suggest that most of these objects are probably chance PN superpositions, compact H II regions, or faint supernova remnants (Ciardullo et al. 1991). However, it is also possible that the overluminous objects represent a low-probability tail to the PNLF. If so, future fits to luminosity functions at larger distances must include this contribution.

A greater concern about the PNLF lies in the uncertain physics of the phenomenon. In every galaxy examined so far, the shape of the rapid cutoff at the bright end of the PNLF is the same. More importantly, the internal and external tests prove that the position of this magnitude cutoff is insensitive to the details of the stellar population.

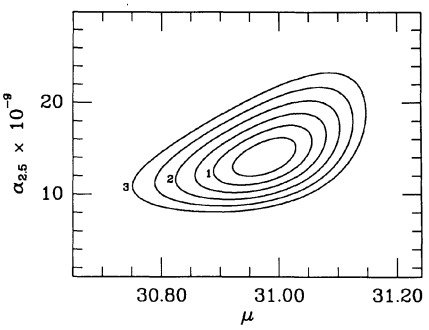

FIG. 17—Probability contours derived from the method of maximum likelihood applied to a homogeneous sample of 59 PN in the Virgo cluster elliptical galaxy NGC 4406. The abscissa is the true distance modulus; the ordinate represents the number of PN within 2.5 mag of the magnitude cutoff M^*, normalized to the amount of bolometric luminosity surveyed. The contours of probability (shown at intervals of 0.5σ) arise from the uncertainty in fitting the model PNLF to the observed luminosity function: horizontal errors reflect the uncertainty in fitting the distance modulus, while vertical errors come from uncertainties in normalizing to the observed number of PN.

This implies that whatever is causing the abrupt magnitude truncation, it does not change much with metallicity or age.

The insensitivity of the PNLF to metallicity is fairly easy to understand. Both the ionizing flux from a PN's central star, and the process of forbidden line cooling in the surrounding nebula depend on metal abundance. In the nebula, the flux emitted at 5007 Å depends on the number of oxygen atoms. However, because oxygen is one of the principal coolants of the nebula, if the abundance of oxygen is decreased, the resulting increase in the electron temperature and collision rate produces an increase in the amount of emission per ion. The result is that the flux emitted at 5007 Å by [O III] is proportional to the square root of the nebula's oxygen abundance (Jacoby 1989). This dependence, however, is almost exactly opposite that calculated for the PN's central star. According to the post-asymptotic branch models of Lattanzio (1986) and Brocato et al. 1990), the maximum luminosity attained by a hydrogen-exhausted core varies inversely with metal abundance, with a factor-of-2 decrease in Z resulting in a $\sim 30\%$ increase in total flux. The net results of these two effects is that distances derived from planetary nebulae should be remarkably independent of metallicity, with $D(\mathrm{PNLF}) \propto Z^{0.06}$! The self-consistent postasymptotic branch models of Dopita et al. (1992) support this analysis, as does the analysis of a metal-poor PNLF formed from observations in the SMC, M32, NGC 185, and NGC 205 (Ciardullo and Jacoby 1992).

The insensitivity of the PNLF to changes in population age and turnoff mass is more difficult to understand. By combining nebular models with postasymptotic giant-branch evolutionary tracks, Jacoby (1989) was able to reproduce the abrupt truncation of the PNLF by assuming a sharp cutoff in the distribution of PN central stars masses. These models show that the PNLF can be recovered if the masses of central stars falloff with a dispersion of σ

$=0.02M_{\odot}$. Dispersions even as large as $0.05\ M_{\odot}$, however, clearly do not fit the data, and although observations of Galactic planetary nebulae (Schönberner 1981; Kaler 1983; Shaw and Kaler 1989) and white dwarfs (Weidemann and Koester 1984; McMahan 1989) do suggest that the distribution of remnant masses is sharply peaked, it is probably not as sharp as what is required. Moreover, most mass-loss laws suggest that the mass of a PN central star depends on the initial mass of its progenitor, but in order to explain all the PNLF observations, this dependence must be virtually nonexistent. Although the measurements of Weidemann and Koester (1983) suggest that for stars with initial mass less than $M<3M_{\odot}$ this might be the case, the PN observations in the Magellanic Clouds and the NGC 1023 group are clearly inconsistent with any PNLF dependence on turnoff mass.

One possible solution to this problem is suggested by the analysis of Magellanic Cloud planetaries by Kaler and Jacoby (1991). These authors have shown that, although the LMC and SMC do contain a number of planetaries with high-mass central stars, when the sample of PN is restricted to those with large [O III] λ5007 fluxes, the mass distribution for central stars *does* agree with the sharp mass cutoff models. The implication is that high-mass remnants must evolve through their high-temperature, high-luminosity phase so quickly that their nebulae never achieve the low densities needed for efficient forbidden line cooling during this phase (Jacoby 1989).

Another possible way of producing a sharp PNLF cutoff which is independent of turnoff mass is through a dredge-up scenario, whereby PN above a certain critical mass have drastically different nebular abundances as a result of previous CNO burning in their envelopes. Such events can increase the emission-line cooling of species such as [N II] $\lambda\lambda$6548, 6584 at the expense of [O III] λ5007 and C III] λ1909 and thereby reduce the [O III] λ5007 flux from high-mass objects by $\sim$0.4 mag. Kaler and Jacoby (1989, 1990) have presented evidence for just such an effect in Galactic and Magellanic Cloud planetaries, but their analysis only deals with nebular abundances, and does not address the question of how envelope CNO burning affects the luminosity and evolution of the ionizing central star.

Still a third mechanism for explaining the PNLF's independence of turnoff mass involves mass loss from post-asymptotic giant-branch stars. The above analyses use as their point of departure the standard postasymptotic branch evolutionary tracks of Paczyński (1971), Schönberner (1981; 1983), and Wood and Faulkner (1986). In these models, the maximum UV flux emitted by a PN central star depends very strongly on its mass (cf. Fig. 14). However, new self-consistent models by Vassiliadis and Wood (1992) which include mass loss at all stages along the evolutionary path suggest that it is possible for stars of widely different initial masses ($1M_{\odot}<M<2.5M_{\odot}$) to converge in the $\log L-\log T_{\rm eff}$ diagram and produce the same maximum UV flux. If this is true, then the invariance of the PNLF to population age is a natural consequence of this degeneracy.

8.5 Future Needs and Directions

At the present time, the most serious deficiency in the PNLF program is a lack of reliable external comparisons. Because the PNLF measurements to date have concentrated on elliptical and S0 galaxies, only three galaxies have both a PNLF and Cepheid distance determination: M31 (the PNLF calibrator galaxy), the LMC (which has a sparse PNLF, and thus a relatively large internal error), and M81 (whose Cepheid distance is based on only two objects with uncertain reddening). Although PNLF measurements in late-type spirals are difficult, such measurements are critical for understanding possible systematic errors in the method.

Also needed for a better understanding of the PNLF are observations of PN in the light of other species. Until now, planetary-nebula luminosity functions have only been measured in [O III] and Hβ. However, one of the best ways of exploring the physics of bright planetaries is to perform observations in [N II] λ6584 and C III] λ1909. Both nitrogen and carbon are important coolants in the nebula, and their luminosity functions are predictable using the modeling techniques of Jacoby (1989). If the dredge-up of partially burned material indeed plays a role in the rapid λ5007 cutoff, then this effect will be reflected in the PNLF of [N II] and C III] as well. For example, if an increase in nitrogen occurs at the expense of carbon in stars above a certain core mass, then this abundance change will not only cause an abrupt truncation in the C III] λ1909 luminosity function, but will also help truncate the [O III] λ5007, since nitrogen becomes very efficient at cooling these objects. The observations of the C III] λ1909 luminosity function in the bulge of M31 will therefore be an important test of this scenario.

9. SURFACE-BRIGHTNESS FLUCTUATIONS

9.1 Background

An image of an elliptical galaxy with milliarcsec resolution would look like an enormous globular cluster, but even when the resolution is a thousand times worse, the discreteness of the stars causes measurable bumpiness in its surface brightness. This phenomenon, dubbed "surface-brightness fluctuations," has been recognized for many years and is sometimes referred to as "incipient resolution." (When there are only a few stars per seeing resolution element, the eye perceives this characteristic mottling as barely resolved stars.)

Observations of external galaxies from which fluxes could be determined for individual stars, drawn from a significant part of the stellar luminosity function, would provide us a wealth of information about the distances of galaxies, their stellar populations, and their formation history. The first steps in this direction were taken by Baade (1944), who first resolved individual Population II stars in Local Group galaxies, and Baum and Schwarzschild (1955) who observed the top of the luminosity function in the bulge of M31 and NGC 205. Improvements of this work include papers by Mould et al. (1983, 1984), by Pritchet and van den Bergh (1988), and by Freedman

(1989). However, the resolution required to observe any but the most luminous stars in galaxies significantly beyond the Local Group will not be achieved in the near future.

Although we cannot determine the fluxes of individual stars without resolving them, we can nevertheless measure a very useful flux that is characteristic of the stellar population. This effect was quantitatively discussed in another context by King (1966) who realized that average profiles of globular clusters could best be determined at the bluest wavelengths where these fluctuations are minimized. Baum (1986, 1990) has investigated the possibility of measuring fluctuation amplitudes by examining the histogram of pixel amplitudes.

The first measurement of surface-brightness fluctuations was by Tonry and Schneider (1988), who described a method by which the fluctuations could be quantified. Subsequent papers include Tonry et al. (1988) which gives additional observations and revised analysis technique, Tonry et al. (1989) which is a first report on 1989 observations of Virgo galaxies using the KPNO 4-m telescope, Tonry et al. (1990) which provides a final analysis of those Virgo observations and describes improved analysis methods, and Tonry and Schechter (1990) who report on fluctuation observations of NGC 5128. Tonry (1991) discusses a completely empirical calibration of fluctuation absolute magnitudes, observations of four galaxy clusters, and the application of fluctuations to the distance scale. Note that the distances in the papers prior to 1991 all need to be corrected to the new, empirical calibration for $\bar{M}_I$.

Surface-brightness fluctuations are fundamentally a very simple effect, and Fig. 18 illustrates this with a cartoon of two galaxies, one twice as distant as the other. A grid representing a CCD's pixels is superposed on the images, and we must imagine that we can only measure the total flux within each pixel. We do not resolve individual stars in this case, but we can measure both the mean flux per pixel and the rms variation in flux from pixel to pixel. The two galaxies cannot be distinguished on the basis of mean flux per pixel (surface brightness) because the number of stars projected into a pixel of fixed angular size increases as distance squared (d^2) and the flux per star decreases as d^{-2}. If N is the mean number of stars, the mean flux is $N\bar{f}$, and the variance in flux is $N\bar{f}^2$, where $\bar{f}$ is a mean flux per star. In Fig. 18, N scales as d^2, $\bar{f}$ scales as d^{-2}, and so the variance scales as d^{-2} and the rms scales as d^{-1}. The galaxy which is twice as distant appears twice as smooth as the nearer galaxy. We can now determine the mean flux $\bar{f}$ as the ratio of the variance and the mean.

The mean luminosity, $\bar{L}$, is simply related to the moments of the luminosity function of the stellar population we are sampling. If n_i is the expectation of the number of stars of luminosity L_i, the average luminosity is the ratio of the second and first moments of the luminosity function:

$$\bar{L}=\Sigma n_i L_i^2/\Sigma n_i L_i \qquad (20)$$

(Tonry and Schneider 1988). This luminosity is roughly that of a giant star, and it is the first ratio of moments which has the dimensions of luminosity and is not dominated by the poorly known faint end of the luminosity function.

9.2 Method

There are two aspects to determining a distance from surface-brightness fluctuations: (1) measurement of a fluctuation flux, and (2) conversion to a distance by assumption of a fluctuation luminosity. The two are coupled, but it is worth discussing them separately because they involve very different problems. It is useful to bear in mind that for typical old, metal-rich stellar populations the absolute fluctuation magnitudes are roughly $\bar{M}_B=+2.5$, $\bar{M}_V=+1.0$, $\bar{M}_R=+0.0$, and $\bar{M}_I=-1.5$, with sensitivity to metallicity and age ranging from very high in B to fairly low in I. The results which are discussed in detail below can be summarized as follows:

(1) This method is applicable to relatively dust-free systems such as E and S0 galaxies, spiral bulges, or globular clusters.

(2) Observation times must be long enough to collect more than 5–10 photons per source of apparent magnitude $\bar{m}$, and the point-spread function (psf) must be well sampled and uniform. The formal measurement errors in $\bar{m}$ can be as small as 3% times the square of the product of psf FWHM (in arcsec) and distance (in 1000 km s^{-1}).

(3) The I band is preferred for distance measurement because $\bar{M}$ is so bright at redder wavelengths that it overcomes the disadvantages of brighter sky background. Use of the I band also minimizes dust absorption. Observations of cluster galaxies shows us how $\bar{M}_1$ depends on mean color: redder populations have fainter $\bar{M}_I$. The intrinsic scatter of $\bar{M}_I$ about this relation appears to be smaller than 0.08 mag.

(4) Calibration of the zero point of $\bar{M}_I$ can be based on theoretical stellar populations, galactic globular clusters, or Local Group galaxies. The latter calibration has been made, and preliminary indications are that the first two will be consistent at the 0.10 mag level.

The basic procedure in measuring a fluctuation flux is to perform the usual observations and reductions so as to obtain an image which is as flat and uniform as possible and for which a photometric calibration is known.

The fluctuation signal grows proportional to time, since we are observing real (albeit statistical) lumps in the galaxies. If we observe long enough to collect several (ideally 10 or more) photons per giant star, we have passed the regime of being dominated by photon-counting statistics into a regime where we are dominated by star-counting statistics. Thus the observation time required is independent of the size of a galaxy, and in the absence of sky background, all points in a galaxy would simultaneously have the same ratio of fluctuation variance to photon-counting variance. If the ratio of sky to galaxy brightness is significant, the number of photons collected per $\bar{m}$ should be increased by one plus that ratio.

We then essentially measure an average flux and an average variance in some region and get a fluctuation flux $\bar{f}$ from the ratio of the two. There are a number of com-

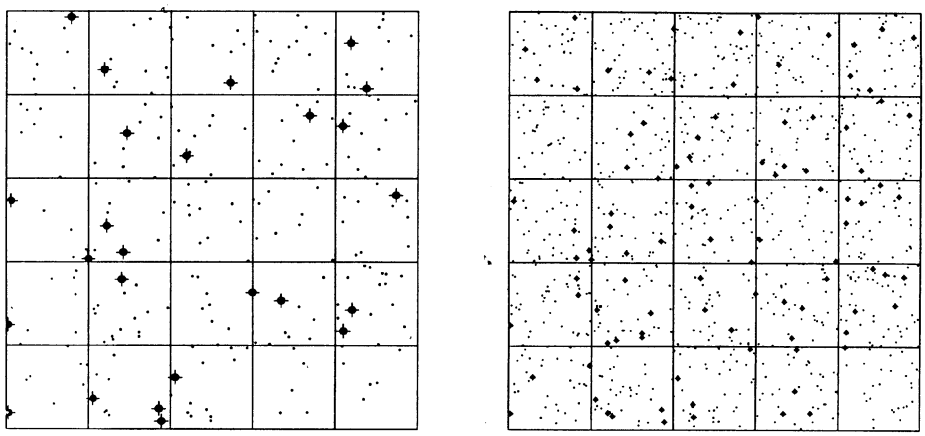

FIG. 18—The schematic galaxy at the right-hand side is twice as distant as the one on the left-hand side. Large dots symbolize giant stars, small ones main-sequence stars, and the grid represents the pixels of a CCD. Although the mean surface brightness collected in a CCD pixel is the same for the two galaxies, since $f \propto d^{-2}$ and $n \propto d^2$, the rms fluctuation from pixel to pixel relative to the mean varies as d^{-1}. The image at the left is about as mottled as an I-band image of a real galaxy would be at its effective radius if the galaxy were 200 kpc distant and the scale of CCD pixels were 1″.

plications: (1) there are many other contributors to variance besides the Poisson statistics of the number of stars present: (2) the image has been smeared by a psf which affects the variance: (3) there is a possibility of the image being mottled or dimmed by dust obscuration: and (4) the assumption that adjacent pixels are independent samples of a stellar population may be comprised by intrinsic correlations such as spiral arms. The details of the measurement are described in Tonry et al. (1990), but some points will be reiterated in order to evaluate the strengths and weaknesses of the method.

Apart from star counts, variance in an image gets contributions from CCD flaws such as traps and bad columns, CCD read noise, and residual flattening problems of CCD images. In addition, each pixel carries Poisson noise from the number of photons collected from the source. Variance also arises from cosmic rays, foreground stars, and background galaxies scattered across the image, and lumps intrinsic to the galaxy being observed such as globular clusters and spiral arms. Patchy obscuration can modulate the flux from the galaxy and create variance, and smooth obscuration can reduce the variance which we measure and hence the flux we derive.

By restricting ourselves to clean E and S0 galaxies we can minimize problems with patchy dust obscuration, but fluctuations can also be measured in spiral galaxies with large bulges, provided that there is sufficient resolution in a blue enough band to determine which regions are contaminated by dust. M31 and M81, for example, have patchy obscuration throughout their bulge. Failure to excise the dust patches which are visible in V-band images of those systems results in an I-band variance which is 10%–20% larger than when the obvious patches are removed. Presumably when the obvious patches have been removed there is negligible power from the remaining obscuration, although this has yet to be tested by using bluer wavelengths or better seeing.

Another advantage accruing from early-type galaxies (or bulges) is that their velocity dispersions are so high that only very dense lumps such as globular clusters survive, and there are negligible pixel-to-pixel correlations from gravitational clumping.

The method by which we discriminate against these unwanted sources of variance is to subtract a smooth fit to the galaxy, remove all areas contaminated by CCD flaws, point sources, and dust, and then measure the variance from the Fourier power spectrum. This has an additional advantage that the zero-wave-number limit of the power spectrum is the power in the image before it was convolved with the psf. Read noise, cosmic rays, and photon statistics all have a white power spectrum which can be distinguished from the power spectrum of fluctuations, stars, globular clusters (GCs), and background galaxies, which have the power spectrum of the psf. The GCs and galaxies remaining in an image at the excision limit are so poorly resolved that there is negligible difference between their power spectrum and that of the psf. Most of the power from patchy obscuration and poor flattening occurs on scales which are very different from the psf and, affecting mainly very low wave numbers, disturb the fluctuation measurement only slightly.

Figure 19 illustrates a power spectrum. The model fitted to the data consists of a constant P_1 (from the white-noise component) plus another constant P_0 multiplying the power spectrum of the psf determined from stars in the image. There is clearly extra noise at very low wave numbers, but there is a substantial range of wave numbers where P_0 is very tightly constrained by the data. The fluctuation variance in the image depends on the product of $\bar{f}$ and the mean galaxy flux; we prefer to scale Fig. 19 by this mean flux so that the power plotted as the ordinate gives us $\bar{f}$ directly in detected photons.

The P_0 component of the variance has contributions P_{flux} from fluctuations and P_τ from point sources remaining in the image. Use of an automated photometry program permits us to find all point sources in the image to some completeness level, excise all objects brighter than that

level, and then examine the luminosity function to estimate P_τ. if we fit a model to the observed luminosity function which allows for stars, globular clusters, and background galaxies, we can consistently estimate P_τ with an accuracy of about 20% from the integrated variance of the model beyond the excision limit. This procedure is illustrated in Fig. 20.

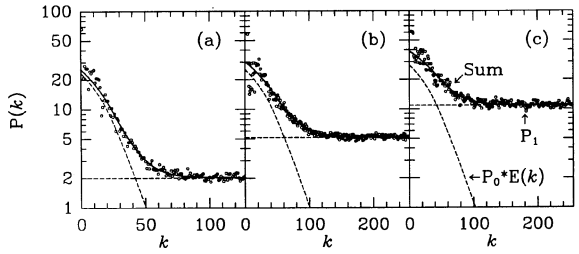

FIG. 19—Azimuthal averages of power spectra from the following three regions of NGC 4552 in the I band: (a) annulus with an inner radius of 64 and an outer radius of 128 pixels, (b) annulus with radii 128 and 256, (c) southeast quadrant of an annulus with radii 256 and 400. The data points are plotted along with the fit to the data and the two components of the fit, $P_0 \times E(k)$ and P_1, where $E(k)$ is the expectation power spectrum for unity fluctuation power. All are scaled by $E(0)$; P_0 is approximately 25 e^- (i.e., each source of apparent magnitude $\bar{m}_I$ contributes about 25 e^- during this 1024-s exposure on the KPNO 4-m telescope). P_0 increases slightly with radius as P_τ increases; the P_1 component increases with radius as the ratio of the sky to galaxy increases.

9.3 Uncertainties

Fluctuation fluxes are subject to the usual photometric calibration errors. Fundamentally, we need to transfer the known magnitude of a standard star to the power spectrum of the psf that we fit to a data power spectrum, since the zero wave number of a power spectrum is just the squared integral of the flux of the psf. Applying the same photometric reduction to the standard star and the psf star accomplishes this transfer with an accuracy of roughly 1%–2%. Uncertainties in atmospheric extinction, galactic extinction, and extinction within the galaxy vary, but can also contribute an error of 1%–2% (or more if there is considerable intervening dust).

There is a substantial systematic error in fluctuation measurements if the fluctuation component of the power spectrum is buried by the white-noise component. The reason for this can be seen by referring to Fig. 19. The variance (power) in fluctuations is equal to the total number of photons collected per pixel times the number of photons collected per $\bar{m}$. The variance due to photon statistics is just the total number of photons collected. In Fig. 19, where the variance has been divided by the mean number of photons per pixel from the galaxy, the photon statistics level is constant with exposure time at 1 plus the ratio of sky to galaxy brightness. The fluctuation signal, however, rises proportional to time. Until the fluctuation signal has cleanly emerged from the photon statistics background at wave numbers which are uncontaminated by low-frequency noise, it is not possible to make an accurate measurement of the fluctuation amplitude. In practice this contributes an error which is roughly 30% of (P_1/P_0), or about 3% if there are 10 photons detected per $\bar{m}$.

Depending on the density of point sources and the depth of the photometry, P_τ may be a large or small fraction of P_0. The fundamental limitation in any photometry is the noise found within a region of area w^2, where w is the FWHM (measured in pixels) of the psf. psf fitting photometry programs such as DOPHOT (Mateo and Schechter 1989) and DAOPHOT (Stetson 1987) approach this limit. The fundamental limitation of observations of point sources seen against a galaxy background is in the fluctuations themselves, because, unlike photon statistics, their amplitude increases proportional to time. When we have reached the point that P_0 emerges from P_1, we obtain no further advantage from longer observations in measuring point sources. These considerations lead to a fundamental photometry limit at a magnitude which depends on the galaxy surface brightness s (magnitude per pixel), the fluctuation apparent magnitude $\bar{m}$, and the signal-to-noise limit η of the point-source detection (typically 5 or greater). This limit is approximately

$$m_{\rm lim} = [(\bar{m}+s)/2] - 2.5 \log(\eta w). \qquad (21)$$

It is a coincidence that, regardless of the distance of a galaxy, the density of globular clusters at the peak of the GC luminosity function turns out to be comparable to that of background galaxies of similar brightness, since the (magnitude) luminosity function of galaxies is roughly a power law of slope -1. Thus we simultaneously have to remove GCs and background galaxies, but we can expect not to be overwhelmed by background galaxies as we push to greater distances. (In fact, in the I band the relative numbers of galaxies to clusters decreases slightly with distance.)

An accurate assessment of P_τ must be carried out for any region that we analyze, but a good rule of thumb is that the P_τ variance per pixel is the square of the flux corresponding to $m_{\rm lim}$ multiplied by the density of point sources $n(m_{\rm lim})$ (number per pixel per magnitude) at $m_{\rm lim}$. At the distance of Virgo, 1 arcsec seeing, with a specific frequency of globular clusters of 6 (number per $M_V = -15$), the residual point sources contribute an error of about 6% in the V and 3% in the I band. Equation (21) shows that, given sufficient observing time to reach the photometry limit, the limiting magnitude depends on the product of distance and seeing. The errors above go roughly as the square of that product.

A source of error which is difficult to assess is the error in P_0 that leaks in from low wave numbers. Sources of this error include poor flattening, uneven sky flux from fringing in the CCD, poor fitting of the mean galaxy profile, or mottling from uneven dust absorption. At the distance of Virgo, the ratio of fluctuation rms to galaxy brightness is about 1% within a 1 arcsec area, and these effects are all small relative to 1%, provided that the detector is good and the seeing is 1 arcsec or better. With worse seeing or at greater distance these effects become appreciable, and they

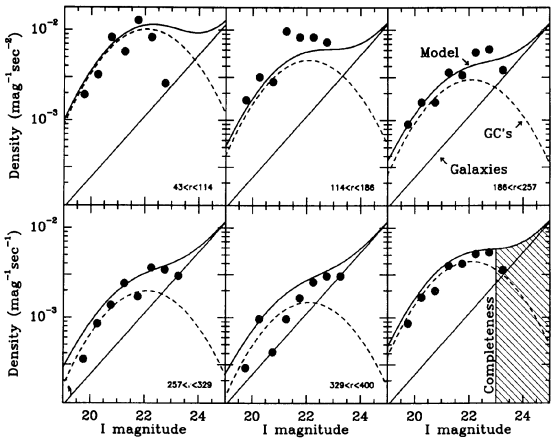

FIG. 20—Luminosity functions of objects in the I image of NGC 4552 in annuli of different radius. Each panel shows as a function of magnitude the observed number density, the model number density, and its two components, globular clusters and background galaxies. The lower right-hand panel shows the luminosity function over the entire area of the image analyzed (although the analysis uses the radially dependent model), and a possible value for $m_{\rm lim}$ is indicated by the completeness line.

are certainly a concern at the 0.2% level, encountered at distances five times that of Virgo. We routinely estimate this contribution by performing the fluctuation analysis on blank sky and looking for excess variance above that expected from residual point sources.

9.4 Calibration

A real strength of the fluctuation method is that it is based on the luminosities of stars for which we think we have a good fundamental understanding. Thus, the luminosities of the stellar populations we observe can be evaluated theoretically or empirically in systems whose distance we know.

Tonry et al. (1990) discussed the fluctuation luminosities of theoretical stellar populations constructed from the *Revised Yale Isochrones* (hereafter referred to as RYI—Green et al. 1987). The results were that the fluctuation luminosity in blue photometric bands depended strongly on the metallicity, age, and IMF of a stellar population, but that the luminosities were quite insensitive to population parameters in the I band. These theoretically calculated values for $\bar{M}_I$ showed a small scatter of about 5% around a mild dependence on the mean color of the population with redder stars having *brighter* $\bar{M}_I$. However, observations of M32 (Tonry et al. 1990) gave $\bar{m}_I=22.81$. If M32 is 0.7 Mpc distant, this corresponds to $\bar{M}_I=-1.42$. These theoretical isochrones predicted $\bar{M}_I=-1.87$ for the $(V-I)$ color of M32, so there was a discrepancy of 0.45 mag.

The numerator in the expression for $\bar{L}_I$ given in Eq. (20) is proportional to the square of the luminosity at the tip of the giant branch and the number of stars there. It appears that the reason for the discrepancy between M32 and the RYI is that the RYI bolometric corrections for these very luminous, very red stars do not adequately account for molecular opacity of their atmospheres at the solar metallicities found near the centers of external galaxies. It seems expedient therefore to abandon temporarily the use of isochrones to calibrate $\bar{M}_I$, and turn to clusters and local group galaxies.

Tonry et al. (1990) found that the Virgo galaxies show a scatter in $\bar{m}_I$ which is consistent with the depth of the Virgo cluster, confirming the expectation that $\bar{M}_I$ is quite uniform (varying less than about 20%), but precluding the possibility of investigating the variation in $\bar{M}_I$ from $\bar{m}_I$. This situation was addressed by Tonry (1991), where observations of the much more compact Fornax and Eridanus clusters permitted this comparison to be made.

Without any correction for galaxy color, the scatter in $\bar{m}_I$ measured among the galaxies in these clusters was about 0.15 mag. The data spanned a range of galaxy luminosity of about a factor of 50, and included both E and S0 galaxies. There was a trend for redder galaxies to have *fainter* $\bar{m}_I$, contrary to the predictions of the RYI. The scatter was reduced to about 0.08 mag about this trend, and a suggestive correlation with galaxy type. The two galaxies observed in the Leo cluster confirmed this predicted trend, but again the Virgo cluster has too much depth to be useful at this level of precision. Nevertheless, the derived distance moduli for Virgo galaxies showed no trend with color or luminosity over a range of 100 in luminosity.

The $\bar{m}_I$ in the bulge of M31, M32, and NGC 205 also confirm this relationship, and give us an absolute calibration. For an assumed distance of 0.77 Mpc, and an assumed A_B extinction of 0.31 mag to M31, Tonry (1991) derived

$$\bar{M}_I=-4.84+3.0(V-I). \qquad (22)$$

This, of course, should be modified for different assumptions about the distance and extinction to M31, and the uncertainty in the zero point depends directly on these assumptions. There also appears to be an intrinsic scatter of about 0.08 mag about this relation. Figure 21 illustrates this relation for the Local Group, Leo, Fornax, and Eridanus clusters by shifting the observed $\bar{m}_I$ by the assumed distance modulus for M31 and the derived relative distance moduli.

Comparison with other distance estimators suggests that this relation is universal. Tonry (1991) found that surface-brightness fluctuation distances agree with the PNLF distances for ten galaxies is common with a scatter in the difference of 7%. The relative mean distances of the four clusters (Virgo, Leo, Fornax, and Eridanus) agree with the results of the infrared TF relations with a scatter in the difference of only 2%. The relative distance between M31 and M81 determined by surface-brightness fluctuations agrees well with the relative distance from Cepheids. Figure 3 of Tonry (1991), however, shows that agreement with the D_n-σ results is much poorer for reasons not yet understood. (We discuss comparisons between the surface-brightness fluctuation distances and the other methods in greater detail in Sec. 11.)

Recent work on the fluctuation luminosity in galactic globular clusters (whose distances can be determined from their horizontal branches) indicates that they also agree with this relation, and can serve to establish the zero point to about 10% (Ajhar 1992). Globular clusters with a metallicity of about 0.1 solar lie just at the intersection of the empirical calibration shown here for galaxies and the RYI calibration from Tonry et al. (1990).

9.5 Future Needs and Directions

Measurements of fluctuation fluxes are accurate in comparison with traditional distance estimators. They are also relatively cheap in terms of telescope time. However, the uncertainties rise rapidly with distance and degraded seeing. Table 2 lists the required observing times and errors in $\bar{m}_I$ (in percent) that we might encounter observing with a CCD on a 4-m telescope in the I band. Note that these numbers assume a galaxy with a typical specific frequency of globular clusters ($S=6$), and do not account for errors which will creep in when we try to push to fluctuations smaller than 0.2% of the overall signal. Under nonideal conditions the errors might be a factor of 2 larger, but they should not be a factor of 3 larger (so the 32% error measurements may be impossible, but the 16% ones are not). The observation times are based on collecting 20 photons per star with a CCD which has 50% QE in the I band.

The most important task for this method is to verify that $\bar{M}_I$ behaves universally according to the trend with color and to calibrate its zero point. The first test can be carried out by observing galaxies in tight groups whose distances are identical. The calibration problem is more difficult. The bulge of M31 has been observed as well as some of the other elliptical galaxies in the Local Group whose distances are known, but we must worry about possible systematic differences between calibrator (primarily the bulge of M31) and application (primarily giant ellipticals). An important test will be observations of a number of other spiral bulges such as NGC 7331, NGC 4565, NGC 4594, NGC 3368, and NGC 2841, which can be compared with their elliptical neighbors or with other distance estimates. Preliminary results from observations of $\bar{M}_I$ in the bulges of NGC 3031, NGC 4565, and NGC 4594 show no discrepancy with the current calibration with mean color. It is also possible to use galactic globular clusters as calibrators as well as clusters in the LMC and SMC, but even the most metal-rich clusters will have brighter M_I than most galaxies.

There are potentially large improvements in the theoretical calibration of $\bar{M}_I$. Improved theoretical isochrones at solar metallicity and better observations in the I band to which bolometric corrections can be tied are necessary. The connection between fluctuations and actual stellar populations in Local Group galaxies needs to be improved. Freedman (1989) has reported observations of the brightest two magnitudes of the luminosity function of M32, and with slightly deeper observations $\bar{m}_I$ could be calculated directly from Eq. (20).

There is some potential for improving the measurement of $\bar{m}$. The dominant source of error comes from the residual point sources, and there are a number of approaches that may improve the situation. Since the fluctuations are redder than most point sources, the point sources can perhaps be identified in a blue image and excised from the I-band image. This leads to difficulties with the unknown colors of the unseen sources, but some improvement should be possible. Improvements in seeing are enormously helpful; they not only make the point sources easier to detect, but they also make the fluctuation amplitude larger. This is an important consideration at distances greater than about three times that of Virgo, because it is difficult to obtain a CCD image which is flat and unfringed at the 0.3% level.

As infrared arrays improve, it will be worthwhile observing in the K band. $\bar{M}_K$ is very bright, $\bar{M}_K \approx -5.6$ (Luppino and Tonry 1992), and the seeing is typically better in the IR. Thus the fluctuation signal is substantially larger, both in absolute terms and relative to point sources for which $(V-K)\approx 3$. The variability of $\bar{M}_K$ with stellar population is currently unknown, but $\bar{M}_K$ in M31 and M32 differ by only 0.3 mag. A significant drawback is that the sky is substantially brighter in the K band, $(V-K)=7$–8, but of course the extinction due to dust at K is smaller by about a factor of 4 relative to the I band.

In the future we can hope to be able to observe with a psf whose FWHM is 0.1 arcsec or better and with CCDs capable of signal-to-noise ratios significantly better than 1000. Such an observation could measure the fluctuations in a galaxy at 20 000 km s^{-1} distance with sufficient accuracy that it would just be possible to determine peculiar velocities and to resolve the depth of a cluster of galaxies. Until that time we will have to be content with high accuracy in our own supercluster and vicinity.

10. THE D_n-σ RELATION FOR ELLIPTICAL GALAXIES

10.1 Background

The use of elliptical galaxies as distance indicators developed from studies aimed at determining their physical properties. The discovery of the relationship between luminosity and central velocity dispersion, $L \propto \sigma^4$, by Faber and Jackson (1976) marks the beginning of the potential use of normal elliptical galaxies as standard candles. Following that discovery, automatic, quantitative techniques based on Fourier or cross-correlation methods for measuring velocity dispersions came into frequent use (Sargent et al. 1977; Tonry and Davis 1980; Davies 1981). The use of these quantitative methods led to a growth of work on the properties and distances of elliptical galaxies, notably the suggestion by Terlevich et al. (1981) of a second parameter at work in the Faber–Jackson relation and the use of that relation by Tonry and Davis (1981) to measure the infall of the Local Group towards the Virgo cluster. The uncertainty in the distance to a single galaxy in Tonry and Davis' use of the Faber–Jackson relation was 32%.

Further work investigating the nature of the second parameter in the Faber–Jackson relation led to the develop-

ment of the D_n-σ relation, where the diameter D_n incorporates both luminosity and surface brightness into a single parameter (Dressler et al. 1987b). The largest uniform body of D_n-σ data was collected in the first half of the 1980's by the collaboration which has become known as the "7 Samurai" (7S) and is to be found in Davies et al. (1987) and Burstein et al. (1987); the work is summarized in Faber et al. (1989). The data formed the basis for the first and currently most extensive application of the method. They combined velocity dispersions measured using quantitative analysis of digital spectra with diameters derived from concentric aperture photoelectric photometry and some CCD photometry. By incorporating surface brightness as the second parameter in the Faber–Jackson relation they formulated a new distance indicator, σ^x/D_n (Dressler et al. 1987b), where D_n is defined as the diameter which encloses a mean blue surface brightness of 20.75 mag per square arcsec. [Lucey (1986) had noted previously that the use of *fixed* aperture magnitudes in the L, σ relation produced a smaller scatter than the use of total magnitudes.] D_n provides a convenient and close to optimum way of combining luminosity and surface brightness into a single parameter (see Sec. 10.3.1).

The mean surface-brightness level for D_n was chosen to minimize the scatter in the new distance estimator and had the advantage that the aperture photometry measurements frequently spanned the diameter value, allowing D_n to be determined by interpolation using the $r^{1/4}$ law curve of growth. For the 7S sample the uncertainty in relative distance to a single galaxy was 23%. The 7S used these data to measure the pattern of peculiar motions of galaxies and clusters over the whole sky out to recession velocities of 8000 km s^{-1} in the reference frame of the cosmic microwave background. They discovered a large-scale coherence to this pattern (Dressler et al. 1987a), from which they inferred that galaxies in a large volume partake in a large-scale flow towards $l=307°$, $b=9°$ (Lynden-Bell et al. 1988, hereafter referred to as LFBDDTW). They postulated that this flow arises from the gravitational attraction of an overdense region centered on 4500 km s^{-1} extending to the Local Group which Alan Dressler named the "The Great Attractor." Subsequent studies using the method have centered on attempts to confirm (or negate) the existence of the Great Attractor. A review of the status of the Great Attractor is beyond the scope of this discussion; a description of a modified Great Attractor model can be found in Faber and Burstein (1989) and a comprehensive evaluation of the present situation can be found in Burstein et al. (1990, hereafter referred to as BFD).

The availability of sensitive, linear CCDs on small telescopes together with the development of sophisticated analysis software has led to the accurate photometric measurement of luminosity and effective radius (R_e) for a large number of elliptical galaxies (e.g., Lauer 1985; Djorgovski 1985). Both Lauer (1985) and Djorgovski and Davis (1987) discovered the same second-parameter relation for elliptical galaxies independently of the 7S (see Faber et al. 1987) using data of this kind. Djorgovski and Davis (1987) introduced the idea of elliptical galaxies populating

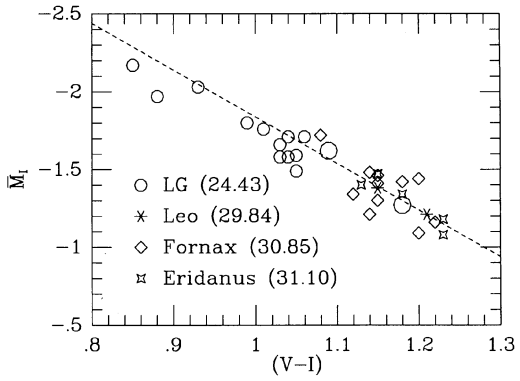

FIG. 21—$\bar{M}_I$ is plotted for cluster galaxies as a function of mean galaxy color ($V-I$). The adopted distance modulus for each cluster is indicated in parentheses. The Local Group (LG) galaxies M31 (red) and M32 (blue) are shown as larger symbols; different patches of NGC 205 comprise the remaining LG points.

a "fundamental plane" in the log L-log R_e-log σ space, so that the Faber–Jackson relation is the projection of that fundamental plane onto the L-σ plane. Note that while both methods rely on the correlation of a global parameter (luminosity and surface brightness) with the velocity dispersion determined *locally* at the galaxy center, the method works in a statistical sense as there is a good correlation between the central value of velocity dispersion and that averaged over a more representative volume of the galaxy.

CCD imaging data provide (1) the potential for a more complete photometric characterization of the galaxy and therefore sensitivity to peculiarities in the morphology (e.g., Bender et al. 1989; Peletier et al. 1990), (2) a post-observing opportunity to remove superimposed interfering star and galaxy images, and (3) a greater control over the way in which photometric parameters are determined. These advantages make CCDs the detectors of choice for future work despite the increase in reduction and analysis effort and the added overhead required for absolute calibration.

The distribution and physical properties of elliptical galaxies make them attractive as potential distance indicators because of the following:

(1) They are luminous galaxies so that their global properties can be measured accurately at large distances. The D_n-σ method can be used to measure distances both within the Local Supercluster and out to distances more than twice that of the Coma cluster.

(2) They are strongly clustered so that many galaxies can contribute to the determination of the distance to an aggregate of galaxies. This increases the precision of the distance estimate and reduces systematic "Malmquist-like" biases.

(3) They have a single old stellar population and are free of the obscuring effects of dust.

The method is, however, potentially sensitive to variations in the physical properties of ellipticals: residual star formation, the unknown distribution of intrinsic shapes, variations in the degree of rotational support, the presence

TABLE 2
Observation Times and Uncertainties

Distance		Obs. time	Flux Error (percent) — psf FWHM —		
(km/s)		(min)	1.5"	1.0"	0.5"
700		4	4	3	3
1000	(Leo)	8	5	4	3
1400	(Virgo)	15	9	5	3
2000	(Eridanus)	30	16	9	4
2800	(Centaurus)	60	32	16	5
4000	(Great Attractor)	120	–	32	9
5600	(Perseus)	250	–	–	16
8000	(Coma)	500	–	–	32

of central-velocity dispersion anomalies, and/or the presence of a weak disk.

Unfortunately there are no nearby examples of luminous elliptical galaxies that can be used for absolute calibration using primary indicators. Furthermore, there is no theoretical basis for an absolute calibration of the D_n-σ relation. Thus, the method is best suited to measuring *relative distances* that can then be calibrated by some of the other methods discussed elsewhere in this review. For this reason the method has been applied primarily to measure the peculiar motions of galaxies and aggregates of galaxies, rather than to derive absolute distances for individual galaxies.

10.2 Methods

10.2.1 Precision of and Corrections to Measured Quantities

The implementation of the D_n-σ method requires the measurement of the central-velocity dispersion and luminosity profile (or curve of growth) of each galaxy to sufficient precision that the measurement errors do not contribute to the intrinsic uncertainty of the distance estimator ($\sigma^{1.2}/D_n$). LFBDDTW report a typical scatter of 23% in D_n at fixed σ. Their single measurements of D_n range in precision from 5% to 12% and for σ from 9% to 14% (these estimates were made from repeat measurements which were used to improve the precision). Single measurements of this quality would contribute significantly to the scatter in D_n in the best observed clusters. A reasonable aim for future work is to determine D_n to 6%, and σ to 5%, which in the absence of cosmological scatter would generate a distance determination with an uncertainty $\leqslant 9\%$.

If the peculiar motions of aggregates of galaxies (hypothesized to be at the same distance) are to be determined, then a measurement of recession velocity is required in addition to the parameters which enter into the distance estimator. (Of course, this can be obtained from the same observational data that was used to derive the velocity dispersions.) The measured galaxies must then be assigned to groups on the basis of position and recession velocity using an algorithm (e.g., Geller and Huchra 1983).

Observationally determined values of σ and D_n need to be corrected as follows:

(1) For galaxies covering a range of distances the σ values need to be corrected to a single linear aperture size. This is a statistical correction which, in the mean, accounts for the variation of velocity dispersion as a function of radius in individual galaxies. The corrections are determined using simulated large aperture measurements on the closest galaxies of a sample (see Dressler 1984). The correction is small, 5% between Virgo and Coma (Davies et al. 1987), and will be smaller still for a sample of distant ellipticals. In some cases where radial dispersion profiles are available for many galaxies in a cluster, global values, rather than central values, of the dispersion have been used to reduce the scatter in the D_n-σ relation (Jacoby et al. 1990).

(2) The aperture magnitudes or luminosity profile must be corrected for absorption in the Milky Way. There is a straightforward and accurate prescription for this (Burstein and Heiles 1978) that is satisfactory for most of the sky. In regions where the absorption is large it may be difficult to determine a value with sufficient precision. However, the uncertainty in the correction may contribute to the apparent complexity of galaxy motions in the Centaurus region, where A_B can be as high as 0.47 mag (BFD; Lucey et al. 1989). By measuring diameters in redder bands (R and I), the size of this uncertainty can be reduced.

(3) The aperture magnitudes or luminosity profile must be corrected for K dimming, the cosmological surface-brightness dimming, and other cosmological effects (that depend on the precise cosmological model chosen). These corrections are very small for the nearby samples of ellipticals so far studied and are discussed in Appendix A of LFBDDTW.

Finally LFBDDTW report that galaxies with extreme properties show increased scatter in the distance estimator and they did not use them. They eliminated galaxies having $\sigma < 100$ km s^{-1} and effective surface brightness higher than $B = 19.5$ mag arcsec^{-2}. Low-velocity dispersion galaxies exhibit an increased diversity of physical properties. For example, they exhibit a larger spread in color and a higher frequency of emission lines, indicating that they do not form a homogeneous class of objects and the D_n-σ method should not be applied to those galaxies.

10.2.2 Correction For Biases

In principle, once the above corrections have been applied, the D_n-σ method can be used to estimate relative distances. However, there are two selection biases, which potentially afflict any sample of galaxies chosen in a diameter- or magnitude-limited way, that require correction. The first, a "Malmquist-like" bias, affects principally those galaxies which are not in rich clusters. As there are more galaxies at greater distances in any sample limited by diameter or apparent brightness, there will be more large/bright galaxies erroneously included in the sample from larger distances than there are galaxies omitted from the sample at smaller distances. Thus, a diameter-limited sample is contaminated by galaxies that are measured to be large for their dispersion. This generates the illusion that galaxies are nearer than their true distance and would generate spurious positive peculiar velocities. Unless cor-

rected, the effect of this would be to introduce a *scale* change as if to *overestimate* the Hubble constant. LFBDDTW show that the correction for this depends on the size of the dispersion in the distance estimator (i.e., $\ln D_n$), Δ, and on the distribution of galaxies. If the latter is parameterized as a power law in number density such that the number of field galaxies in an annulus between r to $r+dr$ is $n(r)dr/r$, so that

$$n(dr/r) \propto r^{(\alpha-1)}\, dr \tag{23}$$

(for a uniform distribution of galaxies $\alpha=3$), then the correction for the bias is given by Eq. 2.11 of LFBDDTW:

$$d=d_e e^{(\alpha+1/2)\Delta^2}, \tag{24}$$

where d_e is the raw estimate of the distance and d is the corrected value. The correction is smaller for aggregates of galaxies, falling as $1/N$ when there are N galaxies with independently estimated distances d_e.

The second correction is applied only to galaxies in clusters where the selection by diameter causes the cluster to have an overrepresentation of large galaxies and an underrepresentation of small ones. LFBDDTW estimated the size of the correction for this effect by combining the galaxies with $\sigma > 100$ km s^{-1} from clusters containing three or more galaxies using the preliminary distance estimates and then by truncating the sample at a range of diameters. The correction factors are tabulated in their Appendix B and are typically a few percent for aggregates at 6000 km s^{-1}.

The steps outlined above allow relative distances of aggregates of galaxies to be determined self-consistently and accurately from D_n-σ data for individual and cluster elliptical galaxies. This is one of the two methods of Aaronson et al. (1982): distances are calculated from the distance estimator and the parameters of the flow model are derived by maximizing the likelihood in the velocity-field residuals. The second method of Aaronson et al. (1982) (discussed in the context of the D_n-σ method by LFBDDTW and by Faber and Burstein 1989), involves determining the distance to galaxies on the basis of the observed velocity and a model of the velocity field and using this to predict the velocity dispersion for a given diameter. The model parameters are determined by maximizing the likelihood in the D_n-σ relation. The two methods each have advantages depending on the exact application being pursued; Faber and Burstein (1989) give an extensive discussion of the pros and cons of each method and develop a hybrid approach.

10.3 Physical Basis

10.3.1 Power-Law Relationships

There is no complete physical description of the structure and kinematics of elliptical galaxies. However, starting from some simple physical assumptions a rudimentary justification of the method can be provided. Sargent et al. (1977) pointed out that the assumptions that all elliptical galaxies have the same surface brightness, $L \propto R^2$ (Fish 1964) and mass-to-light ratio (M/L), together with the virial theorem relation $M \propto R\sigma^2$, lead to the Faber–Jackson relation $L \propto \sigma^4$. These ideas were extended by Djorgovski and Davis (1987) and Dressler et al. (1987b) who developed the concept of a fundamental plane in the 3-space of $\log I_e$, $\log R_e$, $\log \sigma$, where I_e is the galaxy surface brightness within the half-light radius, R_e (or diameter A_e). Combining the results of these three studies, the equation of the fundamental plane is

$$R_e \propto \sigma^{1.36} I_e^{-0.85}, \tag{25}$$

or expressed in terms of a modified Faber–Jackson relation:

$$L \propto \sigma^{2.7} I_e^{-0.7}. \tag{26}$$

As Dressler et al. (1987b) show, there are only two independent parameters in the three observables A_e, D_n, and I_e so that D_n/A_e is a function of the normalizing surface brightness only. They find $D_n/A_e \propto I_e^x$, where $x=0.8$. This, together with the empirical (D_n-σ) relation, leads to a formulation of the modified Faber–Jackson relation which is almost identical to Eq. (26). Thus the definition of D_n combines the parameters of the fundamental plane in such a way that it is viewed edge-on and D_n is therefore a close to optimal distance indicator. This is illustrated in Fig. 22 which shows the fundamental plane and its projections, taken from Faber et al. (1987). They point out that the existence of the fundamental plane implies there are no constraints on the global parameter relations for elliptical galaxies other than the Virial theorem. This is perhaps the most important difference between the D_n-σ relation and the Tully–Fisher methods; the latter, being a single-parameter relationship, requires the action for an extra physical constraint which is presumably set during galaxy formation (Gunn 1988). Thus the D_n-σ relation depends on the physics of galaxy equilibrium rather than the physics of galaxy formation.

The D_n-σ relation cannot be justified in terms of a detailed physical model such as can be formulated for type-Ia supernovae or Cepheids. A general physical description has been formulated using power-law relationships between the structural and kinematic variables that illustrates the sensitivity of the method to the assumptions.

10.3.2 Possible Systematic Effects

Here we discuss the physical effects that could systematically bias the method rather than systematic effects in the data which are covered in Sec. 10.5. A thorough discussion of possible systematic effects is presented in the Appendix to BFD where they investigate the dependence of the D_n-σ relation on absolute magnitude, mass-to-light ratio, and cluster properties. They found no significant effects; their plot of residual radial velocity versus galaxy absolute magnitude is reproduced in Fig. 23. Mass-to-light ratio and cluster effects are discussed below.

The constraints on M/L implied by the existence of the fundamental plane led Silk (1989) to suggest that the environments of ellipticals might act to modify M/L and thus cause the zero point of the D_n-σ relation to vary within a cluster or between clusters. Silk proposed that such an effect might introduce spurious large-scale motions. This possibility has been tested by Lucey et al.

(1991b) who found no significant systematic dependence on the zero point of the relation over a factor of 150 in projected local-galaxy density in the Coma cluster. Similarly BFD found no dependence of the peculiar velocity of cluster ellipticals on M/L (as characterized by the strength of the Mg_2 index of the stellar population at a given σ). There are hints in BFD that in a minority of field and group ellipticals the global parameters, in particular line strengths, might be altered by the presence of an intermediate age population. Schweizer et al. (1990) noted that the presence of fine morphological structures (jets, shells, isophote distortions) also loosely correlate with indicators of the age of the stellar population such that galaxies exhibiting fine structure appear to have a younger component, which they suggest was formed at the same time as the event that generated the structure. Gregg (1992) has taken this further and demonstrated that those few galaxies with the most marked morphological peculiarities have systematically positive peculiar motions. While the number of affected galaxies appears to be very small, the effect of these correlations on the application of the D_n-σ method needs to be evaluated further.

Djorgovski et al. (1988) investigated the possibility that cluster properties such as richness, velocity dispersion, and density might affect the form of the D_n-σ relation. They tentatively suggested that cluster richness caused a variation in the slope and intercept of the relation within clusters, possibly due to the effects of interactions. However, these effects were not confirmed by BFD (see Fig. 24) and are not present in the detailed study of the Coma cluster by Lucey et al. (1991b).

The overall agreement of other distance indicators with D_n-σ (see Sec. 11) tends to confirm that environmental effects are not generating mythical large-scale flows. Indeed, a remarkable set of coincidences would be needed to explain the large-scale pattern of peculiar motions in terms of small M/L changes. This is not to say, however, that there are no clusters where the distance determined by D_n-σ is discrepant with that of another method. The most serious case is Abell 2634, where Aaronson et al. (1986) find the cluster to be at rest with respect to the Hubble flow, and Lucey et al. (1991a), using a D_V-σ relation (based on V-band photometry rather than B-band observations), find a peculiar velocity of $> +3000$ km s^{-1}. Such discrepancies need to be resolved.

On balance it seems that environmental effects have not been shown to bias D_n-σ as a standard candle but the absence of a detailed physical model to describe the method demands continuing care to ensure that such systematic effects do not enter into the future application of the method.

10.4 Calibration

There are no elliptical galaxies near enough to the Milky Way to be used for absolute calibration. M32 has both too low a central dispersion ($\sigma < 100$ km s^{-1}) and too high a surface brightness ($I_B < 19.5$) to be a candidate. Furthermore, because the D_n-σ method carries a relatively large uncertainty for distances to individual galaxies, a large number of calibrators would be required to reduce the zero-point uncertainty to $\lesssim 10\%$.

Three attempts have been made to tie the D_n-σ distances to other scales. Dressler (1987) argued on the basis of samples in the Virgo and Coma clusters that the D_n-σ relation for the bulges of S0's and early-type spirals is identical to that for ellipticals. To minimize the effects of disk contamination and dust he used diameter measurements based on a mean enclosed blue surface brightness of 19.75 and calibrated his relation using CCD frames of M31 and M81 and photoelectric photometry from the literature. Using bulge-velocity dispersions of $\sigma = 150$ km s^{-1} for M31 (McElroy 1983) and $\sigma = 166$ km s^{-1} for M81 (Whitmore et al. 1984), and distance moduli of 24.2 for M31 and 27.5 for M81, he estimated the distance to Virgo as 21.3 and 18.3 Mpc from these two galaxies, respectively.

Pierce (1989) calibrated the luminosity–surface brightness–velocity dispersion relation (Djorgovski and Davis 1987) in the Leo I group by assuming a distance of 10.0 ± 1.0 Mpc based on the planetary-nebula luminosity function (Ciardullo et al. 1989). [The distance estimate is in excellent agreement with the distances derived from the globular-cluster luminosity function (10.7 Mpc; Harris 1990), the Tully–Fisher relation (10.5 Mpc; Bottinelli et al. 1985), and the surface-brightness fluctuation method (9.3 Mpc; Tonry 1991).] This calibration gave a distance of 14.1 ± 1.6 Mpc to Virgo and 13.5 ± 2.2 Mpc to Fornax. If the same Leo distance is used to calibrate the D_n-σ relation and the model of LFBDDTW, the distances to Virgo and Fornax become 15.5 ± 2.2 Mpc and 16.6 ± 2.2 Mpc, respectively. The values for Virgo are in good agreement, and, although the Fornax numbers differ by 20%, they fall within the mutual error estimates. Note, however, that two estimates are not completely independent, since Pierce utilized the velocity-dispersion measurements from Whitmore et al. (1985) and the 7S.

More recently Tonry (1991) has used a new calibration of the surface-brightness fluctuation method (SBF) to determine the distances of four groups or clusters (Leo, Virgo, Fornax, and Eridanus) with respect to that of M31 and M32 which he took to be 0.77 Mpc. He then compared these distances to those derived from the planetary-nebula luminosity function (PNLF), infrared Tully–Fisher (IRTF), and D_n-σ methods. The agreement between the SBF and the PNLF method (on a galaxy-by-galaxy basis) was found to be excellent, consistent with the error estimates. Surprisingly the agreement between SBF and IRTF (on a group-by-group basis) was better than would be expected on the basis of the error estimates (but see Sec. 11). The agreement with the D_n-σ method, was found to have greater scatter as would be expected from the larger uncertainty of the D_n-σ method, but with the additional anomaly that the distance estimate to Eridanus derived from the D_n-σ method is greater (by three standard deviations) than from either the IRTF or SBF methods. This difference is difficult to explain other than by noting the small number of galaxies (five) available for the comparison. Note, however, that in Sec. 11 we show that overall

D_n-σ compares to other distance indicators as expected from the error estimates.

10.5 Uncertainties

There are a number of possible sources of uncertainty that enter into the derivation of distances from the D_n-σ relation. These are as follows:

(1) The uncertainty in the estimate of galactic absorption. This can be minimized using red bands (e.g., R, I, or H) for the photometry. The uncertainty is generally small, although in some directions (e.g., in Centaurus), an error of 0.05 mag in the B-band absorption estimate may arise.

(2) The uncertainty associated with assigning particular galaxies to a group. This can be evaluated by perturbing the algorithm used and noting the changes in distance estimates that arise. Assuming that redshift is the basis for the membership criterion, the error in recession velocity enters into the uncertainty, but this is typically too small (<30 km s^{-1}) to contribute significantly to the overall uncertainty.

(3) Perhaps the largest and most easily remedied uncertainty is associated with the precision of measurement of D_n and σ. Diameter- and velocity-dispersion measurements for the more distant clusters are relatively poorly determined. The data of the 7S are such that for the most distant clusters, the errors of measurement contribute to the overall scatter in the D_n-σ relation. Lucey et al. (1991a) have reported measurements of D_n and σ in A2199 that differ systematically from those reported in the 7S work. Lucey et al. find dispersions that are 10% smaller and diameters that are 7.4% larger, leading to an estimate of the distance to A2199 that is 20% smaller than that of the 7S. A2199 is one of the most distant clusters studied to date and exhibits the largest discrepancy of this type in the literature. As studies using the D_n-σ method probe to greater distances, measurements of a quality that result in a reliable and reproducible distance indicator are required.

(4) The degree of physical uniformity of the samples of galaxies. This has been discussed in Sec. 10.2 where mass-to-light ratio, absolute magnitude, and galaxy environment were considered. Other factors that could bias or add scatter to the D_n-σ method include the unknown distribution of intrinsic shapes, the degree of rotational support, the presence of additional subcomponents (e.g., independent cores, disks, or other isophote distortions), and possible dispersion anomalies at the core. Given the uncertain physical basis of the method, continuing searches for systematic effects are appropriate.

(5) The distribution of galaxies is not uniform and yet the treatment described in Sec. 10.2 assumes a correction for a bias which is based on a uniform distribution. The bias can work with either sign; on the near side of a concentration of galaxies the correction required acts to *increase* the estimated distances whereas on the far side the correction acts to *decrease* the estimated distances. Clearly this effect is potentially highly misleading in regions with large galaxy-number density contrasts. An illustration of this is given in BFD. The size of the uncertainty introduced will depend on the distribution of galaxies in any given sample and will vary around the sky.

(6) Seeing can systematically bias the measurement of diameters. D_n is defined by the mean surface brightness it encloses, and as seeing reduces the mean surface brightness at all radii, seeing biases measurements of D_n to smaller values. Saglia et al. (1992) are investigating the magnitude of this effect. Although Lucey et al. (1991a) apply a seeing correction to their data on Abell 2199 and Abell 2634, the 7S did not make such a correction. The initial simulations of Saglia et al. (1992) indicate that in the regime where the seeing diameter is a substantial fraction of the half-light radius, say $(D_{\rm seeing}/R_e)=0.5$, a substantial seeing correction is necessary amounting to approximately 4% when the true D_n is equal to A_e. Thus seeing can cause diameters to be underestimated and therefore distances overestimated.

10.6 Future Needs and Directions

There are several topics which need to be addressed to provide a firmer basis for the use of the method.

(1) Perhaps the most pressing need is for more high-quality, multiple observations of galaxies in clusters to test the reproducibility and precision of the diameter and dispersion measurements and to determine the limiting scatter in the relationship. Apparent differences between authors on the distance to the same cluster (e.g., Abell 2199) and differences between the IRTF and D_n-σ method (e.g., Abell 2634) must be resolved. A substantial amount of work is under way that will address these points: a survey of clusters in the Hercules and Pisces-Cetus region is being undertaken by the EFAR collaboration of Baggley, Bertschinger, Burstein, Colless, Davies, McMahan, Saglia, and Wegner; Lucey and collaborators are also studying a sample of more distant clusters.

(2) Investigations into possible systematic effects that may affect the D_n-σ method must be continued. Differences in star-formation history, structure, or kinematics need to be explored.

(3) The effect of seeing on the measurement of D_n needs to be quantified in a realistic way. Model point-spread functions may not adequately describe the smoothing that occurs. Work by the EFAR group is under way in this area.

(4) The canonical form of the D_n-σ relation must be determined more precisely. Is a simple power law an adequate representation? Is curvature present at low luminosities? The Coma cluster appears to provide the best opportunity for establishing these relationships.

(5) Is it possible to include other early-type galaxies to improve the estimation of distance to galaxy aggregates? Several studies have utilized lenticular galaxies: Dressler's (1987) discussion of Coma and Virgo, the exploration of the far-side of the Great Attractor by Dressler and Faber (1990b), and the recent work on distant clusters by Lucey et al. (1991a) suggests that disk galaxies can be used. The expansion of the technique to include galaxies spanning a wider range of properties has two positive implications. The number of galaxies in an aggregate would typically be

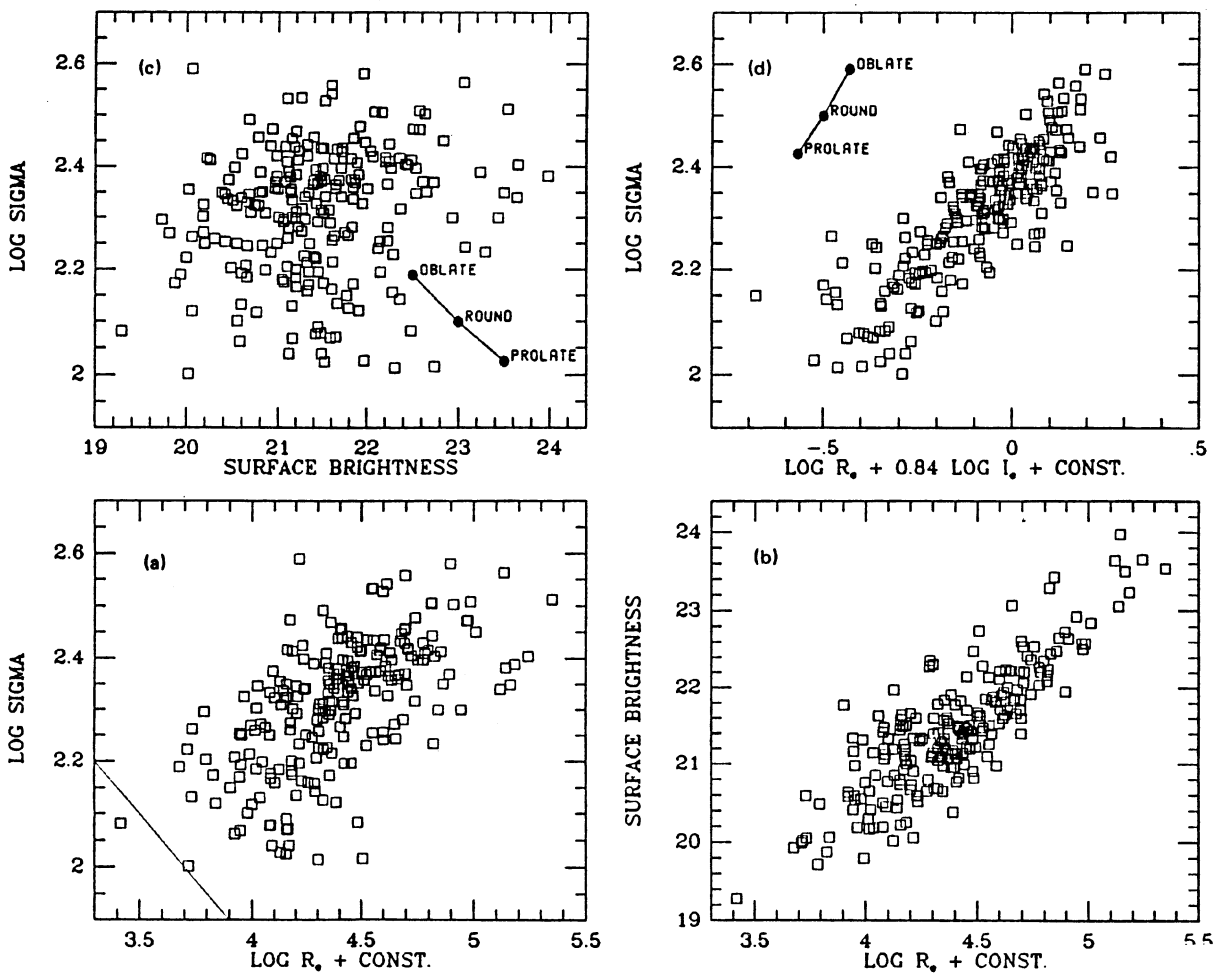

FIG. 22—Structural parameters for group galaxies in the 7S survey, taken from Faber et al. (1987). (a) log σ vs log R_e; the diagonal line of slope -0.5 is the constant mass locus. (b) Surface brightness vs log R_e, showing the fundamental plane almost edge-on. (c) log σ vs surface brightness, showing the fundamental plane nearly face-on; the dots show the effect viewing an E3.6 oblate or prolate galaxy seen at maximum elongation and as round in projection. (d) log σ vs (log R_e+0.84 log I_e) showing the plane exactly edge-on.

doubled if early-type disk galaxies could be included, leading to more accurate distance estimates for those aggregates. Furthermore, if the selection criterion could be used to include galaxies such as M31 and M32, then the method could be calibrated independently, allowing absolute rather than relative distances to be determined.

(6) Finally, a better understanding of the bias introduced by the highly nonuniform distribution of galaxies needs to be developed. The simulations reported by Dekel et al. (1990) suggest that any residual errors which remain after making the correction of Eq. (24) are small. Lynden-Bell (1992) developed Schechter's (1980) method of correcting for the Malmquist-like bias and finds that the correction for the bias depends only on the dispersion in field galaxies and not on distance. Applying it to the elliptical galaxy data he finds results that are almost identical to the original analysis. On the other hand, Landy and Szalay (1991), claim that much of the Great Attractor signal may be due to the Malmquist correction. We look forward to Bertschinger's (1992) review of the subject to clarify the situation.

11. COMPARISON OF DISTANCES

11.1 The Sample

This article would be incomplete without some sort of direct comparison of distances from the various methods. However, it is beyond the scope of the review to try to present a compendium of distances, or to try to reconcile the inevitable discrepancies that will arise. We therefore undertook a blind test of the distance methods, where each of the authors provided distances and error estimates for a set of objects, and the results were not compared until all the distances had been collected. Most of the distances are available from the literature, but some unpublished material is also included.

We chose surface-brightness fluctuations (SBF) as a basis for comparison because it offers good accuracy, a rea-

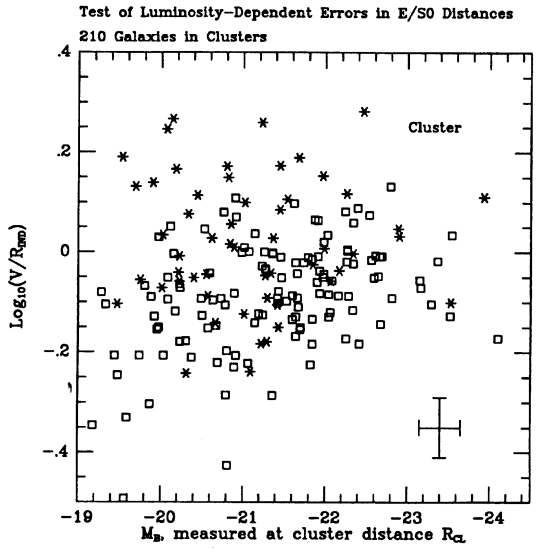

FIG. 23—The logarithm of the ratio of predicted distance corrected for Malmquist bias, to radial velocity in the cosmic microwave background frame, $\log_{10}(V/R)$, as a function of absolute B magnitude of 182 galaxies in clusters, taken from BFD. Galaxies from both the 7S sample (open squares) and BFD (stars) are included.

sonably large data set, and a substantial distance range for comparison. We worked from a list of 44 groups and clusters, based on the groups defined in Davies et al. (1989), and 15 individual galaxies, for which there was overlap between SBF and other distance methods. Cepheids were not included in the comparison because the overlap was largely limited to the fundamental calibrating galaxies. Similarly, novae were not included because of the small number of comparison galaxies.

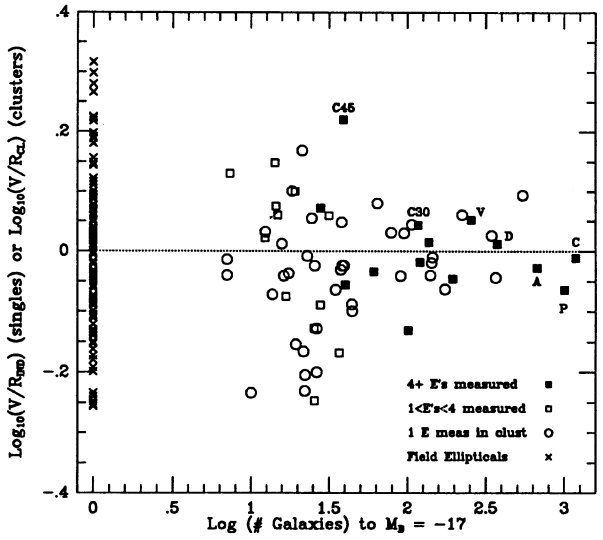

FIG. 24—Ordinate as Fig. 23 shown as a function of the number of galaxies in a cluster with $M_B < -17$ (from BFD). The number of ellipticals in each cluster is indicated. Field galaxies are included at richness 1. The following clusters are identified: Virgo (V), Perseus (P), Coma (C), Abell 1367 (A), Cen 45 (C45), and Cen 30 (C30).

As much as possible, the various distances were adjusted by the authors to the assumption of the SBF calibration: M31 and M32 are assumed to have a true distance modulus of 24.43 and a B-band Galactic extinction of 0.31 mag. Extinctions for the comparison galaxies are taken from Burstein and Heiles (1984). We shall describe briefly what we adopted for the zero point, group averages, and group errors for each method's distances. Someday we hope to understand every systematic error in these distance estimates; at this time, however, unknown systematic errors are suspected to be present and various allowances have been included to account for these errors. We have tried to be as explicit as possible when these are introduced, but justification is not possible within the space constraints of this section.

The SBF group distances are an unweighted average of the distances to the galaxies observed in the group. The distance error for each galaxy is the maximum of the formal uncertainty from the analysis and 5%. The distance error for each cluster is the maximum of the average error for the galaxies and the rms scatter among the galaxies observed, divided by $\sqrt{N}$.

Distance errors from the planetary-nebula luminosity function (PNLF) method are based on the formal uncertainty in the fit of the luminosity function plus other random uncertainties (e.g. standard stars, filter calibrations). Group distances are based on unweighted averages, and errors are the average error for the individual galaxies, divided by $\sqrt{N}$, with an additional allowance of 5% for any systematic error arising from the definition of the M31 PNLF added in quadrature.

Globular-cluster luminosity function (GCLF) distances have errors based on the uncertainty in fitting a luminosity function. The zero point is based on the Milky Way GCLF; the GCLF in M31 has been determined to be 0.2 mag brighter. Thus the GCLF distances do not scale with an assumed distance to M31. Cluster distances and errors are derived from the weighted averages.

D_n-σ distances and errors were taken directly from Faber et al. (1989). Here the zero point is based on distant galaxies, where an undisturbed Hubble flow is presumed to hold. The Coma cluster is an important calibrator, where the D_n-σ distance is found to be 7461 ± 273 km s^{-1}; it has a redshift of 6890 km s^{-1} relative to the Local Group (LG) frame as defined by Yahil et al. (1977), or 7200 km s^{-1} relative to the cosmic microwave background (CMB) frame. The random error in an individual galaxy's distance is reckoned to be 23% in distance; cluster distance errors are reduced by $\sqrt{N}$.

Distances from type-Ia supernovae (SN Ia) have been based on an absolute B-band magnitude of -19.0, and this in turn comes from distances in the *Tully Catalog of Nearby Galaxies,* which uses $H_0 = 75$ km s^{-1} Mpc^{-1} to derive distances. In order to avoid circular reasoning, we have chosen to refer to these distances in terms of velocity by multiplying the factor of 75 km s^{-1} Mpc^{-1} back in. The mean distance derived this way for three SN Ia in the Coma cluster is 7160 km s^{-1}, which is in good agreement with its redshift. We have adopted an error of 0.35 mag in

distance modulus for each supernovae observed, diminishing this by $\sqrt{N}$ for each cluster, since this is roughly the scatter we observe among observations in clusters.

Lastly, distances using the Tully–Fisher (TF) method are founded on Cepheid and RR Lyrae distances to M31, M33, and the Sculptor group. Photographic and photoelectric (primarily *B* band), infrared (primarily *H* band), and CCD (primarily *R* and *I* band) observations have been used, with errors assumed of 0.5, 0.4, and 0.3 mag per galaxy. Cluster distances arise from averaging together individual galaxy distances and assigning errors which are the maximum of the method error and the scatter in a cluster, divided by $\sqrt{N}$. The three types of observations are combined by adopting weights of 0.5:1:1.

11.2 The Comparison

We performed the comparison between methods by determining the mean and the scatter in the natural logarithm of the ratio of a given method's distances and those of SBF. PNLF and GCLF offer sufficient accuracy in a single measurement to warrant comparison on individual galaxies, so these results are reported as well as the comparison of cluster averages.

Table 3 presents the results. Column (1) names the method compared with SBF; column (2) gives the number of objects compared; columns (3) and (4) are the weighted average ratio between the method's distance and SBF and χ^2 for the resulting scatter around this mean; columns (5) and (6) list the unweighted average ratio and the rms scatter in the natural logarithm around this unweighted average; columns (7) and (8) give the median number of galaxies in a group used in computing the average distance from the method and the median error estimate among these galaxies; and columns (9) and (10) list the same quantities for the SBF measurements. Please note in columns (3) and (5) that the ratio between D_n-σ and SBF and SN Ia and SBF has units of km s^{-1} Mpc^{-1}.

There are three entries for D_n-σ because we deemed it interesting to fit the distribution when two outlying points were removed, and to see whether the accuracy of D_n-σ improved with greater number of galaxies averaged together. As expected, the accuracy appears to improve in both instances.

There are three entries for TF because photographic and photoelectric TF measurements are sometimes considered less reliable (see Sec. 7.1.1). Hence, we fitted the distribution after those clusters with only these data were removed. Although *H* and red CCD data do improve the results, the distances are still highly inconsistent with SBF. Thirdly, we fitted the distribution of only those clusters in which at least five spirals had been observed. (The well-mixed groups of Dorado, Telescopium, and Leo are also included in this sample.) In these groups, we believe there is sufficient overlap, or co-mingling between the spirals and early-type galaxies to be confident that both types are at the same distance. In this case, the TF results *are* consistent with those of the SBF.

The comparisons between the various distances are shown graphically in Figs. 25–29. Figure 25 shows the comparison between SBF and PNLF and SBF and GCLF for individual galaxies, and Fig. 26 presents the comparison for PNLF and GCLF using cluster averages.

The agreement between PNLF and SBF gives us reason to believe that the two methods are indeed approaching accuracies of 5%. χ^2 for the individual galaxy comparison shows that there is a small systematic component to the errors of order 5% which needs to be understood, although the empirical allowance in the cluster distance errors is very close to expectations. There is a zero-point difference of about 6% which is significant at the 2σ level, in the sense that PNLF distances are larger than SBF distances.

It appears from the GCLF comparison that the GCLF method is more accurate than its error estimates, perhaps by 40%. There is again an offset in zero point relative to SBF of about 13% in the same sense as with PNLF which is significant at the 2σ level. Either SBF distances are too small by 13%, or the GC's in the early-type galaxies studied here are as much fainter than the GC's in the Milky Way, as the Milky Way is fainter than M31.

Figure 27 plots the comparison for D_n-σ and SN Ia. In these plots the distances have units of km s^{-1}, and the ratios have units of km s^{-1} Mpc^{-1}, and thus represent Hubble ratios in which the zero points have been set using the SBF distances.

D_n-σ works remarkably well. There seems to be a small incidence of galaxies for which D_n-σ is substantially worse than its error estimate, but if these outliers can be identified and removed, the errors seem to be accurate. The mean ratio between D_n-σ and SBF is about 90 km s^{-1} Mpc^{-1}.

The assumed error of 0.35 mag for the SN Ia errors seems to be an underestimate. Because the data are such a heterogeneous mix of old photographic data, it is not possible to make a meaningful comment on the intrinsic value of SN Ia as distance estimators except to say that they are certainly better than 0.5 mag per supernova. The zero point in this comparison results in 85 km s^{-1} Mpc^{-1}, which is in good agreement with D_n-σ and TF.

Figure 28 shows how the TF distances compare with SBF. The very poor agreement between TF and SBF distances is a surprise. χ^2 indicates that the errors in TF distances to groups with ellipticals are significantly worse than the error estimates. The factor is the same for *H*-band and red CCD data as for photographic and photoelectric data, so the latter are not at fault. We plotted the ratio of D_n-σ and SBF against the ratio of TF and SBF, and found no correlation at all, so it is unlikely that the scatter comes from the SBF distances.

In order to explore the hypothesis that this inconsistency arises from the TF distances to spirals which may not be associated with elliptical galaxies with SBF distances, we plot in the upper left-hand panel of Fig. 29 the velocity difference versus the distance difference for the TF clusters with *H* or red CCD data and the corresponding SBF clusters. There is a poor but significant correlation present, suggesting that some of the clusters are separated in space and have a velocity difference arising from an undisturbed Hubble flow. That is, it appears to be more

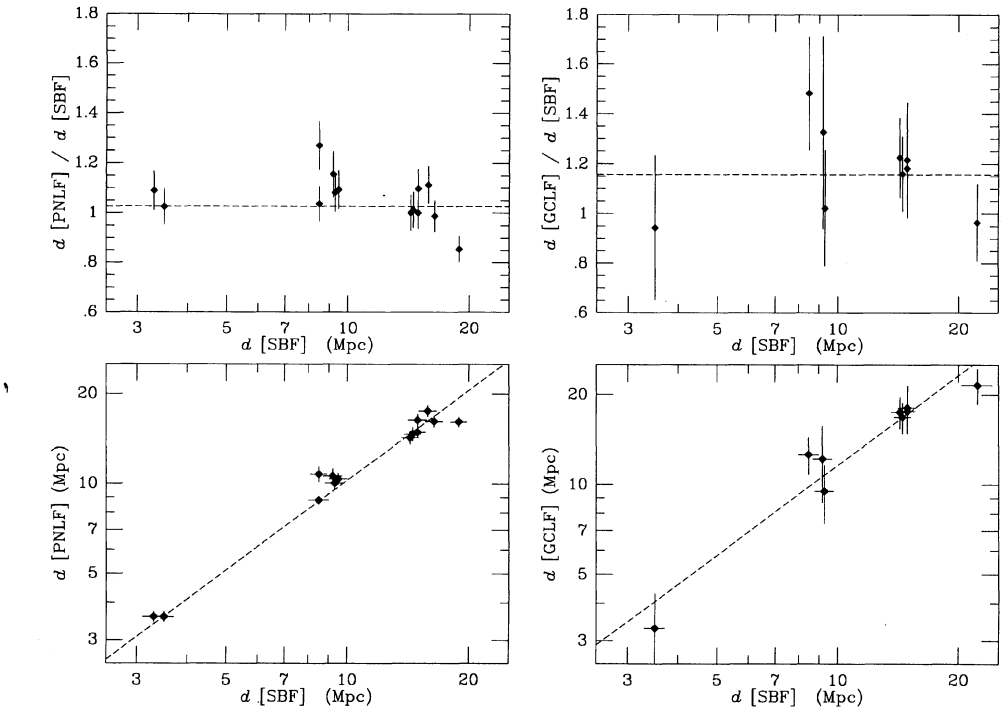

FIG. 25—SBF is compared with PNLF and GCLF for individual galaxies. The left-hand panels are the PNLF distance plotted against the SBF distance, and the ratio of the two plotted against SBF distance. The right-hand panels give the same for the GCLF distances. The dashed lines are drawn according to the weighted mean ratio given in Table 3.

difficult to assign cluster membership to the spirals than to the ellipticals. In the lower left-hand side we reproduce the panel from the lower right-hand side of Fig. 28, with lines showing SBF distance ±8 Mpc. This delineates the envelope of the points fairly accurately, and plausibly reflects the km s^{-1} velocity-selection criterion used to decide whether a spiral group was coincident with an elliptical group.

The right-hand panels of Fig. 29 show the distribution of TF distances relative to SBF distances when the TF sample is restricted to those which are most likely to be closely associated with the adjacent cluster of elliptical galaxies. In this case the differences between TF and SBF become consistent with the errors. The TF-SBF comparison, in general, deals with disparate galaxies (spirals versus ellipticals) in which few, if any, galaxies are common to both methods. Consequently, we see differences that are larger than the formal expectations unless the samples are carefully chosen.

Thus, we believe that the TF error estimates probably are accurate, but that spiral and elliptical groups are often substantially disjoint, more so than is widely appreciated. At the risk of overinterpreting Fig. 29, about half of the outlying spiral groups appear to follow the Hubble flow relative to the elliptical group, and about half have the same velocity at different distances, equally divided between near and far. The implications that this has for cluster virialization and large-scale flows are beyond the mandate of this review.

The ratio of the restricted TF sample and SBF is not significantly different from unity ($\sim 0.98 \pm 0.03$) and the level of agreement is comparable to that of the PNLF-SBF agreement. The larger uncertainties in the TF method are statistically reduced by a larger sample.

TABLE 3
Comparison Results

Method	N	⟨ratio⟩	χ^2	(unwgt) ⟨ratio⟩	rms	Method ⟨n⟩	Method ⟨$\delta d/d$⟩	SBF ⟨n⟩	SBF ⟨$\delta d/d$⟩	Notes
PNLF	14	1.027	23.6	1.054	0.088	1	0.044	1	0.052	Individual galaxies
GCLF	9	1.156	3.7	1.157	0.140	1	0.120	1	0.050	Individual galaxies
PNLF	7	1.072	6.4	1.094	0.078	1	0.056	1	0.057	Cluster averages
GCLF	6	1.117	3.0	1.127	0.152	1	0.160	2	0.052	Cluster averages
SN Ia	6	85.4	20.0	92.4	0.248	2	0.133	2	0.050	
D_n-σ	34	86.5	70.3	92.5	0.227	2	0.149	2	0.052	All clusters
D_n-σ	32	89.3	32.8	92.8	0.165	2	0.149	2	0.045	2.5σ clip applied
D_n-σ	12	91.1	11.8	92.5	0.123	4	0.105	2	0.052	≥ 3 in cluster
TF	34	0.921	100.8	0.909	0.275	4	0.157	1	0.052	All clusters
TF	24	0.960	67.6	0.974	0.237	5	0.122	1	0.050	Has H or CCD data
TF	14	0.986	15.2	0.970	0.127	9	0.083	1	0.055	≥ 5 in cluster

11.3 Virgo—A Case Study

The Virgo cluster has historically played a central role in the determination of the extragalactic distance scale. This is because Virgo is the nearest cluster with a full complement of morphological types so that many different methods of distance determination may be applied. Furthermore, it is sufficiently rich that unusual events occur frequently (e.g., supernovae, novae), it is at high galactic latitude so that foreground extinction is not a serious matter, and it is at low declination so that it may be studied from both northern and southern hemispheres. In addition,

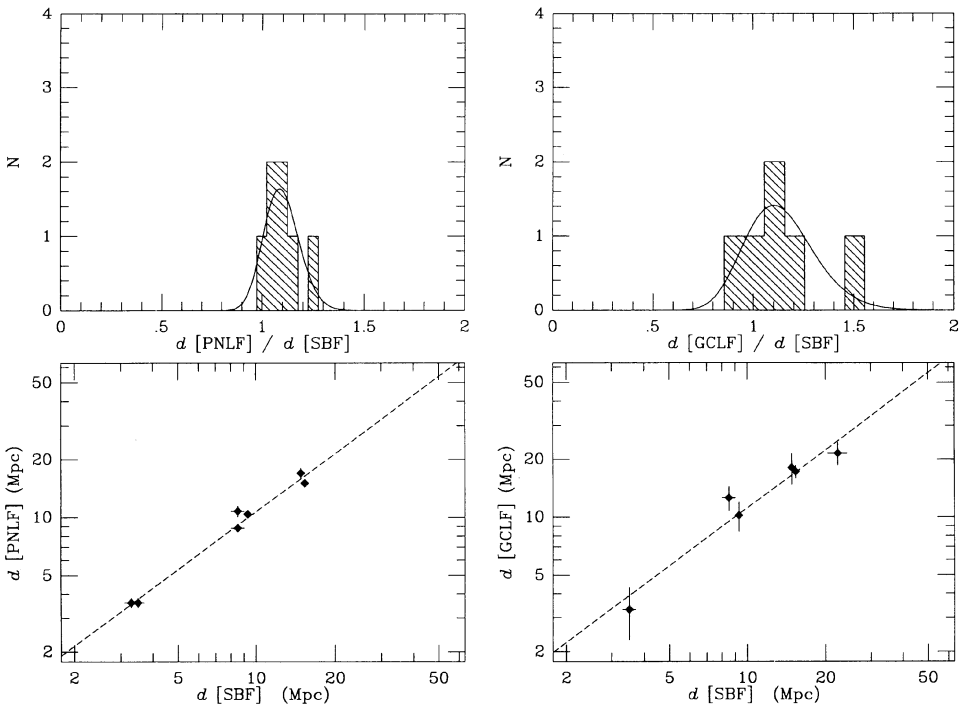

FIG. 26—SBF is compared with PNLF and GCLF using cluster averages. The left-hand panels show the PNLF distance plotted against SBF distance, and the histogram of the ratios. The right-hand panels are the same for GCLF distances. The dashed lines in the distance plots are the weighted mean ratios from Table 3. The smooth curves on the histogram plots are Gaussians using the weighted mean and the rms scatter from Table 3. Note that these are Gaussians in the natural logarithm, and since the abscissa is the ratio itself, the Gaussians are skewed and the peak does not correspond exactly to the mean value.

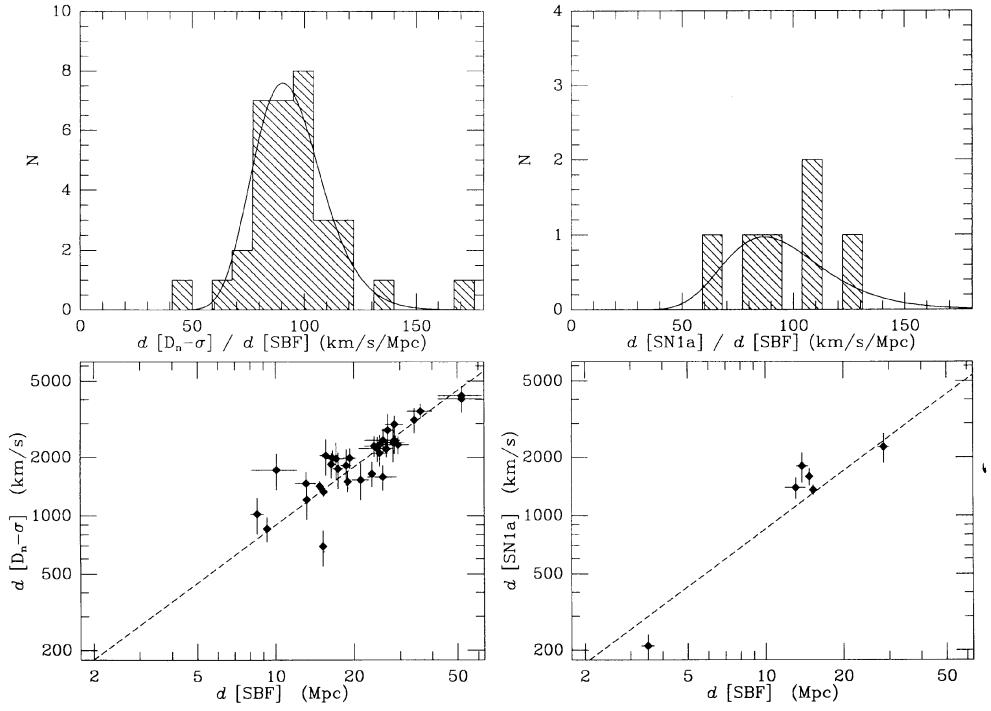

FIG. 27—SBF is compared with D_n-σ and SN Ia. The left-hand panels show the D_n-σ distance plotted against SBF distance, and the histogram of the ratios. The right-hand panels are the same for SN Ia distances. The dashed lines in the distance plots are the weighted mean ratios from Table 3, and the smooth curves on the histogram plots are Gaussians derived from Table 3. The D_n-σ curves come from the fits which have the two outliers removed. In these plots the distances have units of km s^{-1}, and the ratios have units of km s^{-1} Mpc^{-1}.

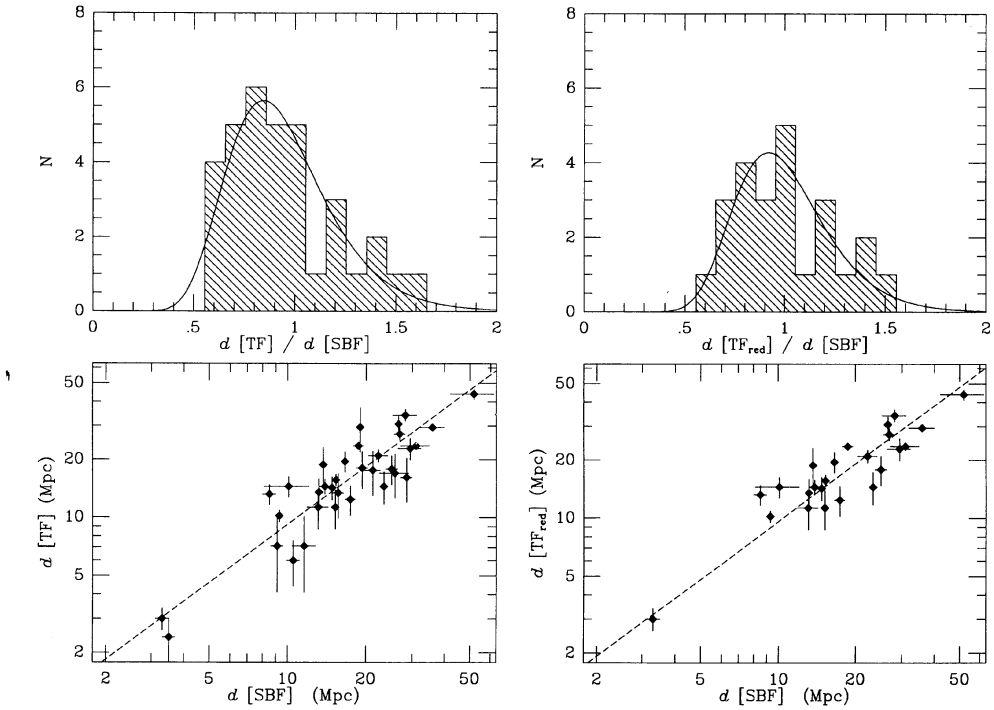

FIG. 28—SBF is compared with TF distances. The left-hand panels show all of the TF data, as in Fig. 26, and the right-hand panels show the TF data which has been pruned of all clusters for which only *B*-band data are available.

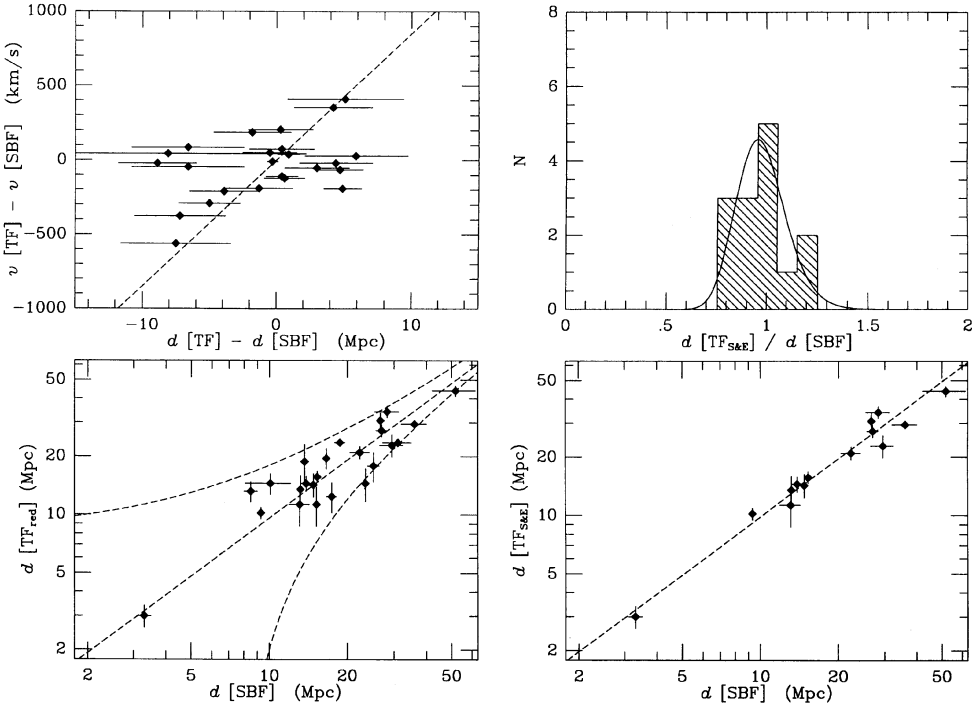

FIG. 29—The upper left-hand panel shows the velocity difference vs the distance difference for the TF clusters with *H* or red CCD data and the corresponding SBF clusters. In the lower left-hand side we reproduce the panel from the lower right-hand side of Fig. 28, with lines showing SBF distance ±8 Mpc. The right-hand panels show the comparison of SBF and TF when the TF sample is restricted to populous groups of spirals which we judged are likely to be co-mingled with their elliptical counterparts.

TABLE 4
Uncertainties to Individual Galaxies (For Galaxies up to 20 Mpc)

Method	$\sigma_{internal}$ (mags)	$\sigma_{external}$ (mags)	Total[a] (mags)
Cepheids	0.10	0.13	0.16
GCLF	0.30	0.27	0.40
Novae	0.33	0.22	0.40
SN Ia	0.20	0.50	0.53
Tully-Fisher[b]	0.25	0.13	0.28
PNLF	0.10	0.13	0.16
SBF	0.10	0.13	0.16
D_n-σ[c]	0.45	0.21	0.50

[a]Total uncertainty is defined as $\sqrt{\sigma_{int}^2 + \sigma_{ext}^2}$
[b]Assumes I or H luminosities; B uncertainties will be larger due to extinction correction errors.
[c]External error is the zero-point uncertainty based on the two Leo I elliptical calibrators.

Virgo is sufficiently distant that most of its recessional velocity derives from the Hubble expansion, and is therefore valuable as a cosmological probe.

We summarize in Table 4 the uncertainties (internal, external, and total) in distance to an individual Virgo galaxy that these seven methods can achieve. (Cepheids are included for completeness, but are restricted to Local Group distances.) Internal errors are taken from the individual sections of this review; external errors are dominated by the uncertainty in the zero-point calibrations. Because most of the methods have common systematic errors(e.g., the Cepheid distance to M31), averaging the distances does not reduce the overall uncertainty.

In Table 5, we present a summary of the results from the seven methods when applied to the Virgo cluster and assuming $E(B-V)=0.02$, which is typical of Virgo galaxies (Burstein and Heiles 1984). The errors in the averages presented in the last rows are rms errors; they have not been reduced by $\sqrt{N}$ statistics because of the systematic errors in common. Note that the total range in distances has an extent (defined as $D_{max}/D_{min}-1$) of only $\sim 37\%$, not the sometimes quoted "factor of 2" (i.e., an extent of 100%). Furthermore, the values exhibit a rms dispersion about the mean of $\sim 12\%$, and all values are contained within a spread of ± 1.6 times this dispersion. A critical element of confusion is that each method includes a different sample of galaxies and intrinsic depth plays a major role approaching or exceeding the level of the dispersion.

TABLE 5
Virgo Distance Estimates

Method	$(m-M)_{Virgo} - (m-M)_{M31}$	Distance (Mpc)[a]
GCLF	6.94 ± 0.40	18.8 ± 3.8
Novae	7.19 ± 0.40	21.1 ± 3.9
SN Ia	7.00 ± 0.50	19.4 ± 5.0
Tully-Fisher	6.57 ± 0.20	15.8 ± 1.5
PNLF	6.50 ± 0.15	15.4 ± 1.1
SBF[b]	6.44 ± 0.12	15.9 ± 0.9
D_n-σ	6.70 ± 0.29	16.8 ± 2.4
unweighted average	6.79 ± 0.26	17.6 ± 2.2
weighted average	6.59 ± 0.22	16.0 ± 1.7

[a]Assumes M31 distance of 770 kpc
[b]Virgo Distance is an average of grouped galaxies rather than a simple average as for other methods

Methods basing their distances on a few galaxies (GCLF, PNLF, Novae, SN Ia) are particularly susceptible to skewed results by including a single near or distant member. In summary, the deviations among the techniques are nearly equal to the accuracies of the techniques. There are no discrepancies of statistical significance.

11.4 Conclusions

The overall agreement between the various distance methods is quite good, but there is room for improvement. SBF and PNLF have a small but significant difference in scale when the same galaxies are compared. SBF agrees well with TF in zero point, but this could be fortuitous if the spirals and ellipticals have conspired to mask a real difference.

The primary results of the comparison are as follows:

(i) SBF and PNLF have errors which are approaching 5%, but each seems to have a poorly understood systematic component of about 5%.

(ii) The GCLF appears to be more accurate than expected, but possibly has a scale error in the sense of overestimating distances by about 13%.

(iii) SN Ia have larger errors than expected, but there is reason to believe that this will improve dramatically as newer data become available.

(iv) D_n-σ seems to have well-understood errors, but with outliers beyond that expected for Gaussian statistics.

(v) TF may have well-understood errors, but a literal interpretation of the distance to an elliptical group may be misleading when the spirals are not well intermixed.

Finally, what about the Hubble constant? All of the distances above, except those from SNe Ia, are based on the RR Lyrae/Cepheid distance scale, and these distances would change proportionately to any change in that scale. It seems unlikely for that scale to change by more than 10%, given that the Magellanic Clouds have so many independent distance estimates, but it is important to bear in mind that the Hubble ratios above are based on an assumption about the distance to M31 and other local calibrators.

Figure 30 illustrates another difficulty. The top left-hand panel shows recession velocity in the LG frame plotted against SBF distance, and the bottom panel shows recession velocity in the CMB frame. It is clear that the CMB frame is inappropriate for nearby galaxies; as has been stressed many times (e.g., Yahil et al. 1977), the local Hubble flow is quite symmetric and linear around the LG frame. Thus, one must use the LG frame to understand the Hubble flow of nearby galaxies.

One could interpret the top left-hand panel of Fig. 30 as evidence that the global value of H_0 is 50 km s^{-1} Mpc^{-1}, and that the deviation of the points starting at about 10 Mpc indicates that all the distance estimators described here share a common bias. An alternative interpretation is that the Hubble ratios near 50 km s^{-1} Mpc^{-1} are the effect of the compression from 85 km s^{-1} Mpc^{-1} by a 300 km s^{-1} infall into the Virgo cluster. The upper right-hand panel of Fig. 30 shows that removal of this effect tightens the velocity-distance relation considerably, and moves all

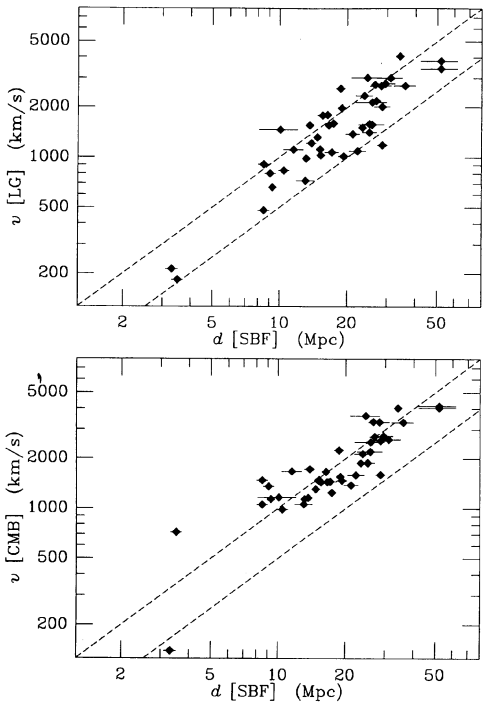

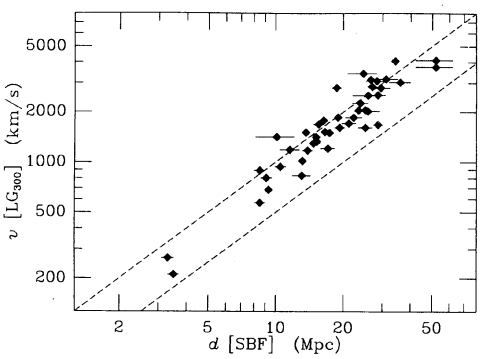

FIG. 30—Various velocities are plotted against SBF distance. The top left-hand panel shows recession velocity in the LG frame, and the bottom panel shows recession velocity in the CMB frame. The two dashed lines show $H_0=50$ and 100 km s^{-1} Mpc^{-1}. The top right-hand panel shows a velocity in the LG frame which has been corrected for the effect of 300 km s^{-1} of Virgo infall.

of the points closer than 20 Mpc up to about 85 km s^{-1} Mpc^{-1} (on the SBF or TF scales).

The evidence presented in this article favors a Hubble constant of about 85 km s^{-1} Mpc^{-1} (on the SBF or TF scales), with rather small uncertainty and good agreement among all the various methods. The Hubble constant would be 6% and 13% smaller if placed on the PNLF or GCLF scales, respectively.

We can also derive the Hubble constant directly from our Virgo averages. There is some question, however, as to the proper velocity to assign to the Virgo cluster; instead we adopt the approach in which the more far-reaching techniques (e.g., type-Ia supernovae, D_n-σ, Tully–Fisher) are used to obtain the distance ratio, 5.6 ± 0.5, for Coma relative to Virgo (Aaronson et al. 1986; Dressler et al. 1987b; Lucey et al. 1991b; Sandage and Tammann 1990). The recessional velocity for Coma is 7160 ± 200 after correcting for Virgocentric infall (Pierce 1989; Sandage and Tammann 1990). These values yield $H_0=73\pm11$ (unweighted Virgo average) and $H_0=80\pm11$ (weighted Virgo average) based on the Freedman and Madore (1990) distance to M31 and an M31 differential reddening value of $E(B-V)=0.08$. These values will be 8.5% higher if the Welch et al. (1986) Cepheid distance for M31 is adopted. Similarly, the values will be 6% higher if we adopt the M31 distance of 725 kpc based on a variety of methods (van den Bergh 1991).

11.5 Summary

We find that the methods described here yield extragalactic distances that are consistent with their expected level of performance. Direct comparisons of the methods for either individual galaxies or groups of galaxies show surprisingly good agreement. Conversely, we do not find any evidence for a discrepancy in the extragalactic distance scale.

We find some evidence that the Tully–Fisher relation yields distances that differ from the early-type galaxy indicators due to true spatial separations of the galaxy populations. Consequently, distances based on this method must be interpreted in that context.

We derive Hubble constants in the range of 73–90 using a variety of approaches based on these distance techniques.

We wish to thank Dr. Paul Hodge, Dr. Paul Schechter, Dr. Sidney van den Bergh, and Dr. Sidney Wolff for their critical reading of an earlier version of this paper and providing an enormous number of suggested improvements. We are also grateful to Dr. Peter Conti, Dr. Tod Lauer, and Dr. Mark Phillips for numerous helpful discussions.

REFERENCES

Aaronson, M., Bothun, G., Mould, J., Huchra, J., Schommer, R. A., and Cornell, M. E. 1986, ApJ, 302, 536
Aaronson, M. et al. 1989, ApJ, 338, 654
Aaronson, M., Huchra, J., and Mould, J. 1979, ApJ, 229, 1
Aaronson, M., Mould, J., Huchra, J., Sullivan, III, W. T., Schommer, R. A., and Bothun, G. D. 1980, ApJ, 239, 12
Aaronson, M., Huchra, J. P., Mould, J. R., Schechter, P. L., and Tully, R. B. 1982, ApJ, 258, 64
Aaronson, M., Mould, J. and Huchra, J. 1980, ApJ, 237, 655
Aaronson, M., and Mould, J. 1983, ApJ, 265, 1
Aaronson, M., and Mould, J. 1986, ApJ, 303, 1
Aguilar, L., Hut, P., and Ostriker, J. P. 1988, ApJ, 335, 720
Ajhar, E. A. 1992, Ph.D. thesis, MIT

Allen, A. J., and Richstone, D. O. 1988, ApJ, 325, 583
Arnett, W. D. 1982a, ApJ, 253, 785
Arnett, W. D. 1982b, ApJ, 254, 1
Arnett, W. D., Branch, D., and Wheeler, J. C. 1985, Nature, 314, 337
Arp, H. C. 1956, AJ, 61, 15
Ashman, K. M. and Zepf, S. E. 1992, ApJ, 384, 50
Baade, W. 1926, Astron. Nach., 228, 359
Baade, W. 1944, ApJ, 100, 137
Baade, W., and Swope, H. H. 1963, AJ, 68, 435
Baade, W., and Swope, H. H. 1965, AJ, 70, 212
Balkowski, C., and Westerlund, B. E. 1977, IAU Colloq., No. 37, Décalages Vers Le Rouge et Expansion de L'Univers, L'Évolution des Galaxies et ses Implications Cosmologiques (Paris, Centre National de la Recherche Scientifique)
Balkowski, C., Bottinelli, L. Chamaraux, P., Gouguenheim, L., and Heidmann, J. 1974, A&A, 34, 43
Barbon, R. 1978, AJ, 83, 13
Barbon, R., Capaccioli, M., and Ciatti, F. 1975, A&A, 44, 267
Barbon, R., Cappellaro, E., and Turatto, M. 1989, A&AS, 81, 421
Barbon, R., Ciatti, F., and Rosino, L. 1973, A&A, 25, 241
Barnes, T. G., Dominy, J. F., Evans, D. S., Kelton, P. W., Parsons, S. B., and Stover, R. J. 1977, MNRAS, 178, 661
Bartel, N. 1991, in Supernovae, ed. S. E. Woosley (New York, Springer), p. 760
Baum, W. 1955, PASP, 67, 328
Baum, W. 1986, Space Telescope GTO proposal 1114-GTO/WFP
Baum, W. 1990, in the ASP Conf. Ser. Vol. 10, The Evolution of the Universe of Galaxies, ed. Richard G. Kron (San Francisco, Astronomical Society of the Pacific), p. 119
Baum, W. A. and Schwarzschild, M. 1955, AJ, 60, 247
Bender, R., Surma, P., Döbereiner, S., Möllenhoff, C., and Madejsky, R. 1989, A&A, 217, 35
Bertschinger, E. 1992, PASP, in preparation
Birkenshaw, M., Hughes, J. P., and Arnaud, K. A. 1991, ApJ, 379, 466
Binggeli, B., Sandage, A., and Tarenghi, M. 1984, AJ, 89, 64
Binney, J., and Tremaine, S. 1987, Galactic Dynamics (Princeton, Princeton University Press)
Bivano, A., Giuricin, G., Mardirossian, F., and Mezzetti, M. 1990, ApJS, 74, 325
Blumenthal, G. R., Faber, S. M., Primack, J. R., and Rees, M. J. 1984, Nature, 311, 517
Bosma, A. 1981, AJ, 86, 1825
Bothun, G., and Mould, J. R. 1987, ApJ, 313, 629
Bottinelli, L., Gouguenheim, L., Paturel, G., and de Vaucouleurs, G. 1983, A&A, 118, 4
Bottinelli, L., Gouguenheim, L., Paturel, G., and de Vaucouleurs, G. 1984, ApJ, 280, 34
Bottinelli, L., Goughenheim, L., Paturel, G., and de Vaucouleurs, G. 1985, A&AS, 59, 43
Bottinelli, L., Gouguenheim, L., Paturel, G., and Teerikorpi, P. 1986, A&A, 156, 157
Bottinelli, L., Gouguenheim, L., Paturel, G., and Teerikorpi, P. 1991, A&A, 252, 550
Bowen, I. S., 1952, in Ann. Rep. Dir. Mt. Wilson & Palomar Obser., No. 51, p. 19
Branch, D. 1981, ApJ, 248, 1076
Branch, D. 1982, ApJ, 258, 35
Branch, D. 1992, ApJ, in press
Branch, D., and Bettis, C. 1978, AJ, 83, 224
Branch, D., Drucker, W., and Jeffery, D. J. 1988, ApJ, 330, L117
Branch, D., Falk, S. W., McCall, M., Rybski, P., Uomoto, A., and Wills, B. 1981, ApJ, 244, 780
Branch, D., Lacy, C. H., McCall, M. L., Sutherland, P. G., Uomoto, A., Wheeler, J. C., and Wills, B. J. 1983, ApJ, 270, 123
Branch, D., and Patchett, B. 1973, MNRAS, 161, 71
Branch, D., Pauldrach, A. W. A., Puls, J., Jeffery, D. J., and Kudritzki, R. P. 1991, in SN 1987A and Other Supernovae, ed., I. J. Danziger and K. Kjär (Garching, ESO), p. 437
Bridges, T., Hanes, D. A., and Harris, W. E. 1991, AJ, 101, 469
Bridges, T., and Hanes, D. A. 1992, AJ, 103, 800
Brocato, E., Matteucci, F., Mazzitelli, I., and Tornambé, A. 1990, ApJ, 349, 458
Brown, J. H., Burkert, A., and Truran, J. W. 1991, ApJ, 376, 115
Burstein, D. 1990, Rep. Prog. Phys., 53, 421
Burstein, D., Davies, R. L., Dressler, A., Faber, S. M., Stone, R. P. S., Lynden-Bell, D., Terlevich, R. J., and Wegner, G. 1987, ApJS, 64, 601
Burstein D., Faber, S. M., and Dressler, A., 1990, ApJ, 354, 18 (BFD)
Burstein, D., and Heiles, C. 1978, ApJ, 225, 40
Burstein, D., and Heiles, C. 1984, ApJS, 54, 33
Burstein, D., and Raychaudhury, S. 1989, ApJ, 343, 18
Buscombe, W., and de Vaucouleurs, G. 1955, Observatory, 75, 170
Cadonau, R. 1987, Ph.D. thesis, Basel University
Cadonau, R., Sandage, A., and Tammann, G. A. 1985, in Supernovae as Distance Indicators, ed. N. Bartel (Berlin, Springer), Lecture Notes in Physics No. 224, p. 151
Caldwell, J. A. R., and Coulson, I. M. 1986, MNRAS, 218, 223
Caldwell, J. A. R., and Laney, C. D. 1990, in IAU Symp. No. 148, The Magellanic Clouds, ed. R. Haynes and D. Milne (Dordrecht, Reidel), p. 249
Caldwell, N., and Phillips, M. M. 1989, ApJ, 338, 789
Caldwell, N., and Schommer, R. 1988, in The Extragalactic Distance Scale, Proceedings of the ASP 100th Anniversary Symposium, PASPC, Vol. 4, ed. S. van den Bergh and C. J. Pritchet (Provo, UT, Astronomical Society of the Pacific), p. 77
Canada-France-Hawaii Telescope Observer's Manual 1990, 4th edition
Capaccioli, M., Cappellaro, E., Della Valle, M., D'Onofrio, M., Rosino, L., and Turatto, M. 1990, ApJ, 350, 110
Capaccioli, M., Della Valle, M., D'Onofrio, M., and Rosino, L. 1989, AJ, 97, 1622
Capaccioli, M. Piotto, G., and Bresolin, F. 1992, AJ, 103, 1151
Cayatte, V., van Gorkom, J. H., Balkowski, C., and Kotanyi, C. 1990, AJ, 100, 604
Chernoff, D. F., and Shapiro, S. L. 1987, ApJ, 322, 113
Chilikuri, M., and Wagoner, R. V. 1988, in Atmospheric Diagnostics of Stellar Evolution; Chemical Peculiarity, Mass Loss, and Explosion, ed. K. Nomoto (Berlin, Springer), Lecture Notes in Physics, No. 305, p. 345
Christian, C. A., and Schommer, R. A. 1987, AJ, 93, 557
Ciardullo, R., Ford, H. C., and Jacoby, G. H. 1983 ApJ, 272, 92
Ciardullo, R., Ford, H. C., Neill, J. D., Jacoby, G. H., and Shafter, A. W. 1987, ApJ, 318, 520
Ciardullo, R., Shafter, A. W., Ford, H. C., Neill, J. D., Shara, M. M., and Tomaney, A. B. 1990a, ApJ, 356, 472
Ciardullo, R., Ford, H. C., Williams, R. E., Tamblyn, P., and Jacoby, G. H. 1990b, AJ, 99, 1079
Ciardullo, R., Jacoby, G. H., and Ford, H. C. 1989, ApJ, 344, 715
Ciardullo, R., Jacoby, G. H., Ford, H. C., and Neill, J. D. 1989, ApJ, 339, 53

Ciardullo, R., Jacoby, G. H., and Harris, W. E., 1991, ApJ, 383, 487
Ciardullo, R., and Jacoby, G. H. 1992, ApJ, 388, 268
Clark, D. H., and Stephenson, F. R. 1977, The Historical Supernovae (Oxford, Pergamon)
Clark, D. H., and Stephenson, F. R. 1982, in Supernovae: A Survey of Current Research, ed. M. J. Rees and R. J. Stoneham (Dordrecht, Reidel), p. 355
Cohen, J. G. 1985, ApJ, 292, 90
Cohen, J. G. 1988, AJ, 95, 682
Cohen, J. G., and Rosenthal, A. J. 1983, ApJ, 268, 689
Cook, K. H., Aaronson, M., and Illingworth, G. 1986, ApJ, 301, L45
Cornell, M. 1989, Ph.D. thesis, University of Arizona
Cornell, M., Aaronson, M. Bothun, G., Mould, J., Huchra, J., and Schommer, R. 1987, ApJS, 64, 507
Corwin, H. G. 1979, in Photometry, Kinematics, and Dynamics of Galaxies, ed. D. S. Evans (Austin, University of Texas Press), p. 125
Courteau, S. 1992, Ph.D. thesis, University of California, Santa Cruz
Courteau, S., and Faber, S. M. 1988, in The Extragalactic Distance Scale, Proceedings of the ASP 100th Anniversary Symposium, PASPC, Vol. 4, ed. S. van den Bergh and C. J. Pritchet (Provo, UT, Astronomical Society of the Pacific), p. 366
Couture, J., Harris, W. E., and Allwright, J. W. B. 1990, ApJS, 73, 671
Couture, J., Harris, W. E., and Allwright, J. W. B. 1991, ApJ, 372, 97
Cox, J. P. 1980, Theory of Stellar Pulsation (Princeton, Princeton University Press)
Cristiani, S., et al. 1992, A&A, in press
Danver, C. G. 1942, Ann. Obs. Lund. No. 10
Daub, C. T. 1982, ApJ, 260, 612
Davies, R. L. 1981, MNRAS, 194, 879
Davies, R. L., Burstein, D., Dressler, A., Faber, S. M., Lynden-Bell, D., Terlevich, R. J., and Wegner, G. 1987, ApJS, 64, 581
Davis, J. 1985, in IAU Symp., No. 111, Calibration of Fundamental Stellar Quantities, ed. D. S. Hayes, L. E. Pasinetti, and A. G. Davis Philip (Dordrecht, Reidel), p. 193
Dekel, A., and Silk, J. 1986, ApJ, 303, 39
Dekel, A., Bertschinger E., and Faber, S. M. 1990, ApJ, 364, 349
Della Valle, M. 1991, A&A, 252, L9
Demers, S., Kunkel, W. E., and Irwin, M. J. 1985, AJ, 90, 1967
de Vaucouleurs, G. 1953, AJ, 58, 30
de Vaucouleurs, G. 1956, Vistas Astron., 2, 1584
de Vaucouleurs, G. 1961, ApJS, 6, 213
de Vaucouleurs, G. 1970, ApJ, 159, 435
de Vaucouleurs, G. 1978, ApJ, 223, 730
de Vaucouleurs, G. 1979, AJ, 84, 1270
de Vaucouleurs, G. 1980, PASP, 92, 576
de Vaucouleurs, G. 1981, in Ann. NY Acad. 10th Texas Symposium on Relativistic Astrophysics, Sci. No. 375, ed. R. Ramaty and F. C. Jones (New York, New York Academy of Science), p. 90
de Vaucouleurs, G. 1982, The Cosmic Distance Scale and Hubble Constant (Mt. Stromlo Observatory Canberra)
de Vaucouleurs, G. 1985, ApJ, 289, 5
de Vaucouleurs, G., and Davoust, E. 1980, ApJ, 239, 783
de Vaucouleurs, G., de Vaucouleurs, A., and Corwin, Jr., H. G. 1976, Second Reference Catalogue of Bright Galaxies (Austin, University of Texas Press)
de Vaucouleurs, G., and Pence, W. D. 1976, ApJ, 209, 687
Disney, M., Davies, J., and Phillips, S. 1989, MNRAS, 239, 939
Djorgovski S. 1985, Ph.D. thesis, University of California, Berkeley
Djorgovski, S., and Davis, M., 1987, ApJ, 313, 59
Djorgovski, S., de Carvalho, R., and Han, M-S. 1988, in The Extragalactic Distance Scale, Proceedings of the ASP 100th Anniversary Symposium, PASPC, Vol. 4, ed. S. van den Bergh and C. J. Pritchet (Provo, UT, Astronomical Society of the Pacific), p. 329
Dopita, M. A., Jacoby, G. H., and Vassiliadis, E. 1992, ApJ, 389, 27
Dressler, A. 1984, ApJ, 281, 512
Dressler, A. 1987, ApJ, 317, 1
Dressler, A., Faber, S. M., Burstein, D., Davies, R. L., Lynden-Bell, D., Terlevich, R. J., and Wegner, G. 1987a, ApJ, 313, L37
Dressler, A., Lynden-Bell, D., Burstein, D., Davies, R. L., Faber, S. M., Terelvich, R. J., and Wegner, G. 1987b, ApJ, 313, 43
Dressler, A., and Faber, S. M. 1990a, ApJ, 354, 13
Dressler, A., and Faber, S. M. 1990b, ApJ, 354, L45
Dwek, E., and Felten, J. E. 1992, ApJ, 387, 551
Eastman, R. G., and Kirshner, R. P. 1989, ApJ, 347, 771
Eather, R. H., and Reasoner, D. L. 1969, Appl. Opt., 8, 227
Eddington, A. S. 1913, MNRAS, 73, 359
Eddington, A. S. 1940, MNRAS, 100, 354
Elias, J. H., Frogel, J. A., Hackwell, J. A., and Persson, S. E. 1981, ApJ, 251, L13
Elias, J. H. Mathews, K., Neugebauer, G., and Persson, S. E. 1985, ApJ, 296, 379
Elson, R. A. W., and Walterbos, R. A. M. 1988, ApJ, 333, 594
Faber, S. M., Burstein, D., Davies, R. L., Dressler, A., Lynden-Bell, D., Terlevich, R. J., and Wegner G. 1987, in Nearly Normal Galaxies from the Planck time to the Present, ed. S. M. Faber (Princeton, Princeton University Press), p. 175
Faber, S. M., and Burstein, D. 1989, in The Proceedings of the Pontifical Academy of Sciences Study Week No. 27, Large Scale Motions in the Universe, ed. G. Coyne, and V. C. Rubin (Princeton, Princeton University Press)
Faber, S., M., and Jackson, R. E. 1976, ApJ, 204, 668
Faber, S. M., Wegner, G., Burstein, D., Davies, R. L., Dressler, A., Lynden-Bell, D., and Terlevich, R. J. 1989, ApJS, 69, 763
Fall, S. M., and Rees, M. J. 1985, ApJ, 298, 18
Fall, S. M., and Rees, M. J. 1988, in IAU Symp., No. 126, Globular Cluster Systems in Galaxies, ed. J. E. Grindlay and A. G. D. Philip (Dordrecht, Kluwer), p. 323
Feast, M. W., and Walker, A. R. 1987, ARA&A, 25, 345
Fernie, J. D. 1969, PASP, 81, 707
Fernie, J. D. 1990, ApJ, 354, 295
Fernley, J. A., Skillen, I., Jameson, R. F., and Longmore, A. J. 1990, MNRAS, 242, 685
Filippenko, A. V. 1989, PASP, 101, 588
Filippenko, A. V., et al. 1992a, ApJ, 384, L15
Filippenko, A. V., et al. 1992b, AJ, in press
Fish, R. 1964, ApJ, 139, 284
Fisher, J. R., and Tully, R. B. 1977, Comm. Astrophys. 7, 85
Fisher, J. R., and Tully, R. B. 1981, ApJS, 47, 139
Ford, H. C. 1978, in IAU Symp., No. 76, Planetary Nebulae, ed. Y. Terzian (Dordrecht, Reidel), p. 19
Ford, H. C., and Ciardullo, R. 1988, in The Extragalactic Distance Scale, Proceedings of the ASP 100th Anniversary Symposium, PASPC, Vol. 4, ed. S. van den Bergh and C. J. Pritchet (Provo, UT, Astronomical Society of the Pacific), p. 128
Ford, H. C., and Jenner, D. C. 1978, BAAS, 10, 665

Foss, D., Wade, R. A., and Green, R. F. 1991, ApJ, 374, 281
Fouqué, P., Bottinelli, L., Gouguenheim, L., and Paturel, G. 1990, ApJ, 349, 1
Freedman, W. L. 1988a, in The Extragalactic Distance Scale, Proceedings of the ASP 100th Anniversary Symposium, PASPC, Vol. 4, ed. S. van den Bergh and C. J. Pritchet (Provo, UT, Astronomical Society of the Pacific), p. 24
Freedman, W. L. 1988b, ApJ, 326, 691
Freedman, W. L. 1989, AJ, 98, 1285
Freedman, W. L. 1990, ApJ, 355, L35
Freedman, W. L., Horowitz, I., Madore, B. F., Mould, J., and Graham, J. 1988, in The Extragalactic Distance Scale, Proceedings of the ASP 100th Anniversary Symposium, PASPC, Vol. 4, ed. S. van den Bergh and C. J. Pritchet (Provo, UT, Astronomical Society of the Pacific), p. 207
Freedman, W. L., and Madore, B. F. 1988, ApJ, 332, L63
Freedman, W. L., and Madore, B. F. 1990, ApJ, 365, 186
Freedman, W. L., Wilson, C. D., and Madore, B. F. 1991, ApJ, 372, 455
Frogel, J. A., et al. 1987, ApJ, 315, L129
Fullerton, A. W. 1986, in The Study of Variable Stars Using Small Telescopes, ed. J. R. Percy (Cambridge, Cambridge University Press), p. 201
Gaposchkin, S. 1962, AJ, 67, 334
Gascoigne, S. C. B., and Shobbrook, R. R. 1978, Proc. Astron. Soc. Australia, 3, 285
Gautschy, A. 1987, Vistas Astron., 30, 197
Geisler, D., and Forte, J. C. 1990, ApJ, 350, L5
Geller, M. and Huchura, J. 1983, ApJS, 52, 61
Giraud, E. 1986, A&A, 174, 23
Giraud, E. 1987, A&A, 180, 57
Green, D. A. 1986, Observatory, 106, 165
Green, E. M., Demarque, P., and King, C. R. 1987, The Revised Yale Isochrones and Luminosity Functions (New Haven, Yale University Press)
Gregg, M. D. 1989, ApJ, 337, 45
Gregg, M. D. 1992, ApJ, 384, 43
Gregory, S., and Thompson, L. 1977, ApJ, 213, 345
Grillmair, C. J., Pritchet, C. J., and van den Bergh, S. 1986, AJ, 91, 1328
Gunn, J. E. 1988, in The Extragalactic Distance Scale, Proceedings of the ASP 100th Anniversary Symposium, PASPC, Vol. 4, ed. S. van den Bergh and C. J. Pritchet (Provo, UT, Astronomical Society of the Pacific), p. 344
Hamuy, M., et al. 1991, AJ, 102, 208
Han, M., and Mould, J. 1990, ApJ, 360, 448
Hanes, D. A., 1977a, MmRAS, 84, 45
Hanes, D. A. 1977b, MNRAS, 180, 309
Hanes, D. A. 1979, MNRAS, 188, 901
Hanes, D. A. 1982, MNRAS, 201, 145
Hanes, D. A., and Whittaker, D. G. 1987, AJ, 94, 906
Hanson, R. B. 1975, AJ, 80, 379
Harkness, R. P. 1987, in Radiation Transport and Hydrodynamics, ed. D. Mihalas and K. H. Winckler (Dordrecht, Reidel), p. 166.
Harkness, R. P. 1991, in Supernovae, ed. S. E. Woosley (New York, Springer), p. 454
Harkness, R. P., and Wheeler, J. C. 1990, in Supernovae, ed. A. G. Petschek (New York, Springer), p. 1
Harris, H. C., Bothun, G. D., and Hesser, J. E. 1988a, in IAU Symp., No. 126, Globular Cluster Systems in Galaxies, ed. J. E. Grindlay and A. G. D. Philip (Dordrecht, Kluwer), p. 613
Harris, H. C., Harris, G. L. H., and Hesser, J. E. 1988b, in IAU Symp., No. 126, Globular Cluster Systems in Galaxies, ed. J. E. Grindlay and A. G. D. Philip (Dordrecht, Kluwer), p. 205
Harris, W. E. 1986, AJ, 91, 822
Harris, W. E. 1987a, ApJ, 315, L29
Harris, W. E. 1987b, PASP, 99, 1031
Harris, W. E. 1988a, in The Extragalactic Distance Scale, Proceedings of the ASP 100th Anniversary Symposium, PASPC, Vol. 4, ed. S. van den Bergh and C. J. Pritchet (Provo, UT, Astronomical Society of the Pacific), p. 231
Harris, W. E. 1988b, IAU Symp., No. 126, Globular Cluster Systems in Galaxies, ed. J. E. Grindlay and A. G. D. Philip (Dordrecht, Kluwer), p. 237
Harris, W. E. 1990, PASP, 102, 966
Harris, W. E. 1991, ARA&A, 29, 543
Harris, W. E., Allwright, J. W. B., Pritchet, C. J., and van den Bergh, S. 1991, ApJS, 76, 115
Harris, W. E., Hanes, D. A., Hesser, J. E., Pritchet, C. J., and van den Bergh, S. 1992, in preparation
Hartwick, F. D. A., and Hutchings, J. B. 1978, ApJ, 226, 203
Haynes, M. P., and Giovanelli, R. 1986, ApJ, 306, 466
Heidmann, J., Heidmann, N., and de Vaucouleurs, G. 1972, MmRAS, 75, 85
Henize, K. G., and Westerlund, B. E. 1963, ApJ, 137, 747
Hesser, J. E., Harris, W. E., VandenBerg, D. A., Allwright, J. W. B., Shott, P., and Stetson, P. B. 1987, PASP, 99, 739
Hodge, P. W. 1966, Galaxies and Cosmology (New York, McGraw-Hill)
Hodge, P. W. 1974, PASP, 86, 289
Hodge, P. W. 1981, ARA&A, 19, 357
Hodge, P. W., and Wallerstein, G. 1966, PASP, 78, 411
Hoessell, J. G., Abbott, M. J., Saha, A., Mossman, A. E., and Danielson, G. E. 1990, AJ, 100, 1151
Hoessel, J. G., Saha, A., and Danielson, G. E. 1991, private communication
Höflich, P. 1991, in Supernovae, ed. S. E. Woosley (New York, Springer), p. 415
Holmberg, E. 1958, Medd. Lunds Astron. Obs., Ser. II, No. 136
Hubble, E. 1925, ApJ, 62, 409
Hubble, E. 1926, ApJ, 63, 236
Hubble, E. 1929, ApJ, 69, 103
Hubble, E. 1932, ApJ, 76, 44
Hubble, E. 1936a, ApJ, 84, 270
Hubble, E. P. 1936b, The Realm of the Nebulae (New Haven, Yale University Press)
Huchra, J. P. 1985, in The Virgo Cluster, ed. O. Richter and B. Binggeli (Garching, ESO), p. 181
Humphreys, R. M. 1983, ApJ, 269, 335
Humphreys, R. M. 1988, in The Extragalactic Distance Scale, Proceedings of the ASP 100th Anniversary Symposium, PASPC, Vol. 4, ed. S. van den Bergh and C. J. Pritchet (Provo, UT, Astronomical Society of the Pacific), p. 103
Jacoby, G. H. 1980, ApJS, 42, 1
Jacoby, G. H. 1989, ApJ, 339, 39
Jacoby, G. H., Ciardullo, R., and Ford, H. C. 1988, in The Extragalactic Distance Scale, Proceedings of the ASP 100th Anniversary Symposium, PASPC, Vol. 4, ed. S. van den Bergh and C. J. Pritchet (Provo, UT, Astronomical Society of the Pacific), p. 42
Jacoby, G. H., Ciardullo, R., Ford, H. C., and Booth, J. 1989, ApJ, 344, 704
Jacoby, G. H., Ciardullo, R., and Ford, H. C. 1990, ApJ, 356, 332
Jacoby, G. H., and Lesser, M. P. 1981, AJ, 86, 185
Jacoby, G. H., Quigley, R. J., and Africano, J. L. 1987, PASP, 99, 672

Jacoby, G. H., Walker, A. R., and Ciardullo, R. 1990, ApJ, 365, 471
Jeffery, D., Leibundgut, B., Kirshner, R. P., Benetti, S, Branch, D., and Sonneborn, G. 1992, ApJ, in press
Jones, R. V., Carney, B. W., and Latham, D. W. 1988, ApJ, 332, 206
Kaler, J. B. 1983, ApJ, 271, 188
Kaler, J. B., & Jacoby, G. H. 1989, ApJ, 345, 871
Kaler, J. B., & Jacoby, G. H. 1990, ApJ, 362, 491
Kaler, J. B., & Jacoby, G. H. 1991, ApJ, 382, 134
Kayser, S. E. 1967, AJ, 72, 134
Kennicutt, R., Balick, B., and Heckman, T. 1980, PASP, 92, 134
King, I. R. 1966, AJ, 71, 276
Kinman, T. D., Mould, J. R., and Wood, P. R. 1987, AJ, 93, 833
Kirshner, R. P., and Kwan, J. 1974, ApJ, 193, 27
Kochanek, C. S. 1991, ApJ, 382, 58
Kowal, C. T. 1968, AJ, 73, 1021
Kraan-Korteweg, R. C. 1986, A&AS, 66, 255
Kraan-Korteweg, R. C., Cameron, L. M., & Tammann, G. A. 1988, ApJ, 331, 620
Landy, S. D., and Szalay, A. S., 1991, preprint
Larson, R. B. 1988, in IAU Symp., No. 126, Globular Cluster Systems in Galaxies, ed. J. E. Grindlay and A. G. D. Philip (Dordrecht, Kluwer), p. 311
Larson, R. B. 1990, PASP, 102, 709
Lattanzio, J. C. 1986, ApJ, 311, 708
Lauer, T. R. 1985, ApJ, 292, 104
Lauer, T. R., and Kormendy, J. 1986, ApJ, 303, L1
Lawrie, D. G., and Graham, J. A. 1983, BAAS, 15, 907
Lee, H. M., and Ostriker, J. P. 1987, ApJ, 322, 123
Lee, Y.-W., Demarque, P., and Zinn, R. 1990, ApJ, 350, 155
Leibundgut, B. 1988, Ph.D. thesis, Basel University
Leibundgut, B., and Pinto, P. A. 1992, ApJ, in press
Leibundgut, B., and Tammann, G. A. 1990, A&A, 230, 81
Leibundgut, B., et al. 1991, ApJ, 371, L23
Lewis, B. M. 1984, ApJ, 285, 453
Lin, D. N. C., and Murray, S. D. 1991, in The Formation and Evolution of Star Clusters, ASP Conference Series 13, ed. K. Janes (San Francisco, Astronomical Society of the Pacific), p. 55
Lucey, J. R. 1986, MNRAS, 222, 417
Lucey, J. R., Bower, R. G., and Ellis, R. S. 1991, MNRAS, 249, 755
Lucey, J. R., Currie, M. J., and Dickens, R. J. 1986, MNRAS, 221, 453
Lucey, J. R., Gray, P. M., Carter, D., and Terlevich, R. J. 1991a, MNRAS, 248, 804
Lucey, J., Guzman, R., Carter, D., and Terlevich, R. J. 1991b, in Observational Tests of Cosmological Inflation, ed. T. Shanks (Dordrecht, Kluwer), p. 193
Lucey, J. R., Lahav, O., Lynden-Bell, D., Terlevich, R. J., and Melnick, J. 1989, in Workshop on Large Scale Structures and Peculiar Motions, PASPC Vol. 15, eds. D. W. Latham and L. N. da Costa (Provo, UT, Astronomical Society of the Pacific), p. 31
Luppino, G. A., and Tonry, J. L. 1992, in preparation
Lynden-Bell, D. 1992, in Statistical Challenges in Modern Astronomy, ed. E. D. Feigelson and G. J. Babu (New York, Springer), in press
Lynden-Bell, D. Faber, S. M., Burstein, D., Davies, R. L., Dressler, A., Terlevich, R. J., and Wegner, G. 1988, ApJ, 326, 19 (LFBDDTW)
Madore, B. F., and Freedman, W. L. 1985, AJ, 90, 1104
Madore, B. F., and Freedman, W. L. 1991, PASP, 103, 933
Madore, B. F., McAlary, C. W, McLaren, R. A., Welch, D. L., Neugebauer, G., and Matthews, K. 1985, ApJ, 294, 560
Madore, B. F., and Woods, D. 1987, ApJ, 323, L25
Malmquist, K. G. 1920, Medd. Lunds Astron. Obs., Ser. II, No. 22
Manduca, A., and Bell, R. A., 1979, PASP, 91, 848
Mateo, M., Olszewski, E. W., and Madore, B. F. 1990, in Confrontation between Stellar Evolution and Pulsation, PASPC Vol. 11, ed. C. Cacciari and G. Clementini (San Francisco, Astronomical Society of the Pacific), p. 214
Mateo, M., and Schechter, P. L. 1989, ST ESO/ST-ECF Data Analysis Workshop, ed. P. J. Grosbøl, F. Murtagh, and R. H. Warmels, p. 69
McAlary, C. W., and Madore, B. F. 1984, ApJ, 282, 101
McAlary, C. W., Madore, B. F., and Davis, L. E. 1984, ApJ, 276, 487
McAlary, C. W., Madore, B. F., McGonegal, R., McLaren, R. A., and Welch, D. L. 1983, ApJ, 273, 539
McElroy, D. 1983, ApJ, 270, 485
McLaughlin, D. B. 1945, PASP, 57, 69
McMahan, R. K. 1989, ApJ, 336, 409
Metcalfe, N., and Shanks, T. 1991, MNRAS, 250, 438
Miller, D. L., and Branch, D. 1990, AJ, 100, 530
Miller, D. L., and Branch, D. 1992, AJ, 103, 379
Monet, D. G. 1988, in The Extragalactic Distance Scale, Proceedings of the ASP 100th Anniversary Symposium, PASPC, Vol. 4, ed. S. van den Bergh and C. J. Pritchet (Provo, UT, Astronomical Society of the Pacific), p. 81
Mould, J. 1987, PASP, 99, 1127
Mould, J., Aaronson, M., and Huchra, J. 1980, ApJ, 238, 458
Mould, J. R., Cohen, J., Graham, J. R., Hamilton, D., Matthews, K., Picard, A., Reid, N., Schmidt, M., Soifer, T., Wilson, C., Rich, R. M., and Gunn, J. E. 1990a, ApJ, 353, L35
Mould, J. R., Han, M. S., and Bothun, G. D. 1989, ApJ, 347, 112
Mould, J., Kristian, J., and Da Costa, G. S. 1983, ApJ, 270, 471
Mould, J., Kristian, J., and Da Costa, G. S. 1984, ApJ, 278, 575
Mould, J. R., Oke, J. B., de Zeeuw, P. T., and Nemec, J. M. 1990b, AJ, 99, 1823
Mould, J. R., Oke, J. B., and Nemec, J. M. 1986, AJ, 93, 53
Mould, J. R., Staveley-Smith, L., Schommer, R. A. Bothun, G. D., Hall, P. J., Han, M. S., Huchra, J. P., Roth, J., Walsh, W., and Wright, A. E. 1991, ApJ, 383, 467
Muller, R. A., Newberg, H. J. M., Pennypacker, C. R., Perlmutter, S., Sasseen, T. P., and Smith, C. K. 1992, ApJ, in press
Neyman, J., Scott, E. L., and Shane, C. D. 1953, ApJ, 117, 92
Nomoto, K., Thielemann, F.-W., and Yokoi, K. 1984, ApJ, 286, 644
Öpik, E. 1922, ApJ, 55, 406
Paczyński, B. 1971, Acta Astron., 21, 417
Panagia, N., Gilmozzi, R., Macchetto, F., Adorf, H.-M., and Kirshner, R. P. 1991, ApJ, 380, L23
Peebles, P. J. E. 1976, ApJ, 205, 318
Peimbert, M. 1990, Rev. Mexicana Astron. Af., 20, 119
Peletier, R. F., Davies, R. L., Illingworth, G. D., Davis, L. E., and Cawson, M. 1990, AJ, 100, 1091
Peletier, R. F., and Wilner, S. P. 1991, ApJ, 383, 382
Persic, M., and Salucci, P. 1988, MNRAS, 234, 131
Persic, M., and Salucci, P. 1990, ApJ, 355, 44
Pfau, W. 1976, A&A, 50, 113
Phillips, M. M., et al. 1987, PASP, 99, 592
Phillips, M. M., Wells, L. A., Suntzeff, N. B., Hamuy, M., Leibundgut, B., Kirshner, R. P., and Foltz, C. B. 1992, AJ, in press
Pierce, M. J. 1988, Ph.D. thesis, University of Hawaii

Pierce, M. J. 1989, ApJ, 344, L57
Pierce, M. J. 1991, in The Evolution of the Universe of Galaxies, PASPC, Vol. 10, ed. Richard G. Kron (Provo, UT, Astronomical Society of the Pacific), p. 48
Pierce, M. J. 1992, in preparation
Pierce, M. J., McClure, R., and Racine, R. 1992, ApJ, 393, 523
Pierce, M. J., Ressler, M. E., and Shure, M. S. 1992, ApJ, 390, L45
Pierce, M. J., and Tully, R. B. 1988, ApJ, 330, 579
Pierce, M. J., and Tully, R. B. 1989, private communication
Pierce, M. J., and Tully, R. B. 1992a, ApJ, 387, 47
Pierce, M. J., and Tully, R. B. 1992b, in preparation
Pottasch, S. R. 1990, A&A, 236, 231
Pottasch, S. R., Goss, W. M., Arnal, E. M., and Gathier, R. 1982, A&A, 106, 229
Press, W. H. Rybicki, G. B., and Hewitt, J. N. 1992, ApJ, 385, 416
Pritchet, C. J., and Harris, W. E., 1990, ApJ, 355, 410
Pritchet, C., and van den Bergh, S. 1985a, ApJ, 288, L41
Pritchet, C. J., and van den Bergh, S. 1985b, AJ, 90, 2027
Pritchet, C. J., and van den Bergh, S. 1987a, ApJ, 318, 507
Pritchet, C. J., and van den Bergh, S. 1987b, ApJ, 316, 517
Pritchet, C. J., and van den Bergh, S. 1988, ApJ, 331, 135
Pskovskii, Yu.P. 1977, Soviet Astron.–AJ, 21, 675
Pskovskii, Yu.P. 1984, Soviet Astron.–AJ, 28, 658
Racine, R. 1968, JRASC, 62, 367
Racine, R. 1991, AJ, 101, 865
Reed, L. G., Harris, G. L. H., and Harris, W. E. 1992, AJ, 103, 824
Reid, M. J. 1989, in IAU Symp., No. 136, The Center of the Galaxy, ed. M. Morris (Dordrecht, Kluwer), p. 37
Renzini, A., and Buzzoni, A. 1986, in Spectral Evolution of Galaxies, ed. C. Chiosi and A. Renzini (Dordrecht, Reidel), p. 195
Rhee, G. 1991, Nature, 350, 211
Rich, R. M. 1987, AJ, 94, 651
Richer, M. G., and McCall, M. L. 1992, AJ, 103, 54
Richter, O.-G., and Huchtmeier, W. K. 1984, A&A, 132, 253
Ridgway, S. T., Jacoby, G. H., Joyce, R. R., Siegel, M. J., and Wells, D. C. 1982, AJ, 87, 680
Ritchey, S. W. 1917, PASP, 29, 210
Roberts, M. S. 1962, AJ, 67, 437
Roberts, D. H., Lehar, J., Hewitt, J. N., and Burke, B. F. 1991, Nature, 352, 43
Rosenblatt, E. I., Faber, S. M., and Blumenthal, G. R. 1988, ApJ, 330, 191
Rosino, L. 1973, A&AS, 9, 347
Rowan-Robinson, M. 1985, The Cosmological Distance Ladder (New York, Freeman)
Rowan-Robinson, M. 1988, Space Sci. Rev., 48, 1
Rowan-Robinson, M., et al. 1990, MNRAS, 247, 1
Rubin, V. C., Burstein, D., Ford, Jr., W. K., and Thonnard, N. 1985, ApJ, 289, 81
Rubin, V. C., Ford, Jr., W. K., and Thonnard, N. 1980, ApJ, 238, 471
Ruiz-Lapuente, P., Lucy, L. B., and Danziger, I. J. 1992, ESO preprint No. 809
Ruiz-Lapuente, Cappellaro, E., Turatto, M., Gouiffes, C., Danziger, I. J., Della Valle, M., and Lucy, L. B. 1992, ApJ, in press
Rust, B. W. 1974, Oak Ridge Natl. Lab. Publ., No. 4953
Saglia, R. P., Bertschinger, E., Davies, R. L., Baggley, G., Burstein, D., Colless, M. C., McMahan, R., and Wegner, G. A. 1992, in preparation
Sancisi, R., and van Albada, T. S. 1985, in IAU Symp., No. 117, Dark Matter in the Universe, ed. J. Kormendy and G. Knapp (Dordrecht, Reidel), p. 67
Sandage, A. 1968, ApJ, 152, L149
Sandage, A. 1973a, ApJ, 183, 711
Sandage, A. 1973b, ApJ, 183, 731
Sandage, A. 1983, AJ, 88, 1108
Sandage, A. 1986, unpublished
Sandage, A. 1987, private communication
Sandage, A. 1988, ApJ, 331, 605
Sandage, A., and Cacciari, C. 1990, ApJ, 350, 645
Sandage, A., and Carlson, G. 1982, ApJ, 258, 439
Sandage, A., and Carlson, G. 1985a, AJ, 90, 1019
Sandage, A., and Carlson, G. 1985b, AJ, 90, 1464
Sandage, A., and Carlson, G. 1983, ApJ, 267, L25
Sandage, A., and Carlson, G. 1988, AJ, 96, 1599
Sandage, A., and Tammann, G. A. 1974, ApJ, 191, 603
Sandage, A., and Tammann, G. A. 1976, ApJ, 210, 7
Sandage, A., and Tammann, G. A. 1981, A Revised Shapley–Ames Catalog of Bright Galaxies (Washington, DC, Carnegie Institute), p. 8
Sandage, A., and Tammann, G. A. 1982, ApJ, 256, 339
Sandage, A., and Tammann, G. A. 1990, ApJ, 365, 1
Sandage, A., Tammann, G. A., and Yahil, A. 1979, ApJ, 232, 352
Sargent, W. L. W., Schechter, P., Boksenberg, A., and Shortridge, K. 1977, ApJ, 212, 326
Schechter, P. 1976, ApJ, 203, 297
Schechter, P. 1980, AJ, 85, 801
Schmidt, T. 1957, Z. Astrophys., 41, 182
Schmutz, W., Abbott, D. C., Russell, R. S., Hamann, W.-R., and Wessolowski, U. 1990, ApJ, 355, 255
Schommer, R. A., Williams, T. B., Bothun, G., and Mould, J. R. 1989, BAAS, 21, 1140
Schönberner, D. 1981, A&A, 103, 119
Schönberner, D. 1983, ApJ, 272, 708
Schweizer, F., Seitzer, P., Faber, S. M., Burstein, D., Dalle Ore, C. M., and Gonzalez, J. J. 1990, ApJ, 364, L33
Secker, J., and Harris, W. E. 1992, in preparation
Shapley, H. 1917, PASP, 29, 213
Shara, M. M. 1981a, ApJ, 243, 268
Shara, M. M. 1981b, ApJ, 243, 926
Shara, M. M. 1989, PASP, 101, 5
Shaw, R. A., and Kaler, J. B. 1989, ApJS, 69, 495
Shobbrock, R. R. 1992, MNRAS, 255, 486
Silk, J. 1989, ApJ, 345, L1
Stenning, M., and Hartwick, F. D. A. 1980, AJ, 85, 101
Stetson, P. 1987, PASP, 99, 191
Strom, R. G. 1988, MNRAS, 230, 331
Sutherland, P. G., and Wheeler, J. C. 1984, ApJ, 280, 282
Tammann, G. A. 1978, Mem. Soc. Astron. Ital. 49, 315
Tammann, G. A. 1982, in Supernovae: A Survey of Current Research, ed. M. J. Rees and R. J. Stoneham (Dordrecht, Reidel), p. 371
Tammann, G. A. 1987, in Observational Cosmology, ed. A. Hewitt, G. Burbidge, and L. Z. Fang (Dordrecht, Reidel), p. 151
Tammann, G. A. 1988, in The Extragalactic Distance Scale, Proceedings of the ASP 100th Anniversary Symposium, PASPC, Vol. 4, ed. S. van den Bergh and C. J. Pritchet (Provo, UT, Astronomical Society of the Pacific), p. 282
Tammann, G. A., and Leibundgut, B. 1990, A&A, 236, 9
Tammann, G. A., and Sandage, A. 1968, ApJ, 151, 825
Teerikorpi, P. 1984, A&A, 141, 407
Teerikorpi, P. 1987, A&A, 173, 39

Terlevich, R. J., Davies, R. L., Faber, S. M., and Burstein, D. 1981, MNRAS, 196, 381
Thompson, L., and Valdes, F. 1987, ApJ, 315, L35
Tonry, J. L. 1991, ApJ, 373, L1
Tonry, J. L., Ajhar, E. A., and Luppino, G. A. 1989, ApJ, 346, L57
Tonry, J. L., Ajhar, E. A., and Luppino, G. A. 1990, AJ, 100, 1416
Tonry, J., and Davis, M. M. 1980, AJ, 84, 1511
Tonry, J. L., and Davis, M. M. 1981, ApJ, 246, 680
Tonry, J. L., Luppino, G. A., and Schneider, D. P., 1988, in The Extragalactic Distance Scale, Proceedings of the ASP 100th Anniversary Symposium, PASPC, Vol. 4, ed. S. van den Bergh and C. J. Pritchet (Provo, UT, Astronomical Society of the Pacific), p. 213
Tonry, J. L., and Schechter, P. L., 1990, AJ, 100, 1794
Tonry, J. L., and Schneider, D. P., 1988, AJ, 96, 807
Trumpler, R. J., and Weaver, H. F. 1962, Statistical Astronomy (New York, Dover), p. 121
Tully, R. B. 1982, ApJ, 257, 389
Tully, R. B. 1988a, Nearby Galaxies Catalog (Cambridge, Cambridge University Press)
Tully, R. B. 1988b, Nature, 334, 209
Tully, R. B., and Fisher, J. R. 1977, A&A, 54, 661
Tully, R. B., and Fouqué, P. 1985, ApJS, 58, 67
Tully, R. B., and Shaya, E. J. 1984, ApJ, 281, 31
Turner, D. G. 1979, PASP, 91, 642
Valentijn, E. A. 1990, Nature, 346, 153
van den Bergh, S. 1969, ApJS, 19, 145
van den Bergh, S. 1970, Nature, 225, 503
van den Bergh, S. 1977, in IAU Colloq., No. 37, Décalages vers le Rouge et l'Expansion de l'Univers, ed. C. Balkowski & B. E. Westerlund (Paris, CNRS), p. 13
van den Bergh, S. 1980, PASP, 92, 122
van den Bergh, S. 1981, ApJ, 248, L9
van den Bergh, S. 1985, ApJ, 297, 361
van den Bergh, S. 1988, Comm. Astrophys., 12, 131
van den Bergh, S. 1989, Astron. Astrophys. Rev., 1, 111
van den Bergh, S. 1991, PASP, 103, 1053
van den Bergh, S., Herbst, E., and Kowal, C. T. 1975, ApJS, 29, 303
van den Bergh, S., and Pierce, M. J. 1990, ApJ, 364, 444
van den Bergh, S., Pritchet, C., and Grillmair, C. 1985, AJ, 90, 595
van den Bergh, S., and Pritchet, C. J. 1986, PASP, 98, 110
van den Bergh, S., and Pritchet, C. J. 1988, The Extragalactic Distance Scale, Proceedings of the ASP 100th Anniversary Symposium, PASPC, Vol. 4 (Provo, UT, Astronomical Society of the Pacific)
van den Bergh, S., and Tammann, G. A. 1991, ARA&A, 29, 363
van den Bergh, S., and Younger, P. F. 1987, A&AS, 70, 125
van Driel, W., and van Woerden, H. 1991, A&A, 243, 71
van Leeuwen, F. 1983, Ph.D. thesis, Leiden University
Vassiliadis, E., and Wood, P. R. 1992, ApJ, in press
Visvanathan, N. 1981, A&A, 100, L20
Visvanathan, N. 1983, ApJ, 275, 430
Wagner, S., Richtler, T., and Hopp, U. 1991, A&A, 241, 399
Walker, A. R. 1987, MNRAS, 224, 935
Walker, A. R. 1988, in The Extragalactic Distance Scale, Proceedings of the ASP 100th Anniversary Symposium, PASPC, Vol. 4, ed. S. van den Bergh and C. J. Pritchet (Provo, UT, Astronomical Society of the Pacific), p. 89
Walker, A. R. 1992, ApJ, in press
Weidemann, V., and Koester, D., 1983, A&A, 121, 77
Weidemann, V., and Koester, D., 1984, A&A, 132, 195
Welch, D. L., McAlary, C. W., McLaren, R. A., and Madore, B. F. 1986, ApJ, 305, 583
Welch, D. L., McLaren, R. A., Madore, B. F., and McAlary, C. W. 1987, ApJ, 321, 162
Wesselink, A. J. 1946, Bull. Astron. Inst. Netherlands, 10, 91
Wheeler, J. C., and Harkness, R. P. 1990, Rep. Prog. Phys. 53, 1467
Whitmore, B., McElroy, D., and Tonry, J. 1984, ApJS, 59, 1
Wilson, T. D., Barnes, T. G., Hawley, S. L., and Jefferys, W. H. 1991, ApJ, 378, 708
Wood, P. R., and Faulkner, D. J. 1986, ApJ, 307, 659
Woosley, S. E. 1990, in Supernovae, ed. A. G. Petschek (New York, Springer), p. 182
Woosley, S. E., and Weaver T. A. 1986, ARA&A, 24, 205
Yahil, A., Tammann, G. A., and Sandage, A. 1977, ApJ, 217, 903
Younger, P. F., and van den Bergh, S. 1985, A&AS, 61, 365
Zinn, R. 1985, ApJ, 293, 424
Zwicky, F. 1936, PASP, 48, 191